Intracellular functions and interactions of Age-Related Macular Degeneration-associated variant B cystatin C.

Thesis submitted in accordance with the requirements of the University of Liverpool for the degree of Doctor in Philosophy

by Christopher John Myerscough

June 2015

In memory of Nora Antonio whose belief in me kept me going

and George Antonio who would be so proud of all I have accomplished

Acknowledgements

With thanks to:

Dr Luminita Paraoan and Professor Malcolm Jackson for extensive advice and assistance throughout this project

Dr. T. Michael Redmond for the gift of D407 cells

Dr Anna Kayani for her assistance with initial ATP assays

Dr Tim Pearson for assistance with both confocal microscopy and the oxytherm oxygen probe

Dr Dave Spiller for technical advice and guidance on cell imaging

Dr Paul Kay for providing the HaloTag materials and oligonucleotides and for lots of excellent advice

Mr Umar Sharif for his expert advice on western blotting

Miss Samantha McDonnell for use of her HaloTag sequencing primers

Professor Rob Beynon, Dr Phillip Brownridge and Dr Deborah Simpson at the University of Liverpool, Centre of Proteomic Research. Without whom the Mass Spectrometry would not have been possible.

Contents

Figures

Tables

List of abbreviations

ADP = Adenosine diphosphate

AGEs = Advanced glycation end products

ALEs = Age-related lipooxidation products

AMD = Age Related Macular Degeneration

ANOVA = Analysis of variance

APS = Ammonium persulphate

ATP = Adenosine triphosphate

CMV = Cytomegalovirus

DMSO = Dimethyl sulfoxide

DNA = Deoxyribonucleic acid

dNTP = Deoxynucleotide triphosphates

EDTA = Ethylenediaminetetraacetic acid

EGFP = Enhanced green fluorescent protein

ESI-FTICR = Electrospray Ionization Fourier Transform Ion Cyclotron Resonance

FCS = Foetal calf serum

GAPDH = Glyceraldehyde 3-phosphate dehydrogenase

LC3 = Light Chain 3 protein

PAGE = Polyacrylamide gel electrophoresis

PBS = Phosphate buffered saline

PCR = Polymerase chain reaction

POS = Photoreceptor outer segments

RPE = Retinal pigment epithelium

ROS = Reactive oxygen species

SDS = Sodium dodecyl sulfate

VEGF = Vascular endothelial growth factor

PhD Thesis Abstract: Intracellular functions and interactions of Age-Related Macular Degeneration-associated variant B cystatin C.

Christopher John Myerscough, June 2015

Age related macular degeneration (AMD) is the leading cause of blindness among the elderly population. It occurs in two forms, a nonexudative "dry" form which can lead to geographic atrophy of the retinal pigment epithelial (RPE) cells in the region of the macula and an exudative "wet" form which involves neovascularisation from the choroid, through Bruch's membrane and the RPE layer and into the photoreceptor layer causing significant damage.

Cystatin C is a cysteine protease inhibitor known to inhibit cathepsin activity. It is a highly abundant transcript in the RPE and is known to be processed through the secretory pathway . A variant form of this protein with an amino acid substitution in its signal sequence results in the protein being retained intracellularly and is found localised with the mitochondria. This variant form has been associated with increased risk of developing exudative AMD.

In this study a number of key cellular processes were examined to elucidate the effect the variant B protein has on the RPE. These processes were respiration, apoptosis, autophagy and oxidative stress; all of which have been implicated in AMD pathology or ageing. In addition the protein-protein interactions of variant B cystatin C were assessed through mass spectrometry analysis of pulled-down cystatin C protein from transfected cell lysates.

No effect on respiration, apoptosis or autophagy was identified. However a statistically significant difference in oxidative stress was identified as a result of overexpression of either wild type cystatin C or variant B cystatin C. Mass spectrometry analysis resulted in two highly promising proteins that were found interacting with variant B cystatin C at a statistically significant level, prohibitin and voltage-dependent anion-selective channel protein 1 (VDAC1).

Although oxidative stress was found for both proteins given the nature of the expression (driven by a CMV promoter) it seems likely that the oxidative stress response is due to a high level of intracellular cystatin C. This suggests that the retention of variant B protein within the cell would lead to increased oxidative stress levels. It can be speculated that this response could be a contributory factor to development of AMD.

VDAC1 and prohibitin may offer an explanation of what happens to the variant B protein within RPE cells. VDAC1 is the major pore-forming protein in the mitochondrial membrane, disruption of its functioning by the binding of variant B protein might be expected to have detrimental effects. Prohibitin is an even more promising target as it has been associated with oxidative stress. In addition it is known to translocate between the nucleus and the mitochondria, offering the tantalising possibility of a complete explanation for the mitochondrial mislocalisation.

Chapter 1

Introduction

1.1 The eye

The eye (figure 1.1) consists of a fluid filled chamber constructed from a number of tissues. Some of these tissues act to focus light, detect it or transmit it and some of which exist to protect and support its function of enabling vision.

The sclera and the cornea comprise the majority of the outer layer of the eye and consist primarily of interwoven collagen fibres arranged differently in the two tissues (Komai & Ushiki, 1991). The sclera is the resilient, white layer which comprises the majority of the outer surface of the eye. The cornea is a similarly tough layer at the front of the eye but is clear , allowing light to pass through. The two are joined by the limbus, a tissue known to contain structures of importance to the balance of pressure in the eye; specifically this region includes Schlemm's canal and other linked vessels which are crucial for removing aqueous humour from the eye and passing it to the circulatory system (van der Merwe & Kidson, 2010). Taken as one these three present a durable and resilient protective outer layer. In addition they provide a surface to which the other layers are anchored in an organised way and help to maintain intraocular pressure. The only interruption to this layer is at the very back of the eye, where the optic nerve penetrates through the sclera.

Behind the cornea is the iris, a flexible layer of tissue containing muscles which allow the pupil to contract and dilate. This allows for adjustment of the amount of light entering the eye, the speed of the response being proportional to the intensity of light (Ellis, 1981). Light passing through the pupil is focussed by the lens, a clear disc which redirects light onto the retina at the back of the eye. The lens is connected to the ciliary body, a muscular ring which is crucial for the adjustment of the refractory capability of the lens.

At the back of the eye are a series of layers to detect and transmit light, as well as the supportive tissue for these layers. The outermost layer (aside from the sclera) is the choroid, a heavily vasculated tissue which supplies the eye with nutrients and removes waste product (1.2.4) The blood vessels within the choroid are thin capillaries, which are very leaky, consequently it is crucial to separate the capillaries from the retina itself. This is achieved by two layers between the capillaries and the retina known as the Bruch's membrane and the retinal pigment epithelium (RPE).

Bruch's membrane (1.2.3) is a flexible layer which separates the RPE from the capillaries. It is a five-layered extracellular matrix made up primarily of elastins and collagens. The RPE is

the support layer for the retina, fulfilling a variety of crucial functions which are essential for the normal functioning of the eye (1.2.2). The innermost layer at the back of the eye is the photoreceptor layer itself (1.2.1), a series of light-sensitive cells interacting with a network of nerve cells which lead back to the optic nerve and, through that, to the brain.

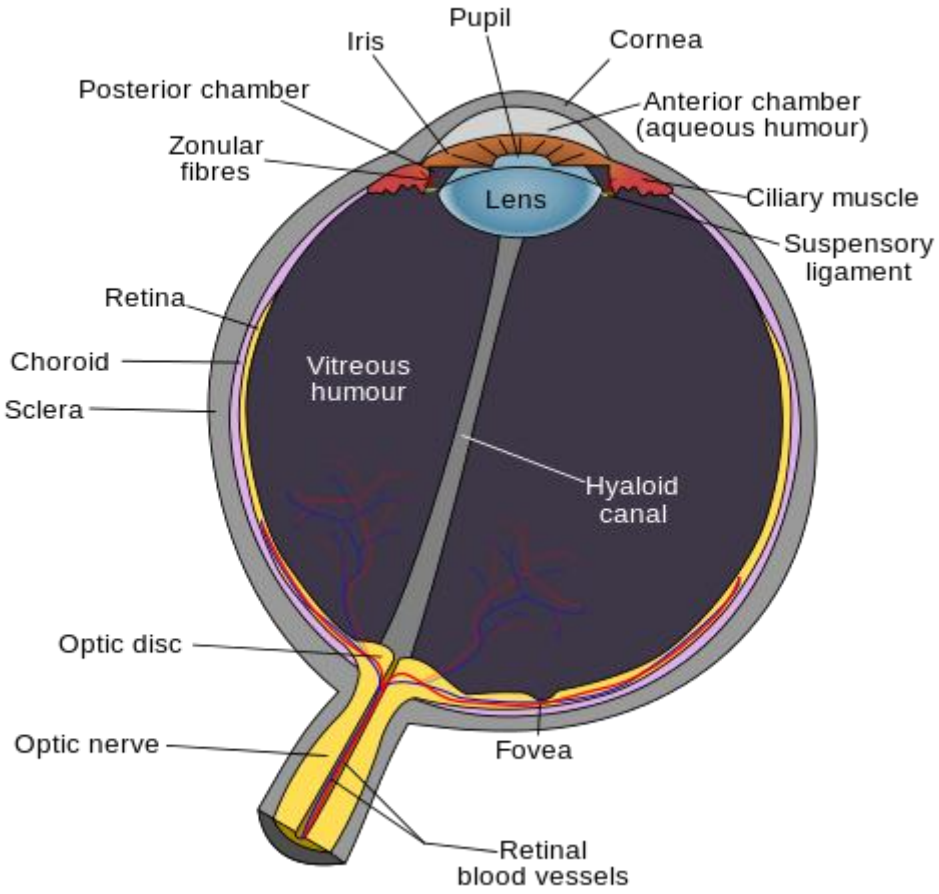

Figure 1.1 Cross sectional representation of the eye. A gross anatomical diagram with major structures labelled. (Public domain image, Wikimedia commons).

1.2 The posterior eye

1.2.1 The photoreceptors and neuronal cells

The most functionally important layer of the eye is the retina. It is defined by its large, complex network of neuronal tissue (Figure 1.2) whose function is to detect the light that falls upon it and transmit signals produced by the reaction to light. This neuronal tissue is layered and detects light through photochemical reactions in specific photoreceptive cells, producing signals in response which are passed on through a series of neurons through the optic nerve to the brain where they can be deciphered.

Photosensitive cells within the retina are organised with their outer segment (containing photosensitive pigment) as the closest structure to the retinal pigment epithelium layer; this outer segment is connected to the inner segment which contains large numbers of mitochondria. The uppermost part of the cell consists of the cell's nucleus with a protruding axon and a synaptic terminal which allows the release of neurotransmitters, initiating the neurological signal resulting from the presence of light. There are two types of photoreceptors known as rods and cones with cones providing superior resolution as well as utilising three different pigments in order to build up a colour image in bright light (Sung & Chuang, 2010). The central vision area of the eye is known as the macula and is responsible for high resolution imaging. In particular the fovea, a small depression in the macula region, is the focal point for central vision and contains an extremely high density of cones (Curcio *et al.*, 1990).

Connecting to the photoreceptor layer is a layer of bipolar cells. These act to transmit signals which originate in the photoreceptors through a network of neuronal tissue with signals diverging or converging as appropriate through these cells. Bipolar cells occur in a wide variety of different types (more than ten) and are crucial to vision, as all information for vision is relayed by these cells (Euler *et al.*, 2014). The signals are then transmitted to ganglion neurons from where they are finally transmitted via the optic nerve to the brain.

Cones in the central vision areas of the eye have divergent signalling by which they link to multiple bipolar cells and, consequently, multiple ganglion cells. This allows for a single stimulated cell to produce a signal in such a way that it can be detected and resolved. Further, this allows for highly sensitive vision as a result of nearby cones being able to detect differing amounts of incoming light and subsequently generating signals

proportional to the input. This central region of the retina is referred to as the macula and is the most crucial region of photoreceptors for high resolution vision.

Peripheral areas of the eye tend to consist of convergently wired rods where a number of photoreceptors feed into one bipolar cell and hence one ganglion cell. Rods contain a single pigment known as rhodopsin (Brown & Wald, 1964) and respond to very low levels of light, as low as a single photon (Kawamura & Tachibanaki, 2008). This results in extremely light-sensitive but poor resolution vision, allowing for vision in low-light conditions but reduced visual acuity. This is particularly important to note in the case of damage to the retina, central areas of the eye are of crucial importance to resolving high resolution images whilst peripheral regions of the eye do not have the same capacity for resolving shapes. Consequently damage to the central region will have a larger impact on visual capability.

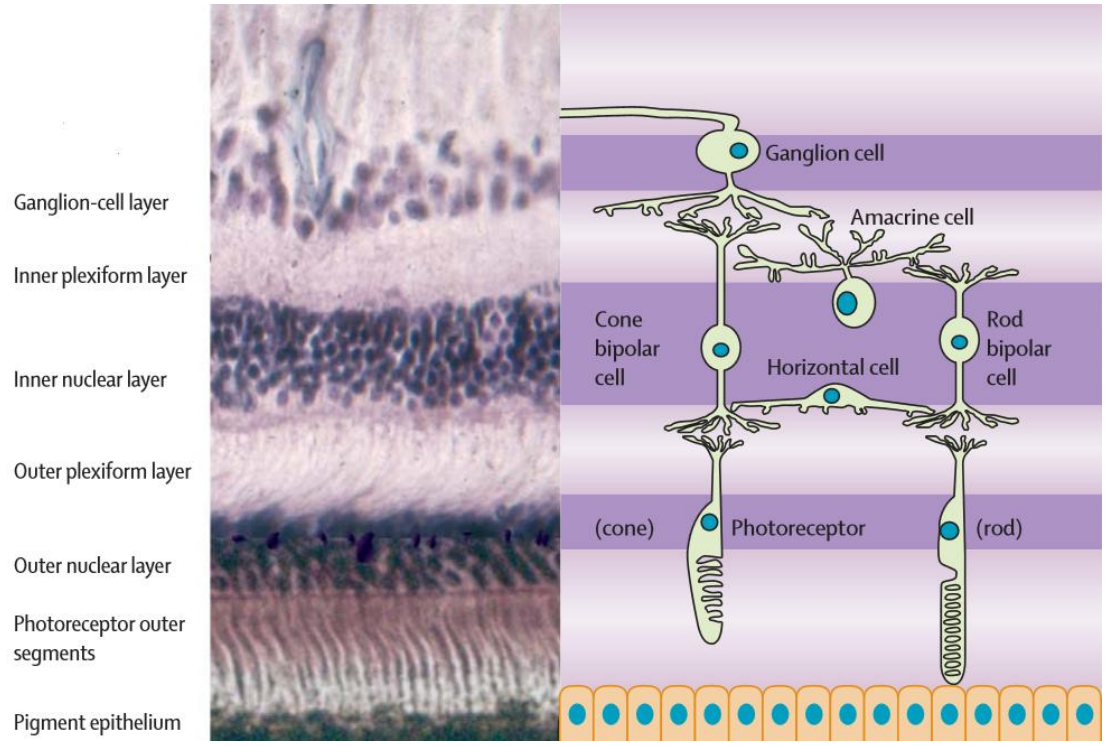

Figure 1.2 Cross section of the layers of the retina. A histological section of the retina showing the photoreceptors and RPE combined with a figure illustrating the various cells at each layer. The retinal pigment epithelium is the bottommost monolayer of cells and is a support tissue for the photoreceptors above. (adapted from Hartong *et al.*, 2006).

1.2.2 The retinal pigment epithelium

1.2.2A Overview

The RPE is a supportive layer in the posterior eye which is crucial for the protection of the retinal cells from a variety of sources of potential damage as well as supporting the cells in their function. These include transport of nutrients and ions between the choroid and the photoreceptors, maintenance of the surrounding tissue by production of growth factors , homeostasis of ions in the subretinal space and recycling of retinal via the visual cycle. Neural retinal cells are highly active due to the constant processing of light signals and consequently have very high upkeep requirements; this is only possible due to these supportive tissues.

1.2.2B Structure of the RPE

The RPE layer is a tightly packed, highly polarised, monolayer cellular structure which acts as a physical barrier in the retina, contributing to protecting it from the choroid and supporting the photoreceptors (Boulton & Dayhaw-Barker, 2001). It is characterised by a dense "cobblestone" appearance and forms a barrier for control of transport.

RPE cells are highly polarised with a structure which facilitates its supportive functions in relation to the retina and the surrounding tissue. The apical side of the RPE consists of a series of microvilli which surround and interact with the ends of the photoreceptor cells (Bok, 1993); these come as a mixture of long and short microvilli. The long microvilli provide a large surface area for transport and easy exchange of ions, and the short microvilli act to sheath the ends of the photoreceptors and to provide a surface for phagocytosis (Boulton & Dayhaw-Barker, 2001). In addition the basal surface of the RPE is infolded (Garron, 1963) which allows for the effective uptake of nutrients and removal of waste products via the choroid, again by providing a large surface area for transport.

The layer as a whole is firmly anchored together by tight junctions. Rizzolo (2007) has reviewed tight junctions, both their development and their effects on the RPE. In brief, these are complex structures that join neighbouring cells and exist to regulate a variety of cellular functions as well as to regulate diffusion through epithelial membranes via the paracellular route. Tight junctions are made up of a variety of proteins that can be broadly

ascribed to four major classes. Transmembrane proteins anchor cells together and they are attached to adaptor proteins. These act as a scaffold to anchor the transmembrane proteins either to the cytoskeleton or to effector proteins. Effector proteins comprise both signalling proteins and transcriptional regulatory proteins; this allows the tight junctions to affect the cell's internal environment. This seal caused by tight junctions allows for the formation of ion gradients by dramatically slowing any diffusion through the spaces between cells. Consequently allowing for ionic gradients to form and be used to drive transport in the RPE cells.

The intracellular structure of RPE cells is organised in such a way as to facilitate the supportive functioning of the retina. Nutrients, ions and waste products must pass through these cells due to the tight junctions, consequently the RPE is crucial in the process of maintaining the environment of the neuronal cells (Bok, 1993). As a result, transport processes of the RPE are complex and utilise a large number of different exchange mechanisms. In addition, ionic balance is of crucial importance as it is ionic gradients that power many of the processes involved.

1.2.2C Functions of and trafficking in the RPE

One way by which the RPE acts to protect the retina is through protecting against excess light that enters the eye. As the name states the cells are pigmented and this pigment acts to absorb light focussed onto the retina by the lens. Excess light has significant potential for harm as a result of photo-oxidation leading to oxidative stress and damage to the cells in the retina.

In addition to the photo-oxidative damage potential illustrated above, the retina itself is a high risk environment for oxidative stress. As photoreceptors are exposed to light over time this leads to a build up of photo-damaged proteins within in the photoreceptor cells and a build up of toxic substances. These damaged components are recycled through the process of shedding old photoreceptor outer segments to be broken down and the construction of new outer segments which occurs at the base of the region. The shed photoreceptor outer segments (POS) are taken up by the RPE by phagocytosis and are subsequently digested, with damaged proteins broken down and intact important molecules are returned to the photoreceptors for use in constructing new outer segments (Bok, 1993). These processes

are both tightly regulated in cooperation with each other as the shedding of POS and the construction of new segments must occur at the same rate in order to ensure that the length of the photoreceptors remains stable. The exact process by which this happens is not fully understood, however it is known that a circadian regulation is involved (La Vail, 1976). This process of phagocytosis of shed photoreceptor outer segments is thus of crucial importance to the retina but is also a source of significant amounts of reactive oxygen species with great potential for causing harm (Miceli *et al.*, 1994).

Perhaps the most important role of the RPE is in the recycling of the photoreceptor photosensitive molecules in what is termed the retinoid cycle. In order for light to be translated into vision it must be transduced into electrical impulses and consequently be passed through the extensive neuronal networks contained within the eye. This is achieved by the light being used to modify the stores of 11-*cis*-retinal contained within the photoreceptors in the form of rhodopisn into all-*trans*-retinal (Hargrave, 2001). However, once this has occurred, the photoreceptors have no way of converting the retinal back into a form which can be triggered by new light. Consequently the RPE cells fulfil a key role in vision itself by acting as the site where retinal can be reisomerised. This occurs in a cycle where all-trans-retinal is converted to all-trans-retinol and transported to the RPE where the retinol is converted back to 11-cis-retinal and returned to the photoreceptors to be used (Tang *et al.*, 2013). In addition a certain amount is also recovered from the shed POS when they are digested and returned to the photoreceptors via a similar pathway.

A significant part of the RPE function is the transport of nutrients and ions; this is essential to both provide the RPE cells what they need to survive as well as to remove waste products. In addition due to the high metabolic activity in the retina a large amount of water is produced and consequently it must constantly be removed. This is achieved by a combination of Müller cells and the RPE cells themselves (Marmor, 1990) and acts to help establish adhesion between the RPE and the retina. In the RPE the removal of water is driven by epithelial transport of chlorine and potassium ions and given the tight junctions and consequent impermeability of the layer the water is primarily extracted by this transcellular pathway (Strauss, 2005).

A large number of ions, nutrients and waste products are shifted across the RPE. With the polarity of the layer combined with the tight junctions making a barrier for careful control of the transport flow. The long microvilli on the apical side of the RPE sheath the photoreceptors and allow for efficient exchange, as do the folds on the basolateral side.

The polarisation of RPE is elegantly reviewed by Marmorstein (2001). However in brief, an apical Na^+-K^+-ATPase provides the driving force for transport, producing a sodium ion gradient that enables the functioning of a variety of cotransporters through which the ions are moved. As mentioned above this includes K^+ and Cl^- ions which are crucial in the uptake of water. However it also includes the removal of lactic acid from the photoreceptors which is the major waste product, found at high subretinal concentrations, and which is taken up by the RPE cells and passed out through the basolateral membrane (Strauss, 2005). In addition glucose is known to be transported from the choriocapillaries to the photoreceptors via the retina in a process which involves the glucose transporters GLUT1 and GLUT3 in a variety of species (Ban & Rizzolo, 2000).

The RPE is also crucial in the development of the retina. The two are co-dependent with specific stages of development of each depending upon corresponding developments in the other. The extension of microvilli of the RPE, for example, is coordinated with the lengthening of the photoreceptor outer segments forming the large surface of interaction necessary for high levels of transport. In addition the RPE is believed to be heavily involved in the development of the Bruch's membrane as it is capable of synthesising the major components necessary in its composition (Booij *et al.*, 2010).

Aside from this developmental importance it is also crucial in the secretion of growth factors for maintenance of the retina. The RPE cells are known to produce and secrete a wide variety of growth factors which are crucial for maintaining a normal environment for the sensitive photoreceptors. Some of these growth factors are of particular importance. For example, the RPE is a source of low quantities of vascular endothelial growth factor (VEGF) which is essential to maintain the choriocapillaries (Adamis *et al.*, 1993).

Finally the RPE acts as part of the barrier between the leaky capillaries of the choroid and the sensitive neuronal tissue of the retina (along with Bruch's membrane). It functions both as a physical barrier and as a regulator, for example by its control of the secretion of VEGF mentioned above. As a physical barrier it prevents blood from entering the retina where it could cause significant harm, damaging and destroying cells and severely disrupting sight. This effect can be seen in neovascular age-related macular degeneration (section 1.3) where blood vessels entering the neuroretina itself leads to blood leakage and damage in the macular region.

1.2.3 Bruch's membrane

Bruch's membrane is located between the RPE layer and the choroid and is commonly described by Hogan's five-layer system (Hogan *et al.*, 1971). Nearest the RPE layer is the RPE basal lamina which is similar in structure to other basal laminas in the body (Curcio & Johnson, 2013) comprising a mesh of fibres and includes a variety of laminins which the RPE cells synthesise and adhere to.

The second layer is the inner collagenous layer, a multilayered cross structure of collagens. Below that, the central layer of Bruch's membrane, is the elastic layer which is primarily a series of elastins forming a sheet, mixed with collagen, fibronectin and various other proteins; collagens from the collagenous layers can also cross into the elastic layer. The elastic layer is the most crucial layer of the Bruch's membrane in resisting angiogenesis as well as being key in its biomechanical properties.

The fourth layer is the outer collagenous layer which in many respects is very similar to the inner collagenous layer, although it also features intercapillary pillars which extend out between the choriocapillaries. Finally the choriocapillaris basal lamina is a very thin layer which is perforated by the intercapillary pillars. It is believed to inhibit cell migration into Bruch's membrane (Roberts & Forrester, 1990).

It is well established that with age Bruch's membrane undergoes a number of changes. There is a tendency for the membrane to thicken with age to varying extents between individuals. This is thought to be a result of misregulation of the extracellular matrix proteins leading to a build up as normal turnover is disrupted (Newsome *et al.*, 1987). Note that this thickening is not uniform across the membrane; the collagenous layers tend to thicken at different rates (the outer layer more than the inner) and the elastic layer tends to thicken at a significantly lesser rate. In addition calcification of the membrane results in increased rigidity as a result of deposition of calcium phosphate onto elastin fibrils (Davis *et al.*, 1981).

In addition Bruch's membrane suffers from protein modification in long-lived proteins. Specifically the formation of advanced glycation end products (AGEs) and age-related lipooxidation end products (ALEs) (Curcio & Johnson, 2013). These together accumulate on Bruch's membrane and are a defining characteristic of ageing. In particular AGEs are the result of protein modification by Malliard reactions and tend to accumulate on long-lived

structural proteins and have been seen to effect the normal functioning of the RPE (Kay *et al.*, 2014). AGEs have been heavily implicated in age-related degeneration of the retina. A study in ARPE-19 cells demonstrated that exposure to AGE treated basement membrane resulted in a mixture of up and down regulation of various mRNAs, particularly those related to extracellular matrix genes and signal peptides as well as lysosomal gene expression (Glenn *et al.*, 2009). In addition an increase in lipofuscin accumulation was identified, a well-known indication of aging (Brunk & Terman, 2002). In addition an assortment of other proteins, such as complement components, are found to build up in aged Bruch's membrane.

More significant is the accumulation of deposits on the surface of Bruch's membrane with age. These are known as drusen and typically form small, hard yellow or white spots on the Bruch's membrane. These are a normal feature of ageing and are comprised of extracellular material and a mixture of proteins and lipids. However they are also linked with disease; large and diffuse drusen being a hallmark of AMD (AMD will be further discussed in section 1.3). Further, the Bruch's membrane has been demonstrated to be digestable in the process of choroidal neovascularisation (Heriot *et al.*, 1984), which means that it is not necessary for the Bruch's membrane itself to be directly damaged for invasion of the retina by the choroid.

1.2.4 The choroid

The choroid is a vascular structure which comprises a large network of blood vessels. Its purpose is to supply the retina with nutrients and oxygen, and to remove waste products. Closest to the Bruch's membrane is the choriocapillary layer, a high-surface-area network of small, fenestrated, leaky capillaries which provide a highly efficient exchange surface for nutrients and waste. These are supported by a network of medium sized blood vessels located immediately underneath this layer, which feed this capillary network, and then a layer of large blood vessels. Taken together these provide a significant supply of blood to the retina in an efficient and organised way. Finally a layer known as the suprachoroid acts as a transition layer between the choroid and the protective layer of the sclera. This layer contains aspects of both structures and effectively anchors the choroid to the sclera. In addition it contains large spaces which are believed to be part of the lymphatic system.

The primary purpose of the choroid is as a transport system of nutrients and oxygen to the retina and waste from the retina. Blood flow in the retina is typically extremely high and tightly regulated in order to ensure an optimal environment for the neuronal components of the eye (Pouranaras *et al.*, 2008). However, blood flow has been shown to decrease with age (Emeterio Nateras *et al.*, 2014) and in patients with age-related macular degeneration (Burgansky-Eliash *et al.*, 2014) which may lead to deficiencies of nutrients within the retina and insufficient removal of waste products. The RPE, Bruch's membrane and choroid all have been implicated in the development of AMD , with a "mutalistic symbiotic relationship" being disrupted in the disease state (Bhutto & Lutty, 2012). Indeed there is a clear link between degeneration of the choriocapillaries and the degeneration of the RPE layer resulting in a 50% decrease in vascular area compared with control eyes for dry AMD (McLeod *et al.*, 2009).

The choroid is also implicated in the development of and production of growth factors necessary for the RPE. As an example transdifferentiation of the RPE to neural retinal cells in embryonic mammals has long been known (Zhao *et al.*, 1995). In addition it is known that the RPE of certain species of newt can regeneratively differentiate into neural retinal cells in a similar manner even in adults; the choroid has been demonstrated to be essential for this process (Mitsuda *et al.*, 2005). In particular specific growth factors such as FGF-2 and IGF-1 appeared to be crucial in this development.

In addition to the involvement of the choroid in supplying the retina and removing waste it is also believed to be involved in thermoregulation. There is some evidence to indicate that the constant high blood flow acts to maintain the retina near the body's core temperature by either dissipating excess heat or providing heat in the cold (Parver, 1991). However this view is not accepted by all, with some arguing that fluctuations in core body temperature would make maintaining a stable retina temperature unlikely (Nickla & Wallman, 2010).

1.3 Age Related Macular Degeneration

1.3.1 Overview of AMD

Age related macular degeneration (AMD) is a leading cause of irreversible blindness in the elderly population (Gehrs *et al.*, 2006). The disease involves the progressive degeneration of the retinal cells in the macular region hence causing loss of central, high resolution, vision.

The disease occurs in two forms which are commonly termed “dry AMD” and “wet AMD”, also known as nonexudative AMD and exudative AMD (Figure 1.3). The dry form of AMD is characterised by the formation of deposits known as drusen in the retina and a progressive, gradual degeneration of sight. The wet form of AMD is characterised by neovascularisation from the choroidal layer penetrating through the Bruch’s membrane and into the retina where the leaky blood vessels cause significant damage leading to vision loss.

"Dry" AMD is caused by a progressive degeneration of the retinal layer itself, with the specific atrophy of the macula region. With age the RPE cells undergo a number of changes (reviewed by Bonilha, 2008) and in AMD they become more pronounced. A key aspect of the disease progression is the formation of drusen plaques, consisting of extracellular debris, between Bruch's membrane and the RPE layer. These commonly occur in older people without AMD and in healthy individuals appear as hard yellow or white spots. However in the case of patients with dry AMD these spots are larger and "softer" with irregular shapes and a lack of a clearly defined edge. Around ten to fifteen percent of cases of dry AMD lead to wet AMD (section 1.3.2).

Although AMD disease progression can be slowed through various treatments there is no treatment available which will reverse the degenerative effects and restore the function of the retina; treatments will be discussed in section 1.3.5. Further, given our limited knowledge it is not possible to prevent progression entirely. A better understanding of the disease is thus crucial, however it is multifactorial in nature and, as such, it is difficult to elucidate the precise mechanism or mechanisms that lead to the degeneration.

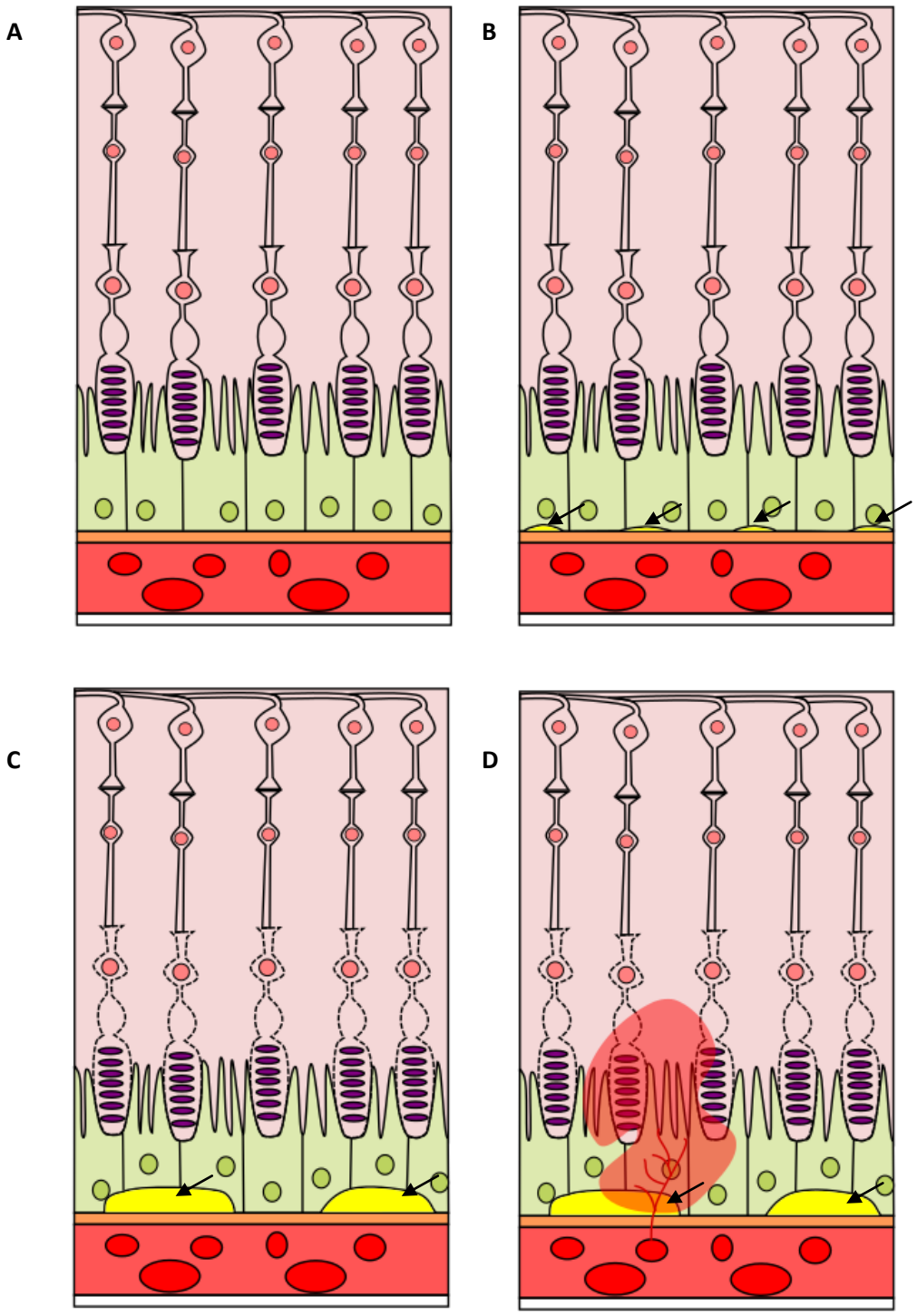

Figure 1.3 Degradation of the retina with age and AMD. A is a representation of a young eye. **B** represents an ageing eye, note the small drusen deposits (arrows). **C** represents an eye with nonexudative AMD, please note the larger drusen (arrows) and degrading photoreceptors. Finally **D** represents an eye with exudative AMD, with neovascularisation penetrating Bruch's membrane and bleeding into the photoreceptor layer. (Author's figure)

1.3.2 Neovascular AMD

Neovascular AMD is also known as exudative AMD and amongst the general population is commonly referred to (and widely known) as "wet AMD". As the name suggests it involves the formation of new blood vessels leading to damage in the retinal layer. More specifically following a gradual degeneration of the retina, new blood vessels develop and pierce the Bruch's membrane and RPE layer before growing into the retina, where blood leaks through the thin capillary walls causing extensive damage.

Dry AMD has no treatments and wet AMD can be treated however the dry form is also far less harmful. The vasculogenesis that occurs in wet AMD leads to heavy and rapid damage done to significant areas of the macular region leading to rapid and extensive vision loss. With both scarring and the blood vessels themselves contributing to the damage. It is multifactorial in nature with both environmental influences such as smoking and diet (Seddon *et al.*, 2006) as well as genetic factors such as the focus of this study, cystatin C.

1.3.3 Similarities to other diseases

AMD is an age-related disease which has a significant aggregation component (the aforementioned drusen). Studies have shown associated elements with a number of other age related diseases; most particularly Alzheimer's disease.

The link with Alzheimer's disease is interesting as Alzheimer's is fundamentally a disease that involves aggregation of proteins into plaques. This is analogous to what happens in AMD given the build up of large drusen plaques in the retina which are a key hallmark of AMD development. However further links beyond this casual association between the diseases are not confirmed. Despite this certain genetic factors found to be risks for AMD, such as variant B cystatin C (discussed in section 1.4.5) have been linked with Alzheimer's disease and has been demonstrated to have impaired secretion in other cells (Benussi *et al.*, 2003). Further a recent study on risk variants for the diseases suggested shared genetic mechanisms between the two (Logue *et al.*, 2014). An almost equally recent population study in an age-matched cohort found no association between the two (Williams *et al.*, 2014); however another study found data supporting a possible association between the diseases (Rozzini *et al.*, 2014). More recently a clear link has been shown between

Alzheimer's Disease and AMD, with the CST3 missense variant leading to the production of variant B cystatin C (section 1.4.5) being associated with both diseases in a meta-analaysis (Butler *et al.*, 2015). The parallel links between AMD and Alzheimer's disease with respect to the presence of amyloid β protein deposition in both senile plaques in the brain and drusen in AMD have been reviewed by Ohno-Matsui (2011). In conclusion these similarities mean that therapeutic techniques for Alzheimer's disease may be applicable to AMD.

Aggregation is, in fact, a key factor in a number of neurological diseases which are believed to be associated with AMD. Proteins found within drusen associated with AMD are common to deposits found in a number of other diseases including atherosclerosis, elastosis, amyloidosis and dense deposit disease (Mullins *et al.* 2000). The evidence for a relationship between AMD and atherosclerosis in particular is noteworthy, with a recent review noting that although there are several differences in studies between groups of patients there is a compelling argument to be made that AMD is associated with atherogenesis (Machalińska *et al.*, 2012). It has been demonstrated, for example, that AMD is associated with an increased risk of certain subtypes of stroke (Ikram *et al.*, 2012) and a weak relationship between carotid plaques and AMD has been identified in population studies (Klein *et al.*, 2013).

1.3.4 Factors associated with AMD

As a multifactorial disease AMD is extremely complex and has a large number of contributory factors which are known to influence incidence of the disease. Consequently, trying to elucidate and target exactly how AMD arises is a difficult process. Further, although the RPE (section 1.2.2) is a crucial tissue involved in AMD it is not the only tissue involved in the process and different processes will be affected in each tissue.

There are a number of genes that are associated with the development of AMD. Examples include apolipoprotein E which is involved in cholesterol metabolism and its' ε2 and ε4 forms are associated with increased risk of AMD (Klaver *et al.*, 1998). In addition, fibulin 5 is a secreted extracellular matrix protein and missense mutations in this protein are implicated in a proportion of AMD cases (Stone *et al.*, 2004). However perhaps the most notable is complement factor H (a regulatory protein of the complement system), a variant of which is associated with AMD and was first identified by Haines *et al.* (2005). This has

since been widely accepted as a major risk factor in the development of the disease. However, some proteins believed to be involved, such as TIMP3, have been eliminated as possibilities (De La Paz, 1997).

In addition to these genetic factors lifestyle choices have also been implicated. Examples of these non-genetic factors include the combination of not smoking, having a healthy diet and being physically active being associated with a 71% reduced risk for AMD amongst women (Mares *et al.*, 2011). Further, increased red meat consumption has been associated with early onset AMD (Chong *et al.*, 2009).

There are a wide variety of factors influencing AMD incidence and consequently a number of cellular processes that are connected to the disease. It is therefore difficult to ascertain the exact pathogenesis of the disease, with many potential targets which are likely to contribute but no apparent overall factor leading to development. The many contributing pathways also make it a difficult disease to treat as only the symptoms can be treated and not the underlying cause.

One intracellular factor implicated in AMD is oxidative stress and the associated reactive oxygen species (ROS) which is of particular relevance to the RPE. ROS are produced in cells as a result of normal cellular functioning, notably from respiration in the mitochondria, which results in the production of large amounts of highly reactive oxidants. This can lead to inappropriate oxidation of cellular proteins leading to damage. Under normal conditions these ROS are unlikely to be harmful as cells have mechanisms by which they control the risk of damage. However under disease conditions there can be a build up of ROS which can lead to severe damage to crucial intracellular mechanisms and impairment of normal function in a non-specific non-directed way. This and other potential mechanisms will be briefly discussed in section 1.5.

1.3.5 Treatments for AMD

Although AMD damage cannot be reversed there are several therapies available to reduce the progression and impact of wet AMD. The most common treatment is the use of vascular endothelial growth factor (VEGF) inhibitors. VEGFs are signal proteins which lead to new blood vessel formation; by therapeutically providing inhibitors for these proteins

their levels can be reduced and consequently the rate and extent of formation can be reduced. Normally the RPE layer itself maintains a very careful balance of growth hormones and inhibitors, however it is apparent that this is insufficient in the case of exudative AMD. However this treatment cannot reverse the damage done as the inhibitors merely act to slow the disease progression by blocking growth signals to the blood vessels. It is worth noting that anti-VEGF agents are increasingly favoured over most other, older therapies (Hanout *et al.*, 2013). The available anti-VEGF agents were thoroughly comparatively reviewed recently by Solomon *et al.* (2014).

Photodynamic therapy (PDT) is a technique developed more than twenty years ago. It involves the injection of a light-sensitive drug into the patient and then activating it specifically where it is needed using a low-powered laser. For AMD treatment this is verteporfin; activation of the molecules by laser induces a phototoxic effect, killing the blood vessels. However side effects include the patient having to avoid sunlight. Further, although PDT slows disease progression, modern VEGF treatment has also resulted in vision improvement. Combination therapy of the two (plus steroids which, although having shown no visual improvement in clinical studies, have various other benefits such as inflammation inhibition) is the subject of much interest and has been reviewed in recent years (Couch & Bakri, 2011; Miller, 2011) but anti-VEGF monotherapy is currently preferred (Lally *et al.*, 2012).

An earlier approach was the direct use of laser surgery on the eye. By utilising a laser to cauterise inappropriately growing blood vessels it is possible to cut off the blood supply and hence cause these vessels to die. This prevents further growth of the blood vessel and restricts the damage that it can do to the retina. As with other treatments, however, this does not repair any damage done, merely prevents further damage from occurring. Further, this treatment is limited to the specific blood vessels treated which can be an advantage. However this therapy tends to be less effective than others and therefore is only used when others cannot be, with a recent review noting it is "not recommended" for subfoveal choroidal neovascularisation (Virgili & Bini, 2007).

Finally radiotherapy has been experimented with in clinical trials. The use of stereotactic radiotherapy has been established in cancer but more recently there have been a number of tests for its effect on AMD. In particular Jackson *et al.* (2014) have been conducting a study which indicates that SRT can significantly reduce the amount of injections required.

1.4 Cystatin C

Cystatin C was originally identified in urine samples by Butler & Flynn in 1961 and dubbed "gamma trace". It was identified and measured as a plasma and cerebrospinal fluid protein with a significant age-related variation in concentration (Löfberg *et al.* 1980). However its amino acid sequence was not described until 1982 when Grubb and Löfberg identified it as a 120 residue chain with a Mr of 13,260 Da and the protein was noted to be localised to the pituitary glands and proposed to be a neuroendocrine protein (Grubb & Löfberg, 1982). However it was also identified in a wide variety of tissues including the thyroid (Löfberg *et al.*, 1983), seminal plasma (Grubb *et al.*, 1983) and alveolar macrophages (Chapman *et al.*, 1990) to name but a few examples. The function of the protein as a cysteine protease inhibitor was finally identified in 1984 by Brzin *et al.* with its ability to inhibit papain and human cathepsins elucidated. In addition its homology with egg white cystatin was noted. The name cystatin C was finally proposed by Barrett *et al.* (1984). Following this the cDNA coding for the precursor protein was sequenced by Abrahamson *et al.* (1987a) and that the protein seemed to have an inhibitory effect via two binding sites (Abrahamson *et al.*, 1987b). The gene coding for the protein, designated CST3, was found to be located in chromosome 20 in 1989 (Abrahamson *et al.*; Saitoh *et al.*) and the structure of the gene completely described a year later (Abrahamson *et al.*, 1990).

As early as 1983 its potential involvement in disease was noted. Cohen *et al.* (1983) described the involvement of a protein “related to the gastroentero-pancreatic neuroendocrine protein, gamma trace” in hereditary cerebral haemorrhage with amyloidosis. This similar protein had been purified from amyloid fibrils in three Icelandic patients dying from the disease and identified in amyloid deposits by immunofluorescence microscopy. Their belief that the protein may not have been just related but actually the same protein was later confirmed by Ghiso *et al.* (1986) who noted the L68Q amino acid substitution near a proposed active site for the molecule. However at this stage it was unsure whether this was due to natural polymorphism in the protein or a point mutation in the coding sequence. By 1987 its involvement was clearly identified with Jensson *et al.* identifying it as a causative agent for the disease, forming amyloid fibril deposits in the walls of brain arteries. Today cystatin C’s involvement in what is termed Icelandic type hereditary cerebral haemorrhage with amyloidosis is well known; reviewed by Levy *et al.* in 2006. However this was just the start in identifying cystatin C’s involvement in aggregation-related diseases; the protein was also proposed as being involved in Alzheimer’s disease

(Coria *et al.*, 1987) and eventually identified as a factor in the development of AMD (discussed in section 1.3.5).

In addition it is well known as a marker for kidney function. As early as 1985 (Simonsen *et al.*) it was considered for this purpose and since then it has been demonstrated to be a good measure of glomerular filtration rate. The traditional method of calculating this is the use of creatinine which has the disadvantage of being highly heterogeneous across populations, varying by muscle mass, exercise and diet; cystatin C by contrast is significantly more uniform and therefore more reliable as a marker (Shlipak *et al.*, 2013).

1.4.1 Structure of cystatin C

The sequence of cystatin C was first established more than twenty years ago and can be seen in figure 1.4. The protein is manufactured by the cell as pro-cystatin C with a mature 120 amino acid cystatin C chain linked to a 26 amino acid targeting sequence at the N-terminus which is essential for targeting to the endoplasmic reticulum (Paraoan *et al.*, 2003).

In the normal course of processing this targeting sequence allows the protein to be processed through the secretory pathway and is cleaved to leave just the mature protein to be secreted from the cell. Consequently the protein only forms its final shape upon the severing of this extra length of amino acids.

In humans it is translated from the CST3 gene which is located on chromosome 20 (Abrahamson *et al.*, 1989; Saitoh *et al.*, 1989) and consists of a series of five β-strands with a large α-helix lying across the surface of the sheet and a short α-helix (Janowski *et al.* 2001) (figure 1.5).

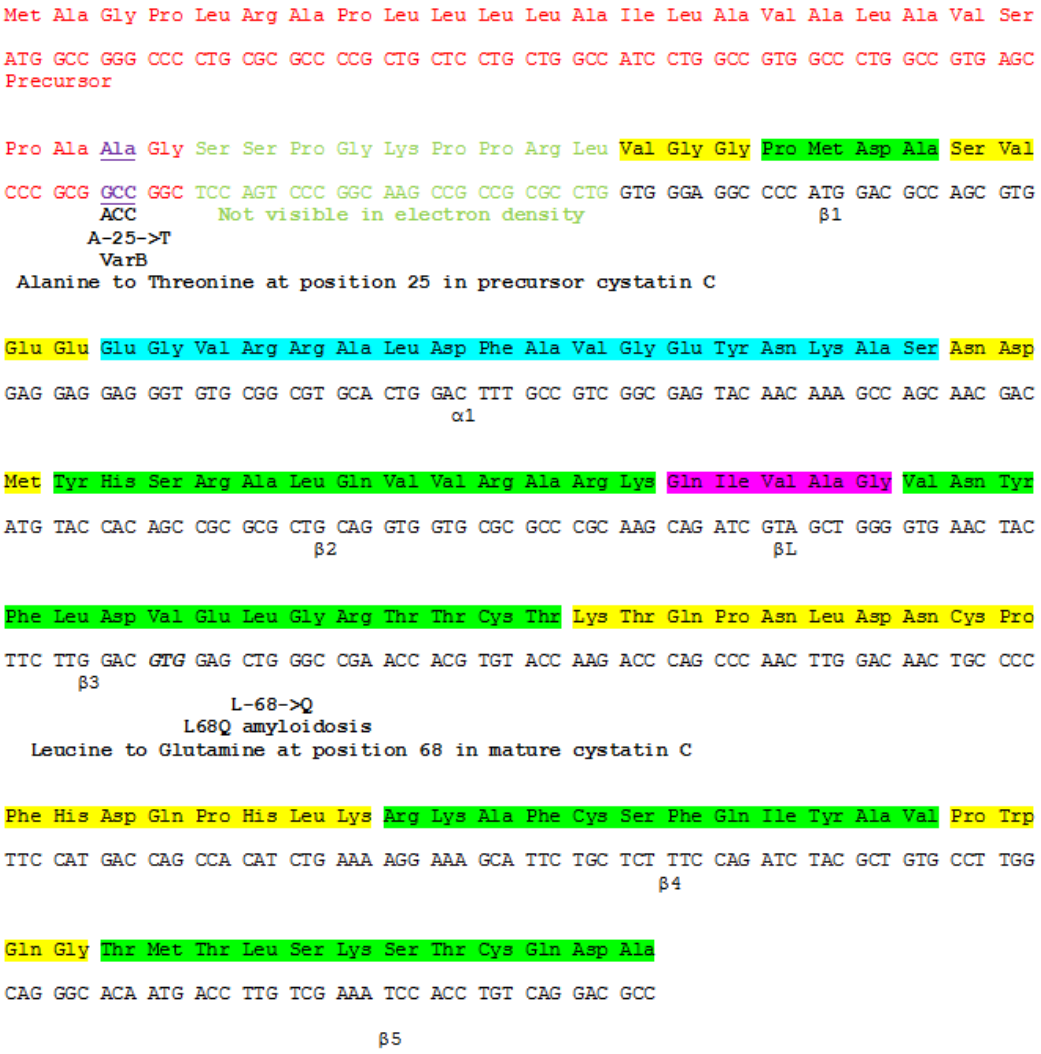

Figure 1.4 DNA sequence and primary protein structure of cystatin C. Red text is the precursor sequence which is cleaved during processing to produce the mature protein, highlighted yellow and pink are link regions, highlighted cyan is the alpha chain, highlighted green are the beta chains. The point mutation in the precursor leading to variant B form cystatin C is indicated. Sequence information from Abrahamson *et al.* (1986) and primary protein structure from Janowski *et al.* (2001).

Cystatin C has been demonstrated to be capable of dimerisation. More specifically it dimerises due to the process of three-dimensional domain swapping (Janowski *et al.*, 2001) in which a hinge region allows for partial unfolding of the protein and combining with similarly unfolded proteins (Jaskólski, 2001). It has been argued that domain swapping in itself is enough for the formation of oligomers (Liu *et al.*, 1998) however this process is known to be effected by other factors. In the case of the amyloid-associated L68Q mutant cystatin C (highlighted in Figure 1.4) the substitution results in a form of cystatin C that has a much greater tendency to dimerise and form aggregates in a manner that is temperature dependent (Abrahamson & Grubb, 1994). Further, it has been demonstrated that the tendency of this disease-causing form of the protein to form amyloid fibrils can be inhibited by preventing domain swapping (Nilsson *et al.*, 2004). In short this provides strong evidence that the structure of cystatin C is crucial to its capacity for aggregation and ability to cause aggregation-related disease.

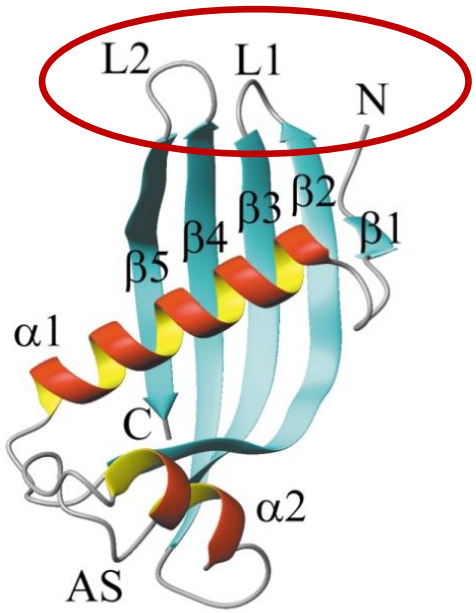

Figure 1.5 Secondary and tertiary structure of cystatin C protein (reproduced from Janowski *et al.* 2001). It consists of a series of antiparallel β-sheets (blue) twisted around the large α-helix (red/yellow). The active site of the mature protein is circled in red.

1.4.2 Mechanism of action and function of cystatin C

Cystatin C is an active cysteine protease inhibitor found extensively throughout the body. Abrahamson *et al.* (1990) found it to be expressed in every human tissue examined ranging from the kidney to the lung to the placenta. Further it is found in almost all bodily fluids with the highest level being seen in seminal plasma but high levels also in the cerebrospinal fluid and blood plasma (Abrhamson *et al.*, 1986).

As a member of the cystatin type 2 gene family, cystatin C is well established as an extracellular protease inhibitor. Consequently the protein is typically produced within the cell and then specifically passed to the secretory pathway (as directed by the signal targeting sequence) where it is processed, packaged and secreted to the extracellular environment. The essential role of the signal sequence in targeting cystatin C to the secretory pathway was demonstrated experimentally by Paraoan *et al.* (2003); loss of this signal sequence led to the protein no longer being targeted to the secretory pathway and instead presenting a uniform fluorescence throughout the cell, indicating it is diffused throughout the cytoplasm and nucleus. This clearly shows that the loss of the signal sequence results in the loss of protein targeting. The combination of its ubiquitous expression and its secretion means it is thus a very important regulator of extracellular protease activity.

Cystatin C is believed to have a variety of functions related to the regulation of levels of a number of different proteins in various bodily fluids and is implicated in several diseases and processes. Furthermore it has been used extensively as a marker for kidney dysfunction and there is a great deal of literature available about the use of it as a biomarker. Given its extracellular nature and abundance, cystatin C is likely to be significantly involved in homeostasis and balance of proteins in extracellular fluid and the modelling of extracellular membranes and structures.

In particular Cystatin C is a potent inhibitor of a number of lysosomal cathepsins (B, H, L and S) and papain (Turk & Bode, 1991; Barrett *et al.*, 1984). Especially cathepsins B, which cystatin C inhibits far more strongly than other cystatins (Barrett *et al.*, 1984); despite the similarities in sequence between the proteins.

Of further note is that cystatin C is a tight-binding but reversible inhibitory protein. It acts through the two hairpin loops and N terminus as seen in figure 1.5 and fits into the active

site of papain (for example) (Bode *et al.*, 1988). The binding mechanism is functionally similar to how small serine inhibitors work, specifically by binding at the protein active site thus blocking it from use. However it is worth noting that the mechanism itself is quite different to the mechanism typically observed for small serine inhibitors.

Specifically in small serine inhibitors the inhibitor binds to the active site of the enzyme in a manner much like that of a substrate, with the blocking effect being a direct blockage of the active site in a "lock and key" type way (Laskowski Jr. & Kato, 1980). For cystatin C, however, the binding sites are dissimilar to a bound substrate, yet it still binds to the active site (Bode *et al.*, 1988). Note that this original model was based upon chicken cystatin, however later experiments demonstrated that this model for binding was also applicable to human cystatin C (Lindahl *et al.*, 1992).

Therefore, to inhibit cysteine proteases cystatin C does not impersonate a substrate but does block the active site itself, preventing the binding of a substrate and therefore blocking the activity of the protease. Specifically the N-terminal region binds to the protein.

1.4.3 Cystatin C in the eye

Cystatin C is found in a wide variety of tissues and fluids in the body. However for the purpose of this work the most crucial site of expression is within the eye, where it is found in high abundance. Specifically cystatin C has been found to be expressed at extremely high levels in the retinal pigment epithelium (top 0.2% of expressed proteins) as well as in the ciliary epithelium (Paraoan *et al.*, 2000; Paraoan & Grierson, 2007).

Cystatin C was originally identified as being expressed in the eye in rats, with cystatin C mRNA being detected in total RNA extractions from the sclera and retina (Barka & van der Noen, 1994). In humans it was identified as being significantly expressed in the retina, as a result of analysis of expressed sequence tags in the RPE (Paraoan *et al.*, 2000). Cystatin C was identified as one of the most abundantly expressed transcripts within the RPE and consequently was noted as likely being of great importance to the normal functioning of the retina.

This was later confirmed by the finding that the protein was mainly localised to the RPE in rat, mouse and human eyes (Wassélius *et al.*, 2001) and it was suggested that the protein

might be involved in regulation of photoreceptor degradation. However cystatin C was found to co-localise with the Golgi apparatus and to be processed through the secretory pathway under normal conditions and passed out of the cell which was confirmed by the detection of cystatin C in cell culture media (Paraoan *et al.*, 2001).

Within the RPE cystatin C is secreted from the basolateral side of the layer (Paraoan *et al.*, 2001). With the amount of protein produced combined with its directional secretion it seems likely to have a crucial role in protein turnover in this region and consequently on the effectiveness of Bruch's membrane in its protective and supportive role

Despite the high level of expression in the retina cystatin C isn't totally segregated in the eye. It has also been found in a variety of tissues of the anterior eye also particularly in the ciliary epithelium (Wassélius *et al.*, 2004), as well as having been documented as being taken up by a variety of cell types, many of which have been shown to contain endogenous cystatin C suggesting its importance in those tissue types and consequently a potentially crucial role in the eye as a whole (Wassélius *et al.*, 2005).

1.4.4 Cystatin C in disease

Given its ubiquitous expression throughout the body it is to be expected that Cystatin C is implicated in different key physiological functions, which in turn may be involved in diseases ranging from cancer to neurodegeneration. Furthermore it has also been established as a kidney function biomarker (Filler *et al.*, 2005) with applications to cardiovascular disease (Angelidis *et al.*, 2013) due to its involvement in modulation of atherosclerotic plaque formation along with cathepsins (Bengtsson *et al.*, 2008). Cystatin C is known to be involved in such diverse diseases such as Alzheimer's, hereditary amyloidosis, Parkinson's disease, and atherosclerosis. Cystatin C has also been linked to a number of eye diseases including congenital X-linked retinoschisis (Joshi *et al.*, 2006; Drenser *et al.*, 2007) and retinitis pigmentosa (Ahuja *et al.*, 2008). Beyond these, however, cystatin C has been most associated with age-related macular degeneration itself; more specifically the association of variant form of the protein known as variant B with development of exudative AMD.

Alzheimer's disease is well established as an aggregation disease with the build up of amyloid β forming amyloid deposits in the brain being a characteristic factor. Of note is that cystatin C has been found to co-localise with amyloid β in these plaques. It was found that overexpression of cystatin C could lead to reduction of the deposition of amyloid β (Kaeser *et al.*, 2007) implying a protective role in Alzheimer's disease by binding soluble amyloid β (Mi *et al.*, 2007) Further, there have been links drawn between Alzheimer's disease and cystatin C polymorphisms; this has been extensively reviewed by Kaur & Levy (2012). Although there is evidence to show that certain polymorphisms believed to be involved in the pathology of the disease are not, and that the cystatin C deposition is a secondary event (Parfitt *et al.*, 1993).

In addition another major disease cystatin C is known to be involved in the pathology of cerebral amyloid angiopathy (Icelandic type). A variant of cystatin C was identified as being the major constituent of the fibrils produced in this disease (Ghiso *et al.*, 1986) and this was later identified to be a polymorphism resulting in a Leu68Gln variant being produced leading to the disease. Interestingly, wild type cystatin C is also sometimes found co-localised with amyloid beta in cerebral amyloid angiopathy and this increases the severity of the disease; furthermore evidence suggests that cystatin C itself could be involved in neuronal cell death by apoptosis (Nagai *et al.*, 2008).

1.4.5 Cystatin C variant B

In 2002 a study by Zurdel *et al.* discovered that a variant form of cystatin C led to a nearly threefold, statistically significant, increase in the risk of developing exudative AMD. This variant, known as variant B, is the result of a single point mutation within the signal sequence leading to an A-25->T amino acid substitution. This small change results in drastic changes to how RPE cells handle the produced molecule. A subsequent study by Paraoan *et al.* (2003) demonstrated that cystatin C lacking the leader sequence was not processed as normal through the secretory pathway of RPE cells, lending support to the hypothesis that the leader sequence is a contributing factor to increased risk of AMD.

Finally another study by Paraoan *et al.* (2004) demonstrated that the AMD-associated variant similarly suffered from a mistrafficking within the cell. Contrasting with the normal secretory pathway processing that wild-type cystatin C undergoes, a large amount of the

variant B form does not pass into the secretory pathway. Instead the modified signal sequence causes the molecule to be retained within the cell in large amounts, leading to a build-up of the protein. However rather than just concentrating within the cytoplasm or being efficiently degraded, the variant form has been found to associate with the mitochondria within the RPE cells.

Interestingly a different mutation at the same site artificially created by Ratnayaka *et al.* (2007) resulted in an intermediate effect on the protein. Rather than the Ala25Thr substitution of variant B this Ala25Ser mutation led to a distribution to both the Golgi apparatus and the mitochondria, with secretion being between variant B and wild type cystatin C. The implication being that an amino acid substitution with a less hydrophobic amino acid is sufficient change to result in the mistrafficking seen with the variant B. A study by Benussi *et al.* (2003) on the same cystatin C variant in skin fibroblasts identified reduced secretion as a result of less efficient cleavage of the signal peptide; with reduced cystatin C secretion into conditioned media from B/B homozygous fibroblasts and less efficient cleavage of a variant B signal peptide-GFP construct.

Given the large number of functions of the RPE and the heavy metabolic activity required for these processes it is likely that this build-up of cystatin C intracellularly would interfere with normal cellular functioning. A breakdown in cell function in an area of the RPE would lead to a harmful reduction in the capability of the RPE to maintain the extracellular environment and protect the photosensitive cells from damage. This is the primary effect observed thus far of the variant B change. Given the association with AMD we believe that the increased risk is caused by a combination of the reduced secretion of cystatin C and its build-up within the cell. This could potentially have a significant effect on the mitochondria given the association, however we do not know how the variant B cystatin C becomes associated in this way. However it has been noted that cystatin C expression increases with exposure to oxidative stress (Alizadeh *et al.*, 2006). Given that oxidative stress is a hallmark of AMD it is possible that the variant B protein interferes with the generation of ROS and consequently contributes via this mechanism.

In short, it is well established that variant B cystatin C is a factor in the development of exudative AMD. It is also well established that the variant is retained intracellularly to a great extent with a consequent reduction in the amount secreted. What is not know, however, is how either of these two events occur and what are their functional consequence. This is what we seek to make the first steps towards addressing.

1.5 Key intracellular processes investigated

1.5.1 Overview

The mislocalisation of the variant B form of cystatin C raises a number of questions over its effect on the mitochondria. Given the crucial importance of the mitochondria in normal cellular functioning it seems likely that this inappropriate association with a protein that is primarily extracellular could result in impairment of such functions.

For this study we selected a number of important intracellular processes which have been associated with the mitochondria or age-related macular degeneration or both. Our intention being to see if the inappropriate intracellular retention of the variant B protein results in disruption in a specific mechanism or mechanisms and consequently informing our knowledge of the process or processes by which the increased risk occurs.

1.5.2 Respiration

1.5.2A The respiratory process

The most important function of the mitochondria is the production of energy from glucose in the form of adenosine triphosphate (ATP) by the respiratory process. This involves a number of ATP producing steps however the majority of ATP is generated through a process of oxidative phosphorylation. A series of proton pumps at the inner mitochondrial membrane, powered by electrons generated by the Krebs cycle, generate an ionic gradient which is used to power ATP synthase, generating ATP (figure 1.6). Consequently this is the most crucial process to begin addressing as impairment of the generation of energy would lead to drastic effects on the cells.

Interfering with any part of this process could lead to significant impairment of normal cellular function in general for any type of cell. A recently published study by Zhang *et al.* (2014) on ATP production in Alzheimer's disease used a mouse model to demonstrate reduced levels of ATP in the brain of affected mice compared with normal control mice; with the effect being more pronounced with the increased age of the mice (and hence the maturity of Alzheimer's disease pathology).

1.5.2B Respiration in the RPE

Given the wide variety of processes in the RPE which are a requirement of its ability to maintain and support the retina and to ensure the stability of the surrounding environment it is possible that disruption of energy generation could lead to the loss of homeostatic balance and damage to the retina. In addition due to AMD being an age-related disease this question is highly relevant. Impairment of mitochondrial respiration with age has been established in other tissues and is believed to be due to interference with the electron transfer chain (Navarro & Boveris, 2010). The combination of the ageing degeneration of capacity for ATP production (Chistiakov *et al.*, 2014) coupled with interference from variant B cystatin C has the potential to result in severe detrimental effects on the RPE and early onset of disease. In particular it has been noted that reduction in ATP levels in human RPE cells can lead to increased oxidative stress and reduced phagocytic and autophagic capacity (Schütt *et al.*, 2012).

A specific example of the importance of ATP in the RPE in particular is highlighted by Bergmann *et al.* (2004). Proton pumps in the lysosomal membrane are crucial in the process of maintaining RPE functions such as degradation of photoreceptor outer segments. These pumps are ATP-driven and it was shown that A2-E was able to inhibit them, with subsequently observed increased intracellular accumulation of photoreceptor outer segments. Given the ATP-driven nature of these pumps it is logical to conclude that a reduction in the availability of ATP could result in a similar decrease in phagocytic activity in the lysosomes.

Although there is at this time no specific prior evidence relating variant B, respiration and AMD it seems undeniable that interference with the respiratory cycle would be severely disruptive to the RPE cells. Given the mitochondrial localisation of variant B it is a critical process to address in this study.

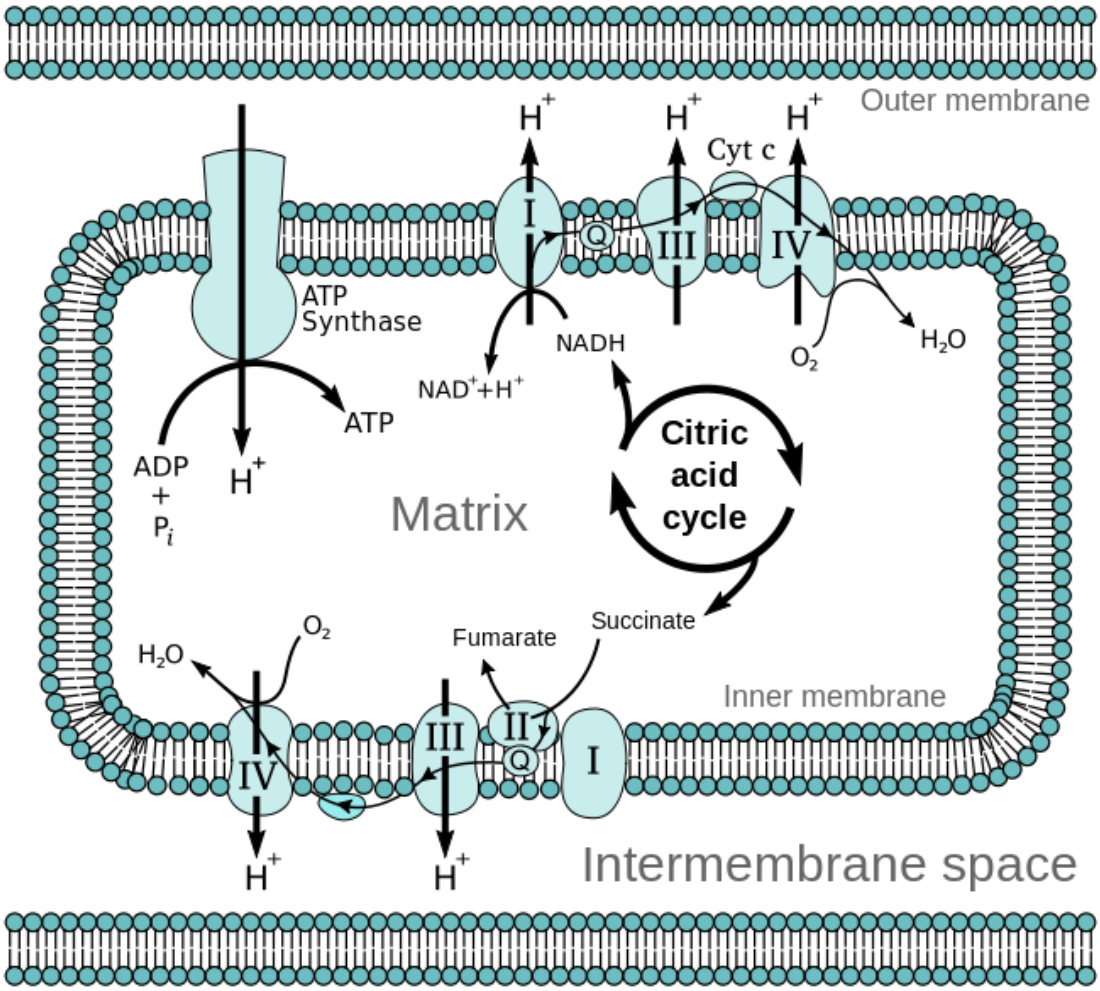

Figure 1.6 Schematic diagram of the mitochondrial electron transport chain. The majority of ATP generated in the mitochondria is via the electron transport chain. Electrons sourced from the citric acid cycle (or Kreb's cycle) are passed along the chain, causing H^+ ions to be pumped out of the matrix and setting up an electrochemical gradient across the inner mitochondrial membrane. This gradient thus causes the diffusal of H^+ ions back into the matrix through ATP synthase, which powers the generation of ATP via oxidative phosphorylation of ADP (public domain image, Wikimedia commons).

1.5.3 Apoptosis

Given that age-related macular degeneration is a degenerative disease there is interest in the process of apoptosis and its potential association with the development of the disease. A recent study on apoptosis by Bhattacharya *et al.* (2012) identified that p53-dependent apoptosis increased in an age dependent manner in human RPE cells via the caspase 3 pathway (figure 1.7 illustrates the caspase pathways of apoptosis). The study concluded that alterations to apoptotic checkpoints in the RPE led to the increase basal rate of apoptosis.

Of particular interest is that JNK inhibition in a mouse model of wet AMD has been shown to reduce apoptosis and neovascularisation (Du *et al.*, 2013). Further, a pan-caspase inhibitor in the same mouse model also results in reduced choroidal neovascularisation, implicating apoptosis in this process. JNK is well establshed as having a role in apoptosis, specifically via Bcl2 and Bax ultimately leading to the caspase cascade (Dhanasekaran & Reddy, 2008).

Further, cystatin C has become well established as being involved in the process of apoptosis in neuronal cells. It has been implicated in apoptosis activation via a JNK-dependent pathway via increased levels of active Bax protein (Liang *et al.*, 2011) and more recently as a trigger in multiple system atrophy (Suzuki *et al.*, 2014). This supports the suggestion that cystatin C variant B may result in inappropriate effects on the apoptotic pathways within the cell.

Preliminary work in our lab suggests activation of the apoptotic pathway in RPE cells expressing variant B protein (unpublished data). However it is worth noting that despite apoptosis being cited frequently as being involved in AMD, some molecular studies suggest that other cell death and degenerative pathways may be more significant (Ardeljan *et al.*, 2014). Given that caspase 3 has long been identified as being a key part in the normal caspase cascade leading to apoptosis (Slee *et al.*, 1999), coupled with the preliminary work suggesting its activation, it is crucial to properly examine this part of the apoptotic pathway.

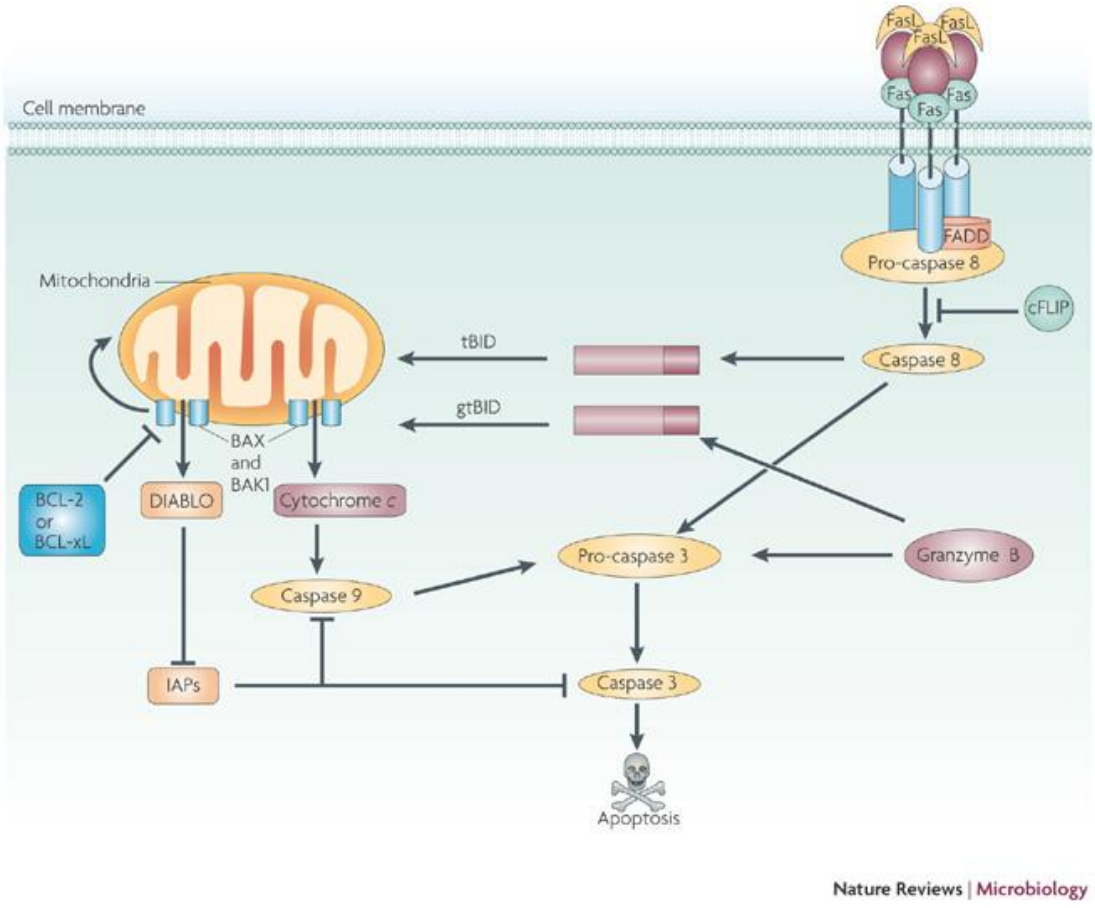

Figure 1.7 The caspase dependent apoptotic pathway. There are two primary routes of caspase-dependant apoptosis. One is by the extrinsic pathway in which FasL binds at the cell membrane, leading to a chain of reactions via caspase 8 which concludes with caspase 3 activation and the triggering of apoptosis. The intrinsic pathway involves the triggering of the release of cytochrome C from the mitochondria which also leads to the activation of caspase 3 and triggering of apoptosis. Caspase 3 therefore represents a point at which apoptosis as a whole via these processes can be monitored. (Clarke & Tyler, 2009)

1.5.4 Autophagy

Autophagy is a crucial process in all cells and is required for the turnover of proteins and organelles (including mitochondria). Without this recycling process defective proteins and misfunctioning organelles could build up within a cell, severely hampering its ability to carry out its normal functions. Not only would this result in the loss and lack of replacement of those which are damaged, but it can result in the processes being actively interfered with due to loss of control and misregulation.

This is of particular importance to the RPE cells; their function as a support tissue necessitates them to carefully modulate their environment and maintain themselves intracellularly. They have a number of roles (discussed in chapter 1.2.2) which require them to process waste products from the photoreceptors. Autophagy has long been cited as a possible key process in the development of AMD (Kaarniranta *et al.*, 2013), with the accumulation of lipofuscin being cited as particularly relevant (Blasiak *et al.*, 2014). Autophagy has been clearly implicated in the development of drusen, with Atg5 (an autophagic maker) being present in drusen of aged eyes (Wang *et al.*, 2009). In short, preservation of autophagy results in healthier cells and a slower cellular ageing process; whereas dysfunction results in poorer cell function and damage to RPE cells (Kaarnirnanta, 2010).

A recent study has firmly established a link between autophagy and oxidative stress; with the impairment of autophagy likely to exacerbate oxidative stress, thus contributing to development of AMD (Mitter *et al.*, 2014). It was noted that autophagy appeared to be impaired in both animal model eyes and in human donor AMD eyes in comparison with control eye specimens, which presented an age-related increase in autophagy.

This recent development is of great interest to the field of AMD research. However it stands in contrast to the way in which cystatin C acts in the brain. Cystatin C has been identified as an inducer of autophagy in the brain which acts as a protective mechanism against neurodegeneration (Gauthier *et al.*, 2011; Liu *et al.*, 2013). This implies that the inappropriate processing of cystatin C resulting from the variant B phenotype (and thus deficiency of mature cystatin C) may well be a causative factor in AMD development.

1.5.5 Oxidative Stress

1.5.5A Oxidative stress and ageing

Oxidative stress is a well established feature of both ageing and age-related diseases. It has long been established as a method by which cells are damaged and has been extensively linked to the mitochondria. It was believed to be central to the gradual degradation of cells over time. Additionally the oxygen supply in the choroid is not autoregulated by the oxygen levels of the tissue (Shen *et al.*, 2003).

Indeed, until recently one of the foremost theories on the process of ageing was based heavily on the principle of oxidative damage resulting from mitochondrial by-products. This was termed the mitochondrial free radical theory of ageing and was extremely popular as a fundamental explanation of why ageing occurs. It has its roots in a paper published by Harman in 1956 which postulated that ageing was the result of accumulated oxidative damage to cells. This theory was refined and added to following the identification of the mitochondria as both a source and target for oxidative stress and the later identification of the mitochondrial genome, in particular, being of key importance due to the lack of repair mechanisms in mitochondria (Fleming et al, 1982; Miquel & Fleming, 1984; Miquel, 1991). The theory states that the accumulation over time of DNA damage within mitochondria results in the production of more ROS and a decrease in mitochondrial capability and resistance to damage leading to further increases in ROS production and cellular damage and loss of respiratory functioning. In short, a vicious cycle of loss of energy production leading to increased ROS production as a result of mitochondrial DNA damage leading to further loss of energy production (Miquel, 1991).

More recent developments, however, have thrown doubt on this theory. Despite the substantial amount of evidence in support of it, questions were raised around the fact that the evidence was largely circumstantial (Jacobs, 2003) and that the discussion around the hypothesis had become influenced by personal opinions. To quote Jacobs (2003):

"...opponents of the hypothesis tend to define it in such a narrow and extreme way that it is almost self-evidently falsified by generally accepted facts. Conversely, its proponents are liable to state the theory in such a vague and general way that it is virtually unfalsifiable experimentally."

Jacob's 2003 paper reviewing the literature behind the theory to that point and calling into question the design of experiments attempting to prove or disprove the theory was in itself controversial; with a rebuttal posted shortly afterwards (Pak *et al.*, 2003). However it is an issue which remains highly topical, being extensively reviewed to this day and inadequately proven neither correct nor incorrect (Sanz & Stefanatos, 2008; Barja, 2013; Edrey & Salmon, 2014; Shokolenko *et al.*, 2014). To summarise the literature indicates that although the mitochondrial free radical theory of ageing may require revisions, and despite the fact that it seems unlikely that mitochondrial DNA damage is the central cause for ageing, the mitochondria and oxidative stress are still a central featuring of the ageing process and are of significant interest.

Further, oxidative stress is implicated as a factor in a number of age-related diseases such as diabetes (Maritim *et al.*, 2003), cancer and neurodegenerative diseases (Thanan *et al.*, 2014). Conversely it is also known that a lower level of oxidative stress than that which causes damage is beneficial for both ageing and resistance to age-related diseases (Yan, 2014). With a number of processes being regulated by moderate levels of ROS including ageing itself (Sena & Chandel, 2012). The explanation for this appears to be that the specific level of oxidative stress is critical; a very low basal level maintains homeostasis within the cell whilst a moderate level results in adaptation to the stress, however severe oxidative stress leads to cellular damage and death (Yan, 2014).

1.5.5B Oxidative stress in the eye and AMD

Oxidative stress is a major issue in the eye. The significant amount of ROS naturally generated by the mitochondria within the cells is coupled with a high level of additional stress caused by photo-oxidation given the exposure of the eye to light. This is further exacerbated by the high metabolic activity levels in the photoreceptor cells, with a consequent high level of oxygen consumption (Shen *et al.*, 2005) resulting in an inherently highly oxidised environment.

For the RPE this can be very damaging. Damage to the RPE and its mitochondria as a result of oxidative stress has been documented (Cano *et al.*, 2014) and the ageing process has been demonstrated to lead to degradation of mitochondria and weaker antioxidant defences even as early as 62 (He & Tombran-Tink, 2010). Oxidative stress has been

associated with a variety of eye pathologies including cataracts (Spector, 1995), glaucoma (Zanon-Moreno *et al.*, 2008) and AMD.

AMD in particular has been well known for its association with oxidative stress for many years. Fifteen years ago an extensive study of the literature by Beatty (2000) stated:

"There is no shortage of research into the relationship between oxidative stress and AMD, but firm evidence of a causal link is still lacking."

Since then, additional research has been carried out but with many different factors contributing to AMD risk it has proven to be a very complicated disease. It was only recently that a study specifically identified that tissue specific induction of oxidative stress in the mouse RPE led to retinal degeneration, in a similar manner to that in dry AMD (Mao *et al.*, 2014). This is further evidence that a contributing causative effect of AMD is oxidative stress, but is evidence against it being the central cause due to lack of other features of the disease such as drusen.

However it is noteworthy that the association of age-related structural changes to the RPE with oxidative stress and decline in function has been established for a number of years (Bonilha, 2008). With oxidative stress also being implicated in other processes, such as apoptosis, with an association with AMD it is an extremely attractive possibility for the mechanism of action by which variant B cystatin C could work; despite some reservations in recent work as to its involvement as the possible primary causative factor for AMD.

1.6 Project aims and objectives

We hypothesise that the inappropriate localisation and intracellular retention of cystatin C leads to detrimental effects in the retina and on the RPE cells in particular. Thus contributing to development of AMD.

This project aims to further the understanding of the effects of variant B cystatin C on retinal pigment epithelial cells and the mechanisms by which this occurs. This, in turn, will further our understanding of the possible ways in which homozygous variant B cystatin C results in an increased risk of exudative age-related macular degeneration.

We examined a selection of intracellular processes of RPE cells as follows:

- Assessed the effect of variant B cystatin C on respiration rate and total ATP content in the cell. This allows for any impact on energy production or turnover of the ATP produced to be identified.
- Examined autophagy and apoptosis markers upon overexpression of variant B cystatin C, these are both crucial degradation processes which involve the mitochondria and are implied in AMD disease progression.
- Tested variant B cystatin C's influence on oxidative stress in cells through levels of reactive oxygen species. Given the extensive involvement of oxidative stress with the retina and its implied involvement in AMD and the crucial role that mitochondria have with respect to the production of reactive oxygen species this was a major goal.

In addition we sought to identify possible binding partners of cystatin C intracellularly using mass spectrometry. This was done in order to provide insight into possible interacting proteins or chaperones. Proteins identified by this study may help explain how and why the variant B protein becomes mitochondrially mislocalised and therefore represent an excellent starting point for further studies on this process.

Chapter 2

Materials and Methods

2.1 Mammalian cell culture

2.1.1 Mammalian cell lines cultured

All experiments were carried out using human-derived immortalised cell lines. RPE cell lines are well established and are highly suitable as models of the *in vivo* tissue when properly maintained. Cultures chosen are detailed below, figure 2.1 contains representative images.

ARPE19 – A well established human retinal epithelial cell line developed and characterised by Dunn *et al.* (1996). Origin: Some departmental stocks, some ATCC, Virginia, United States. Primarily used for preliminary work.

D407 – A human retinal epithelial cell line described by Davis *et al.* (1995). Origin: Gifted by Dr. T. Michael Redmond. These were preferred in later experiments over ARPE19 due to good morphological similarity to RPE cells *in vivo*, faster growth and higher transfection rates.

HeLa – well established human tumour cell line. Origin: Departmental stocks. Used rarely as a control cell line for some experiments.

Limitations of cultures used

The D407 cell line chosen as the primary cell line for experimental work and was utilised extensively. However D407 cells have several limitations noted by Davis *et al.* (1995). Particularly notable is the loss of pigment however this is a common occurrence for RPE cells unless they are foetal in origin. Their apical microvilli are also shorter than those of RPE cells *in vivo*. Further, they express S100 protein which has been associated with transformed cells (as this is a spontaneously transformed cell line).

ARPE19 cells were used for some of the preliminary work, they have been characterised recently as representing a "pathologic or aged RPE" (Ablonczy *et al.*, 2011). For the purpose of attempting to identify the induction of age-related effects through variant B cystatin C overexpression it was judged more appropriate to use D407s for the majority of work in this study.

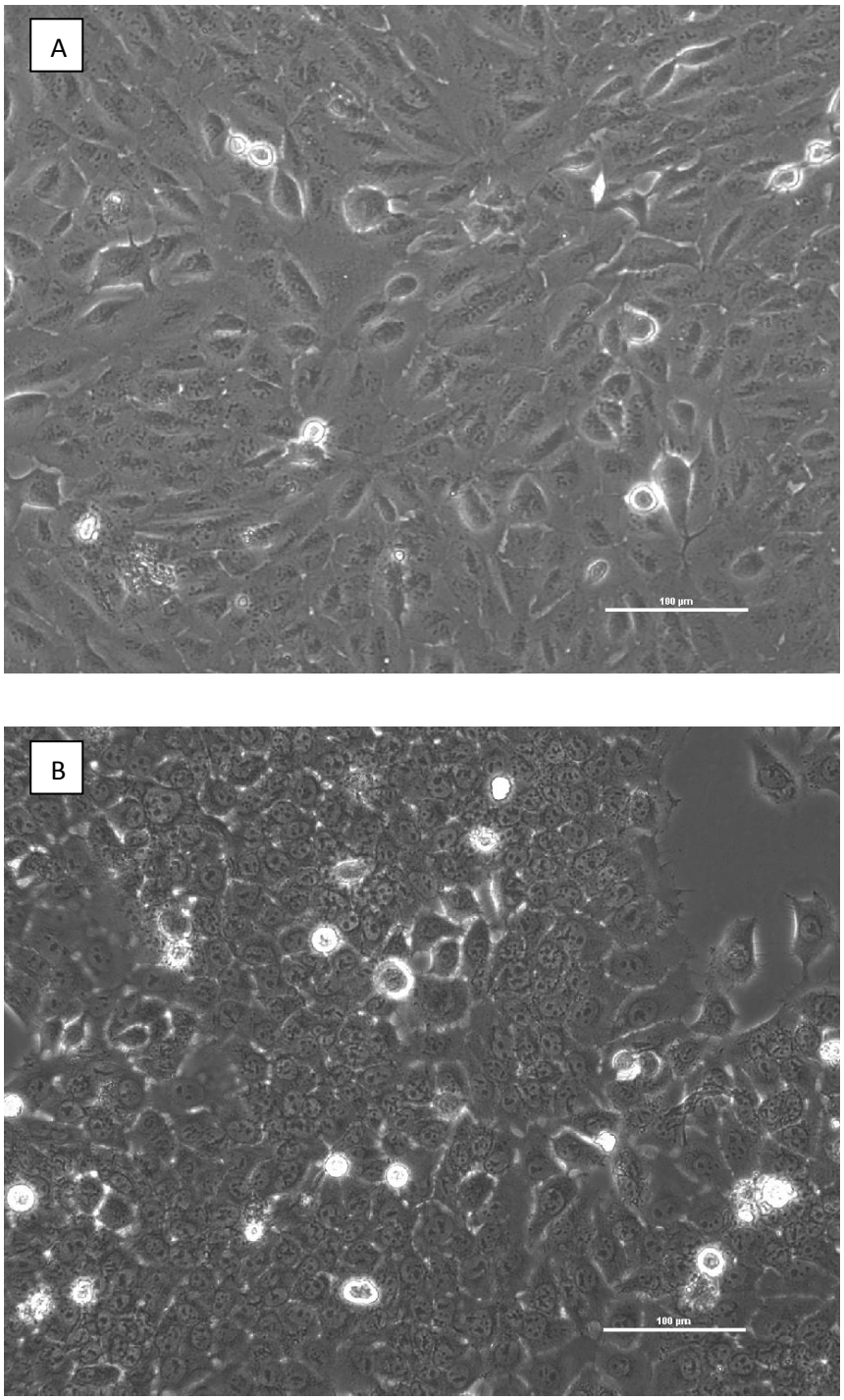

Figure 2.1 Bright field images of ARPE-19 cells (A) and D407 cells (B). ARPE 19 cells typically presented with an elongated morphology until they grew to a high density, at which point they would start to form clusters of cobblestone-like areas. In contrast D407s readily and rapidly formed a cobblestone, RPE-like layer; however unlike the ARPE19 cells they would begin to grow in layers on top of one another after forming a monolayer. Scale bars are 100 µm.

2.1.2 Maintenance of cultures

ARPE19 and D407 cells were grown in Dulbecco's Modified Eagle's Medium/Nutrient Mixture F-12 Ham supplemented with L-glutamine, 15 mM HEPES, and sodium bicarbonate (Sigma-Aldrich Company Ltd., Dorset, England) and was supplemented in our laboratory with 10% Foetal Calf Serum (Sigma-Aldrich Company Ltd., Dorset, England) to facilitate rapid cell growth.

HeLa cells were grown in Dulbecco's Modified Eagle's Medium (Sigma-Aldrich Company Ltd., Dorset, England) supplemented with 1% L-glutamine (Sigma-Aldrich Company Ltd., Dorset, England) and 10% Foetal Calf Serum (Sigma-Aldrich Company Ltd., Dorset, England).

All cell cultures were grown at 37^{o}C, 5% CO_2 and were split using the following procedure (numbers for commonly-used T75 flask, scaled depending on culture vessel). Cells were washed 1-3 times with 10 mL phosphate buffered saline (PBS) (Thermo Fisher Scientific Inc., Waltham, United States). 2.5 mL Trypsin-EDTA (Sigma-Aldrich Company Ltd., Dorset, England) was added to the cells and the flask returned to the incubator until all cells were detached. To neutralise the trypsin ~9 mL warmed complete media was added and the cell suspension transferred to a 30 mL tube. This was centrifuged at 200 g for 3-5 minutes and the supernatant removed, leaving just the cell pellet. The cell pellet was then resuspended in 10 mL media. Cells were seeded into flask with pre-warmed media added until total volume in flask was 10 mL and gently shaken to ensure cells were distributed across the surface before returning to incubator.

Cell counts, where appropriate, were carried out on a haemocytometer using a microscope. Typically this was either for the purpose of loading equal amounts of cells in an experiment or for appropriate levels of seeding into plates or flasks.

Given the extensive use of D407 cells the experimental seeding rate was crucial. Throughout this work the rate typically ~350,000 cells per well for a 6 well plate, ~2.5 million cells for a T75, this resulted in the vessels becoming confluent or close to confluent in ~3 days, with a large number of cells even after 2 days. To reduce the rate of splitting for general maintenance of cultures non-experimental T75s were routinely seeded at ~1 million cells or less which reduced the confluence to around every 5 days. Given that a T75 flask typically yielded between 15 and 20 million cells this would seem to agree with a published D407 doubling time of ~24 hours (Papadaki *et al.*, 2010). ARPE19 cells meanwhile

were typically seeded for normal growth at around 1.5 million cells per T75 flask and typically resulted in around 5-6 million cells per flask by day 5 of growth. This also seems to agree with a recently published ARPE-19 doubling time of 55-65 hours (Iloki Assanga *et al.*, 2013). HeLa cells were typically seeded at ~1 million cells per T75 and, similarly to D407s, appeared to have a doubling time of around 24 hours.

2.1.3 Freezing and thawing cells

Cells were stored as frozen aliquots in liquid nitrogen to ensure their viability. Freezing cells was achieved as follows, the volumes are for a T75 flask and scaled for smaller or bigger culture vessels. Cells were washed 1-3 times with 10 mL phosphate buffered saline (PBS), following this 2.5 mL Trypsin-EDTA was added and cells were returned to the incubator until they were detached. Trypsin was neutralised with the addition of ~9 mL warmed complete media and cell suspension was transferred to a 30 mL tube. The cells were pelleted in a centrifuge at 1000 rpm for 3-5 minutes. The supernatant was removed and discarded and the cell pellet resuspended in 900 µL cold media with 20% FCS. The cell suspension was then transferred to a cryovial, 100 µL dimethyl sulfoxide (DMSO) (Sigma-Aldrich Company Ltd., Dorset, England) was added and the tube sealed. Tubes were frozen at a rate of -1^{o}C/minute in a -80^{o}C freezer overnight. The frozen cryovials were transferred to liquid nitrogen storage.

To thaw the cells, the cryogenic vial was removed from the liquid nitrogen, the cap loosened and the vial placed into a 37^{o}C water bath to thaw. The cells were transferred to fresh flasks containing prewarmed media before overnight incubation at 37^{o}C, 5% CO_2. Following this the flasks were checked by light microscopy to ensure cells had settled and attached and the media was replaced in full with fresh, warmed media.

2.1.4 Transfection

Transfection was carried out using two types of transfection reagent. FuGENE 6 (Roche Applied Science, Indianapolis, United States) was used initially but resulted in relatively lower transfection efficiencies. TurboFect (Thermo Fisher Scientific Inc., Waltham, United States) was used later and resulted in a higher transfection efficiency.

Transfection methods were as follows (volumes for a 6 well plate, scaled appropriately for different sized culture vessels based on manufacturer's guidelines):

FuGENE 6

Cells were seeded at ~ 100,000 cells per well then stored in the incubator until the transfection complex was ready to be added. This consisted of 3 µL of FuGENE 6 reagent added to 100 µL serum-free medium and mixed. This FuGENE/Media mixture was then incubated at room temperature for ~5 minutes. Following this incubation 1 µg plasmid DNA was added with the tube again flicked several times to mix and incubated for at least ~15 minutes at room temperature. Finally the complex was added to the wells and the plate gently swirled to ensure distribution throughout the media. The plate was then returned to the incubator until cells were to be used. One advantage of FuGENE 6 was that the transfection complex could be left on as it was not toxic to the cells.

TurboFect

Cells were seeded at ~350 ,000 cells per well the day before transfection with incubation at 37^{o}C, 5% CO_2 overnight (~16-20 hours) in 4 mL medium. This allowed for the cells to settle, adhere to the surface of the culture vessel and begin to grow.

For the transfection complex, 2-6 µg DNA (optimised per batch of DNA) was added to 400 µL serum-free medium and 6 µL TurboFect to the DNA/media mixture. The tube was flicked several times to mix and then incubated for 20 minutes at room temperature. The mixture was then added to the cells and the plate returned to the incubator overnight. Unlike FuGENE the complex had to be removed if cells were to be kept more than 24 hours as the reagent was shown to kill the cells if incubated for longer.

2.2 Plasmids

2.2.1 Plasmid constructs used

2.2.1A EGFP-based

The plasmid pEGFP-N3 (Clontech) was the backbone vector for EGFP-cystatin C constructs for both wild type cystatin C and the variant B form (figure 2.2). These were previously developed and described in Paraoan *et al.* (2001) and were used extensively throughout this work for overexpressing the two forms of the protein within cells.

The primary advantage of these constructs is the ease by which they can be imaged. Given that the EGFP tag is attached to the protein, it is visible with a fluorescent microscope (excitation maximum 488 nm, emission maximum 507 nm) thus allowing for the localisation within the cell to be easily visualised.

2.2.1B HaloTag-based

Cystatin C-HaloTag plasmids were produced for both wild type cystatin C and variant B cystatin C for the purpose of mass spectrometry experiments; the backbone plasmid for these constructs is presented in figure 2.3. HaloTag is a relatively new technology which relies upon a proprietary protein tag. This tag is not fluorescent itself but is flexible and specific, with the ability to covalently link to a corresponding ligand. As the reactive linker is identical for all HaloTag this allows it to be used for a variety of purposes. For this study the most relevant aspects are the capability for it to be fluorescently imaged intracellularly by the addition of a ligand attached to a fluorescent marker and the ability for it to be pulled down from cell lyates in a highly specific way by the addition of the ligand attached to agarose beads.

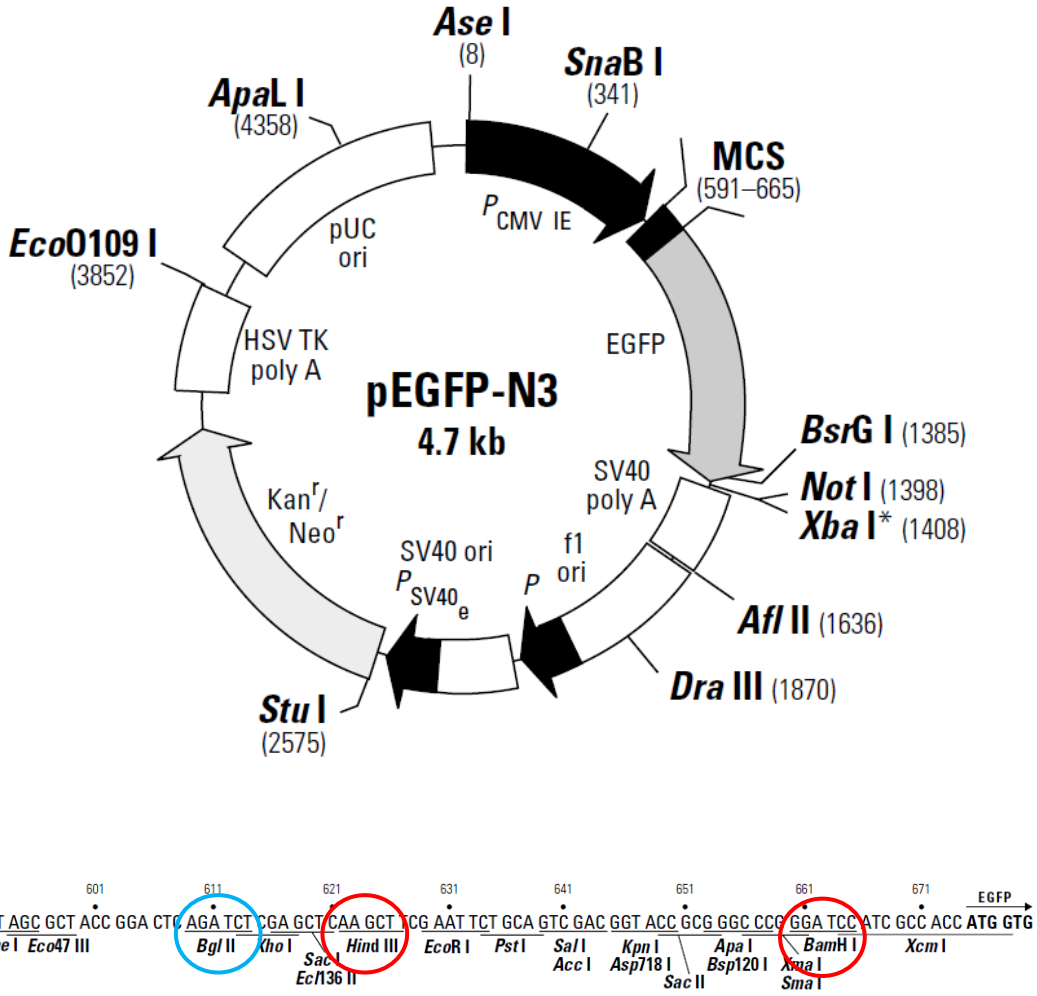

Figure 2.2 Plasmid map for pEGFP-N3 plasmid used for EGFP constructs. Cut sites for insertion are highlighted in red. Confirmation cut site within the plasmid (with corresponding cut in the cystatin C gene) highlighted in blue. (From BD Biosciences Clontech pEGFP-N3 protocol sheet PT3054-5)

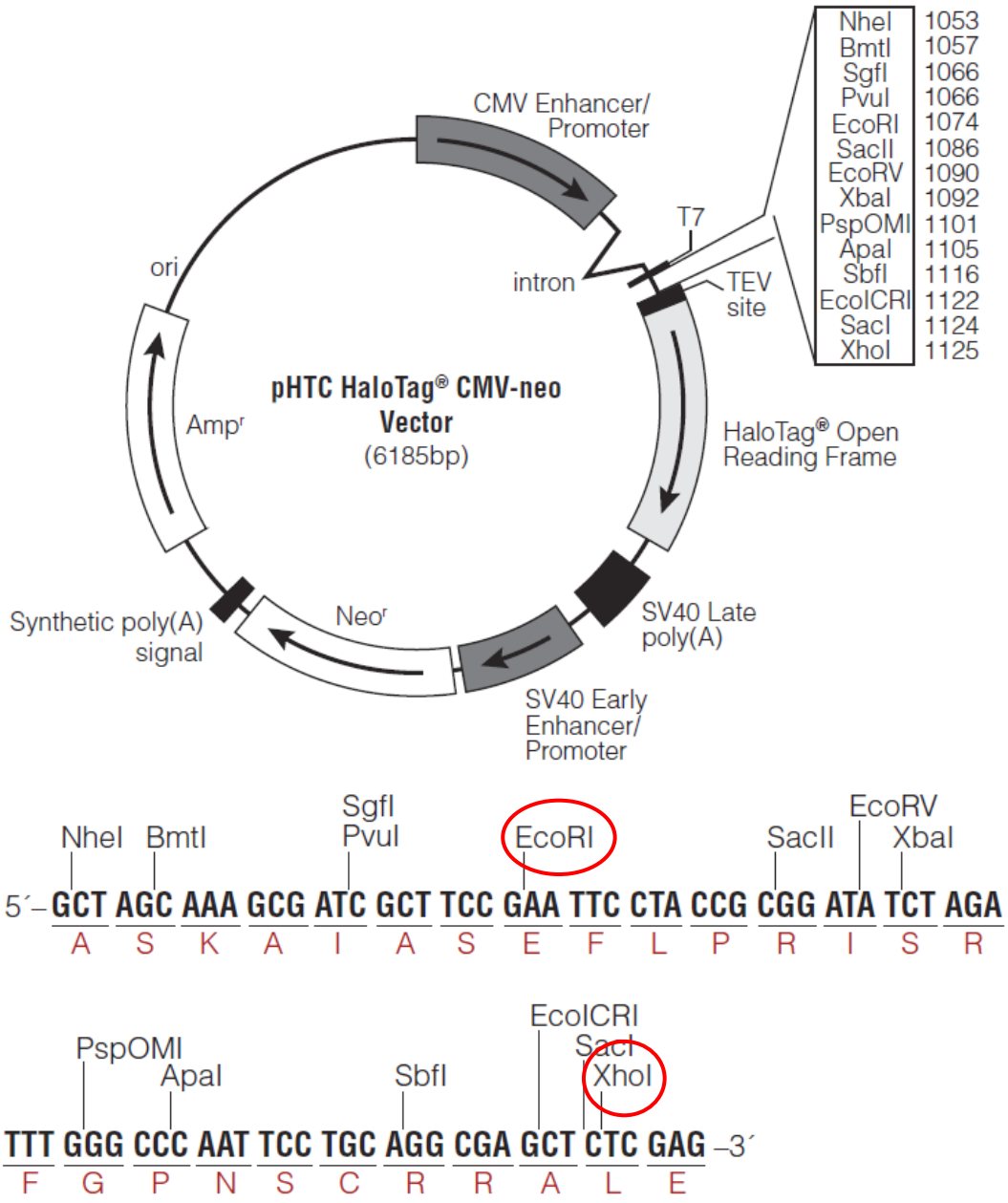

Figure 2.3 Plasmid map for pHTC Halotag plasmid used for Halotag constructs. Cut sites for insertion of cystatin C are highlighted in red. (From Promega pHTC HaloTag® CMV-neo Vector Product Information sheet, 9PIG771)

2.2.2 Bacterial transformation for routine amplification

50 µL of Competent Library-Efficiency DH5α *E. coli* and 15-30 ng of plasmid DNA were transferred to a chilled 1.5 mL tube on ice and mixed. Following 30 minutes of incubation the cells were heat shocked for 1.5 minutes at 42^{o}C. The cells were returned to the ice for 2 minutes before 350 µL SOC medium (Life Technologies, Thermo Fisher Scientific Inc., Waltham, United States) was added.

The bacteria were incubated at 37^{o}C for 1.5 hours on an orbital shaker at ~200 rpm before plating onto LB agar plates containing 50 µg/mL kanamycin sulfate (Sigma-Aldrich Company Ltd., Dorset, England) for EGFP constructs or 100 µg/mL ampicillin (Sigma-Aldrich Company Ltd., Dorset, England) for HaloTag constructs. Bacteria were plated at either 200 µL of culture per plate or 100 µL on one plate and 300 µL on the other to ensure that individual colonies could be picked. Plates were then incubated overnight at 37^{o}C before storage at 4^{o}C.

2.2.3 Plasmid preparation from transformed bacteria

Plasmid preparations were carried out using QIAGEN kits; the QIAGEN Miniprep Spin kit and the QIAGEN Endofree Maxi-prep kit (QIAGEN, Limburg, Netherlands).

Specifically Miniprep kits were used to extract and confirm the presence of plasmid in the bacterial cells and to transfer plasmid from one bacterial strain to another. For this purpose 10 mL of Luria broth containing appropriate antibiotics was inoculated with a single colony of bacteria and incubated overnight with shaking at ~180 rpm at 37^{o}C. DNA was then extracted following the manufacturer's instructions.

Endofree kits were used to produce endotoxin free DNA stocks suitable for our experiments in mammalian cells. These kits incorporate an extra endotoxin removal step to ensure that the DNA is suitable for tissue culture applications. A single colony of bacteria was inoculated into 10 mL of Luria broth containing appropriate antibiotics and the culture was incubated for 6-8 hours at 37^{o}C with orbital shaking at ~300 rpm. From this initial starter culture 200 µL was inoculated into 100 mL of Luria broth and then incubated overnight at 37^{o}C with orbital shaking at ~180 rpm. DNA was then extracted following the manufacturer's instructions. Quantification was carried out by use of either a Nanodrop

(Thermo Fisher Scientific Inc., Waltham, United States) or Qubit with dsDNA kit (Life Technologies, Thermo Fisher Scientific Inc., Waltham, United States).

2.2.4 DNA Restriction digestions and agarose gel electrophoresis

Plasmids were routinely checked by restriction digest followed by agarose gel electrophoresis. The restriction enzymes used are detailed in Table 2.1, all were supplied by Roche Diagnostics Limited, West Sussex, UK.

Table 2.1 Restriction enzymes used for restriction digest of plasmids.

Enzyme	Site cut	Description
HindIII	5'-A|AGCTT-3' 3'-TTCGA|A-5'	Site within EGFP plasmid for insertion of cystatin C. Used for verification.
BamHI	5'-G|GATCC-3' 3'-CCTAG|G-3'	Site within EGFP plasmid for insertion of cystatin C. Used for verification.
BglII	5'-A|GATCT-3' 3'-TCTAG|A-5'	Site for this enzyme found both within EGFP plasmid and within Cystatin C gene. Used for verification of insert.
EcoRI	5'-G|AATTC-3' 3'-CTTAA|G-5'	Site within Halotag plasmid for insertion of Cystatin C. Used for cloning and verification.
XhoI	5'-C|TCGAG-3' 3'-GAGCT|C-5'	Site within Halotag plasmid for insertion of Cystatin C. Used for cloning and verification.

Digests were carried out by mixing 1 µL DNA plasmid, 0.5 µL of the relevant enzyme or enzymes, 1 µL of the buffer appropriate to each enzymes and making the volume up to a total of 10 µL. This was then incubated at 37^{o}C for 1 hour before a brief heat period at 65^{o}C for 10 minutes to inactivate certain enzymes and then held at 4^{o}C before analysis.

DNA was analysed on a 1% Agarose gel made up in TBE buffer (Appendix 2). The agarose gel was prepared by adding 0.5x TBE buffer to molecular grade agarose (Sigma-Aldrich Company Ltd., Dorset, England). This was then heated until the agarose had fully dissolved and the solution allowed to cool to 55-60^{o}C before the addition of SafeView Nucleic Acid Stain (NBS Biologicals Ltd., Cambridgeshire, United Kingdom) in a dilution of 1:10,000 before pouring the gel.

DNA samples were prepared for analysis by adding a 1:6 dilution of DNA glycerol loading buffer (Appendix 2). DNA marker routinely use was Hyperladder I (Bioline, Massachusetts, United States). Gels were run at 100-150 V in 0.5x TBE buffer. Visualisation was carried out on a Bio-Rad Laboratories Chemidoc using the same settings as used for ethidium bromide visualisation.

2.2.5 DNA sequencing

Plasmids were also routinely checked by DNA sequencing. DNA sequencing of all constructs was carried out commercially. Samples were sent by mail and processed by DNA Sequencing & Services, University of Dundee, Scotland. The results were returned in both FASTA format and as a colour-coded sequencing trace. Primers used for sequencing constructs are presented in Table 2.2.

Table 2.2 Sequencing primers used to confirm the integrity of constructs used in experiments.

Primer	Sequence	Description
E1	5'-TATAAGCAGAGCTGGTTTAG-3'	Sequencing primer for sequencing of EGFP plasmid insert (Laboratory stock)
E2	5'-CGTCGCCGTCCAGCTCGACCAG-3'	Sequencing primer for sequencing of EGFP plasmid insert (Laboratory stock)
T7	5'- TAATACGACTCACTATAGGG-3'	Sequencing primer for sequencing of Halotag plasmid insert (provided by DNA Sequencing & Services, University of Dundee, United Kingdom)
SM1	5'- AGCAGCCAACTCAGCTT-3'	Sequencing primer for sequencing of Halotag plasmid insert (designed by Samantha McDonnell)
SM2	5'- TGTCGGATTTGCCCATACCG-3'	Sequencing primer for sequencing of Halotag plasmid insert (designed by Samantha McDonnell)

2.2.6 Site-directed mutagenesis

For the purpose of repairing a point mutation, Agilent Technologies' (California, United States) QuikChange II Site-Directed Mutagenesis Kit was used. Mutagenesis reactions were prepared as per the mutagenesis kit manufacturer's instructions. In brief 1 µL (10ng) of construct DNA with 1.25 µL (125 ng) of each mutagenesis primer detailed in table 2.3 were used in a total final reaction volume of 50 µL. Reaction mixes were then cycled using a thermal cycler with an initial step at 95^{o}C for 30 seconds before twelve cycles consisting of a denaturation step at 95^{o}C for 30 seconds, an annealing step at 55^{o}C for 1 minute and an elongation step at 68^{o}C for 5 minutes.

Table 2.3 Primers used for point mutagenesis of plasmid to repair original EGFP constructs.

Primer	Sequence	Description
c275t	5'-ctacttcttggacgtggagctgggccgaa-3'	Primer used to cause site directed mutagenesis in cystatin C insert
c275t.antisense	5'-ttcggcccagctccacgtccaagaagtag-3'	Primer used to cause site directed mutagenesis in cystatin C insert

Amplification products were cooled on ice for 2 minutes before being incubated with 1 µL of *Dpn* I restriction enzyme at 37^{o}C for 1 hour. This digested the parental plasmids, leaving only the repaired plasmid behind.

Following this 1 µL of DNA from each amplification was added to a 50 µL aliquot of supercompetent XL1-Blue Escherichia coli and incubated on ice for 30 minutes prior to a 45 second heat shock at 42^{o}C in a water bath and returning the cells to ice for a further 2 minutes.

Preheated NZY+ broth (Appendix 2) was then added to the heat shocked aliquots and then transferred to an orbital incubator at 37^{o}C for one hour. The bacteria were then finally plated onto Luria agar containing 100 µg/mL ampicillin to select for growth of transformed bacteria.

2.2.7 Production of new plasmid constructs

For the purpose of mass spectrometry HaloTag® was chosen as a way of producing improved samples to traditional methods. HaloTag® is a recently developed, flexible system produced by Promega for the purpose of tagging proteins; HaloTag is able to covalently bond with a specific ligand which in mass spectrometry is used to specifically pull down the target protein and then elute only the interacting proteins. This ensures that the sample is

not overwhelmed by excessive amounts of the target protein which was greatly appealing for this experiment.

Table 2.4 Primers for amplification of cystatin C. These were used to amplify cystatin C wild type and variant B sequences from the EGFP constructs and to add appropriate restriction digest sites for ligation. (Designed by and obtained from Dr. Paul Kay):

Primer	Sequence	Description
CysC Amplifying Plasmid (forward)	5'- AATTAGAATTCATGGCCGGGCCCCTGCGC -3'	Primer used to amplify cystatin C inserts from EGFP constructs and add Eco RI restriction sites
CysC Amplifying Plasmid (reverse)	5'- AATTACTCGAGGGCGTCCTGACAGGTGGATTTCGAC -3'	Primer used to amplify cystatin C inserts from EGFP constructs and add Xho I restriction sites

Cystatin C was amplified from the EGFP constructs with primers (Table 2.4) constructed to add restriction digest sites to allow it to be inserted into the Halotag plasmid. The amplification reactions were prepared using Phusion DNA polymerase (New England Biolabs) as per manufacturer's instructions. In brief reactions were prepared with 1 µL (10ng) of the respective EGFP construct (wild type and variant B), 2.5 µL of each primer detailed in table 2.4 (10 µM), 10 µL 5x Phusion HF buffer and 1.5 µL DMSO in a final reaction volume of 50 µL.

The PCR thermal cycling conditions as follows, an initialisation step at 98^{o}C for 30 seconds, then 30 cycles consisting of a denaturation step at 98^{o}C for 10 seconds, an annealing step at 55.7^{o}C for 30 seconds and an elongation step at 72^{o}C for 15 seconds. A final elongation step followed these cycles at 72^{o}C for 7 minutes and finally the reaction was held at 4^{o}C.

Amplified DNA was treated with the QIAGEN PCR Purification kit before both the Halotag template and the PCR cystatin C products were double digested with Xho I and EcoRI restriction enzymes in Buffer H in total reaction volumes of 20 µL as described in section 2.2.4.

Digested PCR products were ligated into the plasmid overnight at room temperature by mixing 1 µg of digested plasmid, 1 µg of digested cystatin C PCR product and 5 µL T4 DNA ligase in a final reaction volume of 30 µL.

Following overnight incubation the DNA was transformed into XL1-Blue competent cells (Agilent) and cultured on selective Luria agar containing 100 µg/mL ampicillin at 37^{o}C. Selected colonies were picked and cultured in Luria broth overnight, again selected for by ampicillin at 37^{o}C, and uptake of the plasmid was confirmed by use of a QIAPrep Spin Miniprep kit (Qiagen).

2.3 Polyacrylamide gel protein analysis

2.3.1 Preparation of whole cell lysates

Samples for western blot analysis were produced from transfected and untransfected cells as whole cell lysates. Cells were washed with PBS and Lysis buffer (Appendix 2) was added in a volume sufficient to be able to spread over the cells, approximately 1mL for a T75 flask, and a cell scraper was used to spread the buffer and detach the cells.

Lysates were transferred to 1.5 mL tubes and syringed with a 21G or 23G needle 10 times to shear the DNA and make the sample less viscous. Samples were quantified for total protein content by Qubit® Protein Assay (Life Technologies, Thermo Fisher Scientific Inc., Waltham, United States) in order to enable equal loading.

Loading buffer (Appendix 2) was added to the samples in a 1 in 5 ratio and the samples were heated at 95^{o}C for 5 minutes to denature the protein and make it suitable for loading. Cell lysates were stored in a freezer at -20^{o}C.

2.3.2 Polyacrylamide gel electrophoresis

Protein samples were analysed utilising methods based on the basic process of separating proteins by their ability to move through a polyacrylamide gel (a function of the length and charge of the molecule). Polyacrylamide gels, 15 mm thick, were used to separate protein samples. Resolving gel (Appendix 2) was poured between two glass plates and water saturated butanol was used to level the top and the gel allowed to set for ~30 minutes minimum.

Butanol was removed from the set gel and rinsed off completely with dH_2O. Stacking gel (Appendix 2) was then poured on top of the resolving gel and a comb added to form the wells, then allowed to set for typically up to one hour. Running buffer (Appendix 2) at 1x concentration was used in combination with a Bio-Rad mini-PROTEAN system to separate the samples on the gel.

Protein ladder routinely used was PageRuler Prestained Protein Ladder (Thermo Fisher Scientific Inc., Waltham, United States). The maximum volume of sample applied was 50 µl

in 10 well gels or 30 µl in 15 well gels. Wells were equally loaded by total protein content of sample. The gel was typically run at 80V for 10 minutes to allow the sample to enter and pass through the stacking gel and then 120-150V for 1-1.5 hours to separate on the resolving gel.

2.3.3 Western blotting

Western blotting involves transferring proteins to a membrane which can then be dyed and/or probed with antibodies and imaged. This is achieved in a similar way to the gel separation in that an electrical current is used to make the charged protein pass out of the gel and onto the nitrocellulose surface. All buffers can be found in Appendix 2.

Pieces of nitrocellulose membrane and filter paper were cut to size and soaked in transfer buffer along with two sponge pads per gel, the components assembled in a transfer cassette as per figure 2.4. Transfer to the membrane was carried out using transfer buffer and a Bio-Rad mini-PROTEAN system. The gel was transferred at 100 V for ~60-90 minutes with gentle stirring.

Following the transfer membranes were routinely checked by staining with Ponceau S (Sigma-Aldrich Company Ltd., Dorset, England) for transfer success and the presence of protein bands on the nitrocellulose membrane. Ponceau S stain was added to the membrane for 2 minutes at room temperature with gentle agitation. Then the excess dye was poured off and the membrane washed with dH_2O to reveal the bands. Repeated washes removed the dye entirely allowing the gel to be further analysed.

The membrane was washed in wash buffer twice for 5 minutes each with gentle agitation, then incubated in blocking buffer for at least 1 hour with gentle agitation at room temperature (this could be left longer, if left overnight then incubation was at 4^oC). After the blocking step the membrane was incubated with antibodies diluted as indicated in table 2.5 in 10 mL blocking buffer or 10 mL 5% BSA in wash buffer as appropriate (typically blocking buffer for monoclonal antibodies and 5% BSA for polyclonal antibodies). The membrane was incubated with the antibody with gentle agitation overnight at 4^oC.

Following overnight incubation the membrane was washed three times with wash buffer for 5 minutes each time and incubated with secondary antibody (Table 2.5) at the

appropriate dilution in 10 mL blocking buffer for 1 hour at room temperature. This was followed by another three washes before the membrane was exposed to ECL reagent (GE Healthcare Life Sciences, Buckinghamshire, UK) and incubated for 1-2 minutes. Finally the membrane was visualised on a Chemi-Doc (Bio-Rad Laboratories Ltd., Hertfordshire, UK).

Table 2.5 Antibodies used in western blotting

Antibody target	Dilution	Supplier and code	Description
Cystatin C	1:2000	Millipore ABC20	Rabbit polyclonal antibody
EGFP	1:2000	Clontech 632380	Mouse monoclonal antibody
GAPDH	1:20,000	Abcam 8245	Mouse monoclonal antibody
LC3B	1:500	Cell signalling 3868	Rabbit monoclonal antibody
Caspase 3	1:1000	Abcam 90437	Rabbit polyclonal antibody
Anti-rabbit	1:1000	Sigma-Aldrich A0545	Goat polyclonal antibody
Anti-mouse	1:1000	Sigma-Aldrich A9044	Rabbit polyclonal antibody

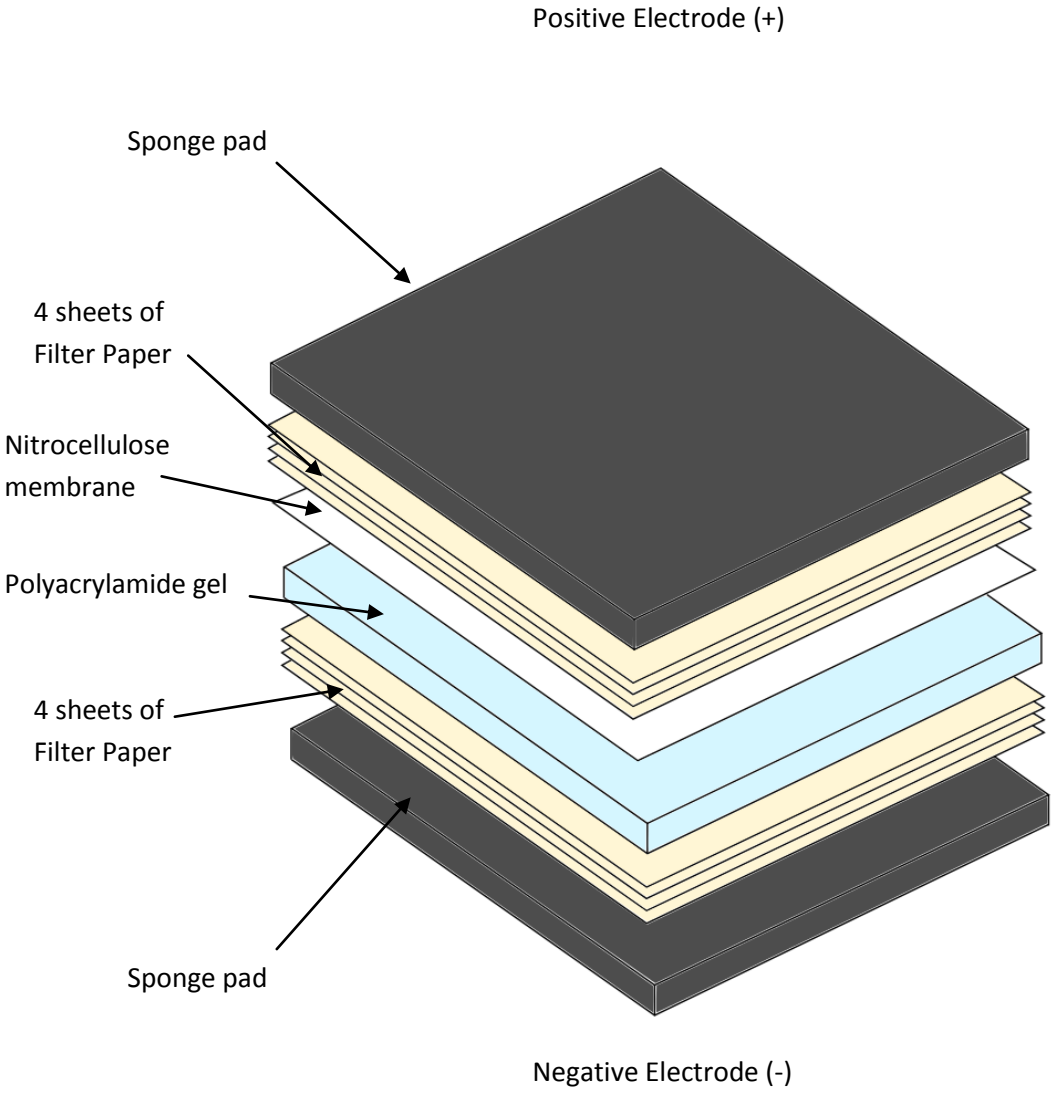

Figure 2.4 Transfer cassette for western blotting and details of transfer process. For transfer of the proteins and subsequent probing with antibodies a nitrocellulose membrane was used. The sponge pads padded the cassette in order to ensure that the gel did not slip. Four pieces of filter paper were found to be optimal, protecting the gel and membrane during the process. All western blot gels were of 1.5 mm thickness. Alignment with the electrical current as shown causes the transfer of the protein from the gel to the nitrocellulose membrane. Larger proteins require longer transfer times. (Author's figure)

2.3.5 Coomassie staining

Coomassie staining is a simple method of visualising proteins on a gel however once the gel is stained it cannot be used for further analysis. First the SDS gel was removed from between the glass plates and placed into a staining tray. Then covered with 10 mL of 0.5% Brilliant Blue R250 (Sigma-Aldrich Company Ltd., Dorset, England) and incubated for 1 hour at room temperature with gentle agitation.

The dye was then removed and the gel washed with 50 mL destaining solution (10% Acetic Acid/30% Methanol) for 1 hour. The destain solution was replaced and destaining was continued overnight with additional destains the next day as necessary to visualise.

2.3.6 Silver staining

Silver staining is a much more sensitive method of visualising the proteins on a gel than coomassie staining. It was primarily used to verify immunoprecipitation samples during optimisation, the Pierce Silver Stain Kit (24612, Pierce, Thermo Fisher Scientific Inc., Waltham, United States) was used for this purpose as per manufacturer's instructions.

In brief, the SDS gel was washed twice for 5 minutes with dH_2O. Fixing solution (30% ethanol, 10% acetic acid) was then added and the gel fixed for 30 minutes with the solution being replaced after 15 minutes. The fixing solution was rinsed off with 10% ethanol (two washes for five minutes each) and then with dH_2O (two washes, five minutes each).

Sensitiser solution (50 µL sensitiser in 25 mL dH_2O) was added to the gel for 1 minute and the sensitiser rinsed off with two 1 minute washes with dH_2O. Staining solution (0.5 mL enhancer in 25 mL stain) was then added and the gel incubated at room temperature for at least 30 minutes (up to overnight). The gel was washed briefly for 20 seconds twice in dH_2O before developing in 25 mL developer solution with 0.5 mL enhancer until bands appeared.

Finally when the bands were sufficiently visible the developing mixture was removed and the gel rinsed with 5% acetic acid for 1 minute before fixing with fresh 5% acetic acid for ten minutes. Gels were then photographed with care taken to ensure that bands could be clearly viewed. Developed gels could be stored in dH_2O at 4^oC until no longer required with no visible degradation of the staining.

2.4 Flow cytometry analysis for oxidative stress

Flow cytometry was performed with CellROX® (Life Technologies, Thermo Fisher Scientific Inc., Waltham, United States) dye. CellROX® is an oxidative stress dye that permeates into the cells and fluoresces upon reacting with reactive oxygen species. It is not specifically localised, instead being distributed throughout the cytoplasm of the cell making it a general oxidative stress marker. In its reduced state it is very weakly fluorescent, with the signal becoming stronger upon oxidation.

The dye is highly photostable compared with other oxidative stress dyes meaning it is significantly easier to work with, although it is still preferable to protect the dye from light where possible. Further there are several forms of the dye with varying excitation and emission wavelengths. Labelling can be carried out in complete media, with the dye being both live cell compatible and certain forms of it also being suitable for formaldehyde fixation. Finally the dye is suitable for flow cytometry, allowing for high throughput assaying of cells.

For these experiments CellROX® Deep Red Reagent was used, which has absorption/emission maximum at ~644/665 nm which allows it to be specifically distinguished from the EGFP fluorescence of the construct tag. Hence it was possible to pick out the fluorescencent and non-fluorescent cells from each sample and take readings from each for comparison.

2.4.1 Cell preparation

Cells were seeded and transfected in 6 well plates and were checked using a fluorescent microscope to ensure that the transfection had been successful. CellROX® dye was then added to cells at a final concentration of 5 µM and incubated for 30 minutes at 37^{o}C.

Following this incubation period the medium was removed and the cells washed three times with PBS to remove excess dye. Cells were then harvested and pelleted before being resuspended in 1 mL chilled PBS/2% FCS and were kept on ice until analysis.

2.4.2 Flow cytometry

A FACSCalibur (BD Biosciences, California, US) was used to analyse the dyed cells. Initially controls were used to assess that the cells had taken up the dye and that a fluorescent population was present. From there the samples were run through the cytometer and each cell processed assessed for EGFP fluorescent signal and the red fluorescent signal of the CellROX dye.

To analyse this dataset, individual transfected cells were explicitly selected as a group (eliminating any double or triple cell clumps that had not properly dissociated) and compared against populations from other samples and with the untransfected population from within the same sample.

2.5 Protein pull-down

Two types of pull-down procedure were carried out during this work. The first was immunoprecipitation of the original EGFP cystatin C constructs, the second was pull-down of the new Halotag cystatin C.

2.5.1 Cystatin C protein immunoprecipitation

Immunoprecipitation of the EGFP constructs was achieved by the use of an anti-cystatin C antibody and Protein-A agarose beads in order to pull down both the fusion construct and the endogenous cystatin C.

Cells were seeded and transfected on 6 well plates; 23 hours post transfection they were imaged to ensure the transfection was successful. The medium was removed and discarded and the cells washed with PBS, then an appropriate volume of RIPA buffer (Appendix 2, ~500 µL for a T75 flask) was added to the cells, which were then incubated on ice for 5 minutes and scraped to remove them from the culture vessel.

The cell suspension was transferred to a 1.5 mL tube and syringed with a 27G needle, the resulting lysate was cleared by centrifugation for 5 minutes at 14,000g. Cleared supernatant was transferred to a fresh tube and 50 µL of cystatin C antibody (sc-73878, Santa Cruz Biotechnology, Texas, US) was added before incubation overnight with rocking at 4^{o}C.

40 µL of Protein A agarose bead slurry was added (9863S, Cell Signalling Technology, Massachusetts, US) and returned to 4^{o}C for 1.5 hours with rocking. The beads were then extracted by centrifugation at 800g for 2 minutes and the supernatant discarded. Four washes using 500 µL RIPA buffer were then carried out, with beads pelleted by 800g centrifugation for one minute each time between each wash.

Finally the protein was eluted from the beads by incubation at room temperature for 30 minutes in 40 µL elution buffer (western blot lysis buffer was used for this purpose to allow immediate loading onto gels). The beads were removed from the sample by a 2 minute centrifugation at 800g to leave the eluted proteins in a solution cleared of beads.

2.5.2 HaloTag® protein pull-down

The Promega Halotag Mammalian Pull-Down Kit (Promega) was utilised in order to specifically precipitate out proteins interacting with cystatin C Halotag constructs and thus minimise contaminants. Due to the nature of Halotag and the covalent bonding to the ligand it was possible to just elute the interacting proteins. The method was modified from the manufacturer's instructions for optimal extraction of the samples.

Cells were seeded and transfected in a T75 flask; 24 hours post transfection the media was removed from the cells and they were washed with chilled PBS. Following this 10 mL of fresh chilled PBS was added and the flasks were gently scraped to detach the cells from the culture vessel and the suspension transferred to a 15 mL tube. Cells were pelleted at 200g for 5 minutes, the PBS removed and the pellet transferred to a -80^{o}C freezer for at least 30 minutes.

The pellets were then thawed and resuspended in 150 µL of lysis buffer and 3 µL of protease inhibitor cocktail, then the suspension was passed 10 times through a 27G needle. Lysate was then centrifuged at 14,000g for 5 minutes to clear. The cleared lysate was then kept on ice for subsequent steps.

Before the addition of resin the lysate was diluted with 350 µL TBS buffer, this diluted lysate was added to Halotag binding resin (prior washed with wash buffer - TBS/0.05% IGEPAL CA630) and incubated at 4^{o}C for at least 2 hours up to a maximum of overnight. This incubation period was to allow the Halotag ligand to covalently bind with the Halotagged cystatin C constructs.

The samples were then centrifuged at 800g for 2 minutes and the supernatant discarded. Then they were washed with 1 mL wash buffer (as above) four times, centrifuging between each wash at 800g for 2 minutes and discarding the wash each time. Finally 1 mL of wash buffer was added and the beads incubated with gentle agitation at room temperature for 5 minutes before finally being pelleted at 800g for 2 minutes and this final wash discarded.

Proteins bound to the cystatin C were eluted with 40 µL of RapiGest (Waters) which was added to each sample and incubated at 80^{o}C for 10 minutes. This released the protein and the beads were subsequently spun down for 2 minutes at 800g and the protein containing supernatant recovered for analysis.

2.6 Mass Spectrometry

D407 cells were seeded in T75 tissue culture flasks and incubated overnight (~12-16 hours) , then transfected with Halotag-Cystatin C constructs before being returned to the incubator for a further 24 hours. Halotagged Cystain C protein was extracted as described in section 2.5.2 and the proteins bound to the construct eluted with 40 µL *Rapi*Gest (Waters).

Samples were then transferred on ice to the University of Liverpool Proteomics facility (Technology Directorate, University of Liverpool, England) to be processed. The samples were analysed by Electrospray Ionization Fourier Transform Ion Cyclotron Resonance (ESI-FTICR) and the results returned as both a mass spectrometry trace and mass spectrometry data spreadsheets.

Data returned included normalised ion abundancies, raw abundancies, spectral counts and ANOVA analysis of the results automatically generated, calculated in Progenesis QI for proteomics (a standard software package to analyse mass spectrometer outputs). In addition the individual Mascot search files were provided. The mass spectrometry runs and initial analysis were carried out by Dr Deborah M Simpson of the Centre for Proteome Research, University of Liverpool.

2.7 Respiration assays

2.7.1 Oxygen probe measurement of respiration rate

To assess the effect of cystatin C wild type and variant B on the respiration rate of cells the rate at which oxygen is depleted was examined. An oxygen probe was used to achieve this, this probe measures the concentration of oxygen within a solution within the chamber, thus allowing for the concentration of oxygen at different time points to be measured and the rate of depletion calculated. Given that oxygen is consumed by the respiratory process this rate allows the rate in the cell to be assessed indirectly by the consumption of oxygen without having to extract and assess the mitochondria directly (thus potentially compromising the physiological relevance of the data).

Cells were transfected in 6 well plates; 23 hours post transfection plates were imaged, 24 hours post transfection cells were washed with PBS, harvested and pelleted. Cells were then resuspended in PBS/10 mM potassium orthophosphate/10 mM HEPES buffer, counted and kept on ice until use. An Oxytherm oxygen electrode unit (Hansatech Instruments, Norfolk, United Kingdom) was prepared according to manufacturer's guidelines and allowed to stabilise for 3 minutes before 1 million cells were loaded into the chamber. Four minutes later glutamate (2.5 mM) and malate (2.5 mM) were added to supplement respiratory activity. Finally after 11 minutes total had passed ADP (1 mM) was added to ensure that this was not a limiting factor for the rate of respiration.

Readings were taken for each sample every second until at least 30 minutes total had passed since the initial loading. The gradient of the graph produced for each sample, following the additions of supplements, was calculated, indicating the rate at which oxygen was being used and hence the rate of respiratory activity.

2.7.2 Total ATP content assay

To assess the total ATP content of transfected and untransfected cells as a measure of normal cell functioning the luciferase-based CellTiter-Glo® kit (Promega) was used. Although primarily designed for assaying cell viability it achieves this by a measure of ATP in samples, consequently loading equal numbers of cells will allow for relative ATP quantification.

Cells were seeded and transfected in a 6 well plate , imaging was carried out 23 hours post transfection for the purpose of correcting for differing transfection rates; 24 hours post transfection the cells were harvested. Cells were resuspended in 1 mL media and counted to allow for equal loading onto plates.

For analysis, 40,000 cells were seeded in triplicate for each sample into a white-bottomed 96-well plate and the total volume of each well made up to 100 µL with additional media. Plates were then equilibrated at room temperature for 30 minutes before the addition of 100 µL of CellTiter-Glo reagent to each well.

Two minutes of agitation at room temperature was followed by incubation at room temperature for 10 minutes. Finally the luminescence was recorded on a Promega Glomax Multi+ plate reader to give relative luminescent levels correlating to relative ATP levels.

2.7.3 Preliminary ATP measurements

Preliminary analysis involved direct measurement of ATP produced by isolated mitochondria. Cells were transfected in a 6 well plate and incubated for 24 hours before the fluorescence was checked and the cells harvested. A Miltenyi Biotec Human Mitochondrial Isolation kit was used, as per manufacturer's instructions, to extract mitochondrial protein (and thus mitochondria) from the samples. In brief cells were lysed in the kit's lysis buffer with a 25g needle. Following this the lysates were diluted with separation buffer and Anti-TOM22 magnetic microbeads were added for magnetic labelling.

A Miltenyi Biotec QuadroMACS separator was used for the extraction of the magnetic beads from the samples, allowing for four simultaneous extractions to be carried out. Columns were prepared and the samples passed through the columns, with washing, before the beads, with attached mitochondria, were flushed out as per manufacturer's instructions.

Beads were then spun down at 13,000g for 2 minutes and resuspended in 30 µL ROS buffer (125 mM KCl, 10 mM MOPS, 5 mM $MgCl_2$, and 2 mM K_2HPO_4 (pH 7.44)). Protein was quantified by Qubit® Protein assay (Life Technologies).

On a white-bottomed 96 well tissue culture plate 5 µg of total mitochondrial protein was suspended in 100 µL of ROS buffer. This was incubated in the plate reader for 5 minutes at 37^{o}C. Following incubation 0.5 µM rotenone and 5 mM succinate were added to drive respiration through complexes I, III and IV and 2.5 mM glutamate and 2.5 mM malate were added to stimulate the process. Then 100 µL of luciferase reagent from Roche's ATP Bioluminescence Assay Kit CLS II along with 1 mM ADP were added to each well and luminescent measurements were taken every twenty seconds for approximately six minutes. The rate of ATP production could then be calculated from the increase in luminescence signal over time.

2.8 Statistics and calculations

2.8.1 T-test

Unpaired T-tests were routinely used as a statistical test unless otherwise specified. These were calculated automatically using Microsoft Excel's t-test function for ease of data manipulation in data spreadsheets.

T-test P values are reported throughout the results and was the standard way by which results were assessed. It is a highly effective method by which results can be assessed for statistical significance in a comparison between two data sets. Given that much of the comparisons in the analysis are between the means of independent sets of data it was deemed to be suitable.

2.8.2 ANOVA

ANOVA analysis was carried out automatically on mass spectrometry data by the Progenesis QI for Proteomics software.

In addition an ANOVA was used as a preliminary statistical analysis for some sets of data, but these are not presented. ANOVA was typically used as a statistical test to indicated the potential for notable results within a sample and consequently as a way to draw attention to particularly notable sample sets and was never used alone.

2.8.3 Combining standard deviations

To combine standard deviations for samples with technical replicates the square root of the pooled variances was used. This allowed for variation in technical replicates to be preserved in the final variances appropriate and was achieved utilising the following calculation:

$$SD_{combined} = \sqrt{\frac{SD_{sample\ 1}{}^2}{n_{sample\ 1}} + \frac{SD_{sample\ 2}{}^2}{n_{sample\ 2}} + \frac{SD_{sample\ 3}{}^2}{n_{sample\ 3}}}$$

Chapter 3

Mitochondrial associated cellular mechanisms

3.1 Introduction

The primary focus of this study is what happens to variant B cystatin C within retinal pigment epithelium cells, encompassing both the interactions of the variant protein with other intracellular proteins and the consequent effects on intracellular mechanisms. The mislocalisation to the mitochondria indicates that it is possible that this variant interferes with the normal functioning of the mitochondria. Given the importance of mitochondria within the cell this would likely be highly disruptive to the cellular environment.

As a result, key intracellular mechanisms were selected for examination. In each mechanism chosen there is reason to believe that the process either may be impaired by the mislocalisation or the process has been implied in the development of AMD.

3.2 Preparation of constructs

Initial preparation and sequencing of stocks of the previously produced EGFP constructs (Paraoan *et al.*, 2004) identified an inappropriate point mutation resulting in a GCG codon replacing a GTG codon, and a consequent amino acid change of Valine to Alanine. This change resulted in potential detrimental effects on the protein structure. This mutation was present in both the cystatin C wild type and variant B plasmid constructs.

Both of these amino acids are uncharged and hydrophobic with similar pKa values which may initially indicate that this substitution would have no effect. However Alanine is highly associated with alpha-helices and Valine with β-sheets, further this base is in the middle of the third β-sheet in the protein and thus might be expected to have a disruptive effect on the structure of the protein. This is of importance with respect to cystatin C's role as a protease inhibitor as the inability to bind with its typical substrates may lead to it being ineffective. Furthermore with respect to the variant B form of the protein this could lead to interactions which are not seen *in vivo* and hence result in misleading conclusions regarding its involvement in disease.

Consequently a point mutation repair was carried out on the plasmids in order to revert the DNA code to its normal human sequence. Amplification primers were designed to substitute the inappropriate base for the correct one using PCR thermal cycling. Bacterial

cells were then transformed with the repaired plasmid, selected and subject to miniprep plasmid extraction utilising a QIAprep Spin Miniprep kit.

The repair was confirmed by DNA sequencing of miniprep samples produced from the transformed bacteria. This established that the point mutation had been successfully reverted and consequently fixed the amino acid substitution error in the protein. Sequence readings in this region were clear, with clean peaks demonstrating no ambiguity. The substituted base and change in amino acid are illustrated in figures 3.1 and figure 3.2.

A

ATG GCC GGG CCC CTG CGC GCC CCG CTG CTC CTG CTG GCC ATC CTG GCC GTG GCC CTG GCC GTG
AGC CCC GCG GCC GGC TCC AGT CCC GGC AAG CCG CCG CGC CTG GTG GGA GGC CCC ATG GAC GCC
AGC GTG GAG GAG GAG GGT GTG CGG CGT GCA CTG GAC TTT GCC GTC GGC GAG TAC AAC AAA GCC
AGC AAC GAC ATG TAC CAC AGC CGC GCG CTG CAG GTG GTG CGC GCC CGC AAG CAG ATC GTA GCT
GGG GTG AAC TAC TTC TTG GAC GTG GAG CTG GGC CGA ACC ACG TGT ACC AAG ACC CAG CCC AAC
TTG GAC AAC TGC CCC TTC CAT GAC CAG CCA CAT CTG AAA AGG AAA GCA TTC TGC TCT TTC CAG
ATC TAC GCT GTG CCT TGG CAG GGC ACA ATG ACC TTG TCG AAA TCC ACC TGT CAG GAC GCC

B

ATG GCC GGG CCC CTG CGC GCC CCG CTG CTC CTG CTG GCC ATC CTG GCC GTG GCC CTG GCC GTG
AGC CCC GCG GCC GGC TCC AGT CCC GGC AAG CCG CCG CGC CTG GTG GGA GGC CCC ATG GAC GCC
AGC GTG GAG GAG GAG GGT GTG CGG CGT GCA CTG GAC TTT GCC GTC GGC GAG TAC AAC AAA GCC
AGC AAC GAC ATG TAC CAC AGC CGC GCG CTG CAG GTG GTG CGC GCC CGC AAG CAG ATC GTA GCT
GGG GTG AAC TAC TTC TTG GAC GTG GAG CTG GGC CGA ACC ACG TGT ACC AAG ACC CAG CCC AAC
TTG GAC AAC TGC CCC TTC CAT GAC CAG CCA CAT CTG AAA AGG AAA GCA TTC TGC TCT TTC CAG
ATC TAC GCT GTG CCT TGG CAG GGC ACA ATG ACC TTG TCG AAA TCC ACC TGT CAG GAC GCC

C

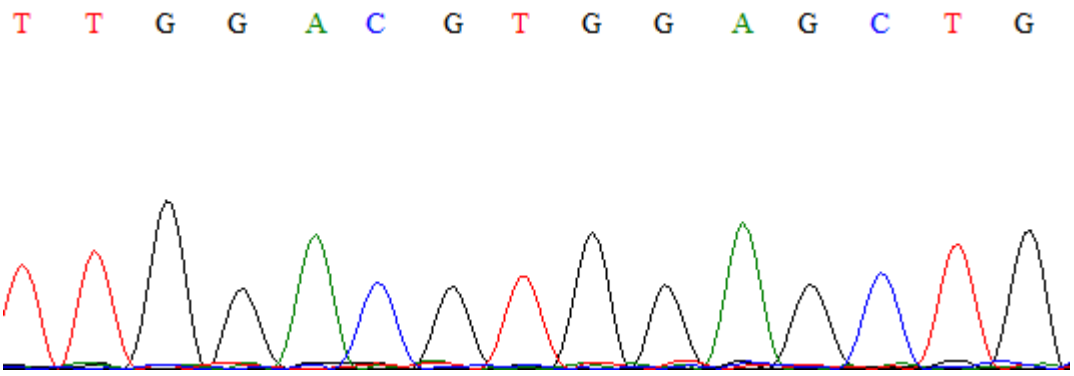

Figure 3.1 DNA substitution repairs in wild type cystatin C fusion protein. The sequence of cystatin C from Abrahamson (1987a) is presented in **A**. **B** is the sequenced cystatin C from the pEGFP-N3 vector post-repair. Green highlights the area where the expected sequence matches with the sequencing output, which represents the entirety of the sequence. Red highlights the area where the substitution repair was completed. The underlined codon is that which is modified in the variant B form of cystatin C and in this wild type form matches with the Abrahamson sequence. **C** is the associated sequencing spectrum for the region where the repair was carried out, illustrating that the sequence peaks for the repair are clear and defined with little to no background from other bases.

A

ATG GCC GGG CCC CTG CGC GCC CCG CTG CTC CTG CTG GCC ATC CTG GCC GTG GCC CTG GCC GTG
AGC CCC GCG GCC GGC TCC AGT CCC GGC AAG CCG CCG CGC CTG GTG GGA GGC CCC ATG GAC GCC
AGC GTG GAG GAG GAG GGT GTG CGG CGT GCA CTG GAC TTT GCC GTC GGC GAG TAC AAC AAA GCC
AGC AAC GAC ATG TAC CAC AGC CGC GCG CTG CAG GTG GTG CGC GCC CGC AAG CAG ATC GTA GCT
GGG GTG AAC TAC TTC TTG GAC GTG GAG CTG GGC CGA ACC ACG TGT ACC AAG ACC CAG CCC AAC
TTG GAC AAC TGC CCC TTC CAT GAC CAG CCA CAT CTG AAA AGG AAA GCA TTC TGC TCT TTC CAG
ATC TAC GCT GTG CCT TGG CAG GGC ACA ATG ACC TTG TCG AAA TCC ACC TGT CAG GAC GCC

B

ATG GCC GGG CCC CTG CGC GCC CCG CTG CTC CTG CTG GCC ATC CTG GCC GTG GCC CTG GCC GTG
AGC CCC GCG ACC GGC TCC AGT CCC GGC AAG CCG CCG CGC CTG GTG GGA GGC CCC ATG GAC GCC
AGC GTG GAG GAG GAG GGT GTG CGG CGT GCA CTG GAC TTT GCC GTC GGC GAG TAC AAC AAA GCC
AGC AAC GAC ATG TAC CAC AGC CGC GCG CTG CAG GTG GTG CGC GCC CGC AAG CAG ATC GTA GCT
GGG GTG AAC TAC TTC TTG GAC GTG GAG CTG GGC CGA ACC ACG TGT ACC AAG ACC CAG CCC AAC
TTG GAC AAC TGC CCC TTC CAT GAC CAG CCA CAT CTG AAA AGG AAA GCA TTC TGC TCT TTC CAG
ATC TAC GCT GTG CCT TGG CAG GGC ACA ATG ACC TTG TCG AAA TCC ACC TGT CAG GAC GCC

C

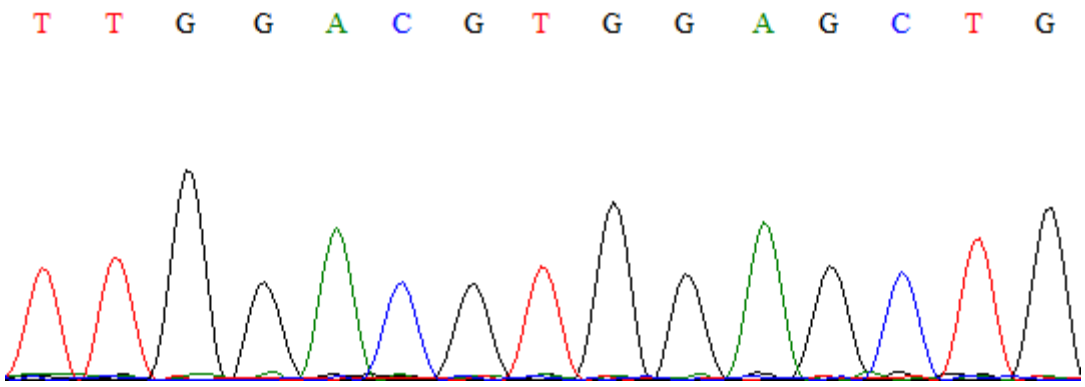

Figure 3.2 DNA substitution repairs in variant B cystatin C fusion protein. The sequence of cystatin C from Abrahamson (1987a) is presented in **A**. **B** is the sequenced cystatin C from the pEGFP-N3 vector post-repair. Green highlights the sequence areas where the expected sequence matches with the sequencing output, which represents the entirety of the sequence. Red highlights the area where the substitution repair was completed. The underlined codon is that which is modified in the variant B form of cystatin C and in this variant B form does not match with the Abrahamson sequence, instead presenting the A25T substitution. **C** is the associated sequencing spectrum for the region where the repair was carried out, illustrating that as for the wild type the sequence peaks for the repair are clear and defined with little to no background from other bases.

Confirmation of localisation of the repaired construct was also carried out (Figure 3.3). This was an essential final step to confirming the similarity of the repaired construct to the previous work done on the wild type and variant B protein; ensuring the mitochondrial localisation of the variant.

ARPE19 and D407 cells were seeded into glass-bottomed 35mm dishes and transfected with the repaired plasmid constructs and grown overnight. Following this growth period the cells were incubated for 30 minutes at 37^{o}C with Mitotracker Red diluted to 250 nM in media. This cell-permeable dye accumulates within mitochondria and fluoresces upon exposure to appropriate wavelength light (exciting at a wavelength of 581 nm and emitting at 644 nm).

Cells were imaged using a confocal microscope and fluorescence images taken for both the EGFP green channel and Mitotracker red channel. This allowed for the co-localisation of the protein to be checked based on overlap of the two different fluorescence patterns, given the EGFP tagging of the protein and the Mitotracker accumulation within mitochondria.

EGFP only transfected cells demonstrated a diffuse green fluorescence present throughout the cell as expected. The wild type cystatin C-EGFP construct did not show as diffuse fluorescence as the tag alone, instead demonstrating specific localisation; however that localisation was not specifically localised with the mitochondria staining. In contrast the variant B cystatin C-EGFP construct demonstrated a high degree of localisation with the red straining of the mitochondria accumulated red dye.

Given the confirmation of the plasmid by both restriction digest DNA gel and by sequencing and the confirmation of the protein localisation of the variant B protein the repair was deemed to be successful. The newly repaired pEGFP-N3 cystatin C wild type and cystatin C variant B constructs were subsequently used for the majority of following experiments. They were routinely checked by the use of agarose gel electrophoresis and periodically tested via DNA sequencing throughout the studies to ensure their integrity.

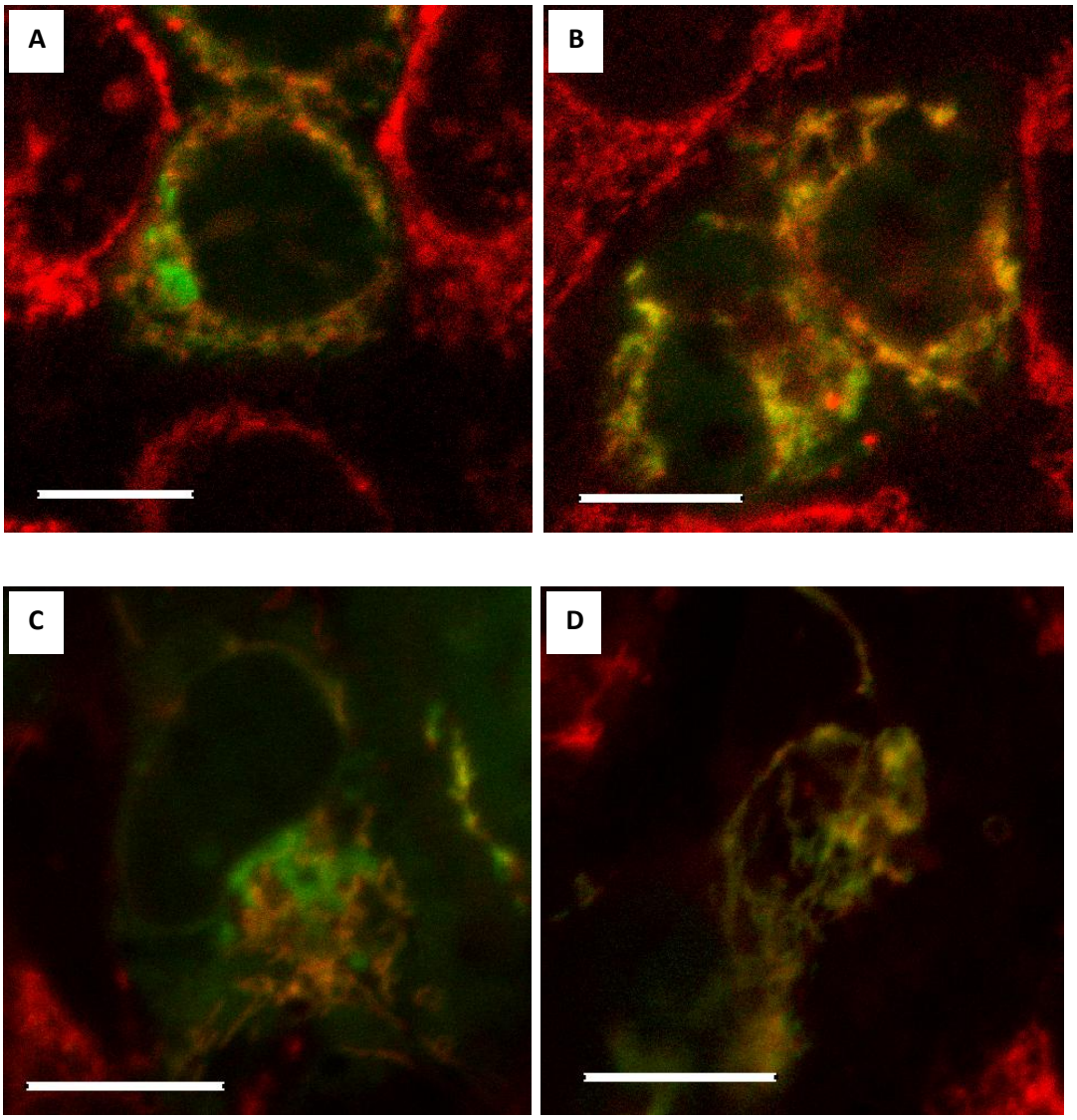

Figure 3.3 Localisation of repaired EGFP cystatin C constructs. A and **B** are D407 cells. **C** and **D** are ARPE19 cells. Fusion protein localisation is green whilst the mitochondria are visible in red (stained with Mitotracker Red dye), areas of yellow indicate co-localisation. **A** and **C** are both transfected with the wild type cystatin C EGFP vector construct and present a wild type distribution pattern, that is to say not specifically mitochondrially localised. **B** and **D** are both transfected with the variant B cystatin C EGFP vector construct and present the mitochondrial co-localisation as described in Paraoan *et al.* (2004). Scale bars are 10 µm. Typical transfection rates ~25-30% for cystatin C wild type construct and 10-15% for variant B construct following transfection optimisation.

3.3 Respiration

Respiration is the most crucial process of the mitochondria. It is absolutely essential for the normal functioning of cells as it is the primary source of energy in the cell in the form of ATP. This is of particular relevance to the RPE cells given the many different processes that are essential for its role within the eye.

There are a two main ways that the respiration rate can be assessed. Either by analysing the amount of ATP produced by the cells/mitochondria directly or by measuring the usage of oxygen in a closed system and its rate of depletion. Both of these were attempted.

3.3.1 Preliminary respiratory measurements

As an initial test for rate of respiration an attempt was made to measure the rate of production of ATP from the mitochondria. Standard fluorescence kits were utilised which produce a signal based upon the amount of ATP within a sample, allowing for direct measurement of the levels and thus a calculation of rate of production. For this purpose whole mitochondria were extracted from cells, initially by subcellular fractionation and later by the use of magnetic separation.

The former of these two methods is a well established methodology of separating cellular fractions, typically to isolate specific types of organelle by density, and is widely used for producing crude purifications. The disadvantage is that it is fairly nonspecific and crude method; it does not specifically select out the mitochondria, instead typically leaving a series of fractions containing significant amounts of different cellular components with around the same density (sometimes along with contaminating elements from other fractions). It also requires extensive high speed centrifugation cycles for significant lengths of time.

In comparison magnetic separation is a relatively new technique which relies upon antibodies attached to magnetic microbeads to select targets within a cell lysate and from there use a powerful magnet to extract the beads out with the target attached. By using microbeads with antibodies for a mitochondria specific protein (TOM22) it is possible to selectively extract the mitochondria from the lysate intact without relying upon high speed centrifugation that is likely to result in significantly more contamination.

Untransfected ARPE19 cells and cells transfected with the cystatin C EGFP constructs were grown in T75 flasks and mitochondria were extracted using a Miltenyi Biotec MACS Mitochondrial extraction kit. Given the selectivity of this kit this results in good recovery of intact mitochondria from cells as a high purity fraction attached to the beads from where they could be used for functional assays. The extract was quantified by BCA assay and 5 µg of protein was loaded per well on a white-bottomed 96 well plate for measurement in a luminometer.

The isolated mitochondria, supplemented with ADP and other key components of respiration, were allowed to respire in the presence of luciferin and luciferase enzyme. This resulted in a fluorescent signal produced in proportion to the level of ATP present which was measured in a plate reader over a short period of time to measure the rate of production of ATP.

No significant difference was detected between the untransfected and cystatin C transfected samples or between wild type cystatin C and variant B cystatin C transfected cells. This is presented in figure 3.4.

However this approach had a number of drawbacks. Firstly, following this work an improved method of transfection was identified, resulting in significantly better transfection rates; consequently any difference is less likely to show up in this dataset than in subsequent work. Secondly the extraction method was somewhat inconsistent with some samples containing large amounts of protein (used as a measure of relative quantity of mitochondria) and some containing very little. Finally the method was extremely volatile between readings resulting in a significant amount of variation between samples and even between technical replicates of the same sample. It is unknown if this is the result of different rate of production, of inconsistent use of the ATP by the mitochondria or of variation in the reagent itself. Another possibility was damage to the mitochondria caused by the extraction processes. A further limitation was that mitochondria had to be loaded by protein quantification, with any potential contamination from the lysate being retained having significant consequences on equal loading. Given that the measured amounts of ATP were very small this variation resulted in significant error in the results.

This preliminary study of ATP generation is valuable as a way of testing for any gross changes resulting from the overexpression of variant B protein, but not for identifying subtle changes. As a result it was decided that measuring the rate of ATP production

directly from mitochondria in this way was not the best way to approach this question and that a method utilising higher numbers of transfected cells with a more sensitive and consistent assay was needed.

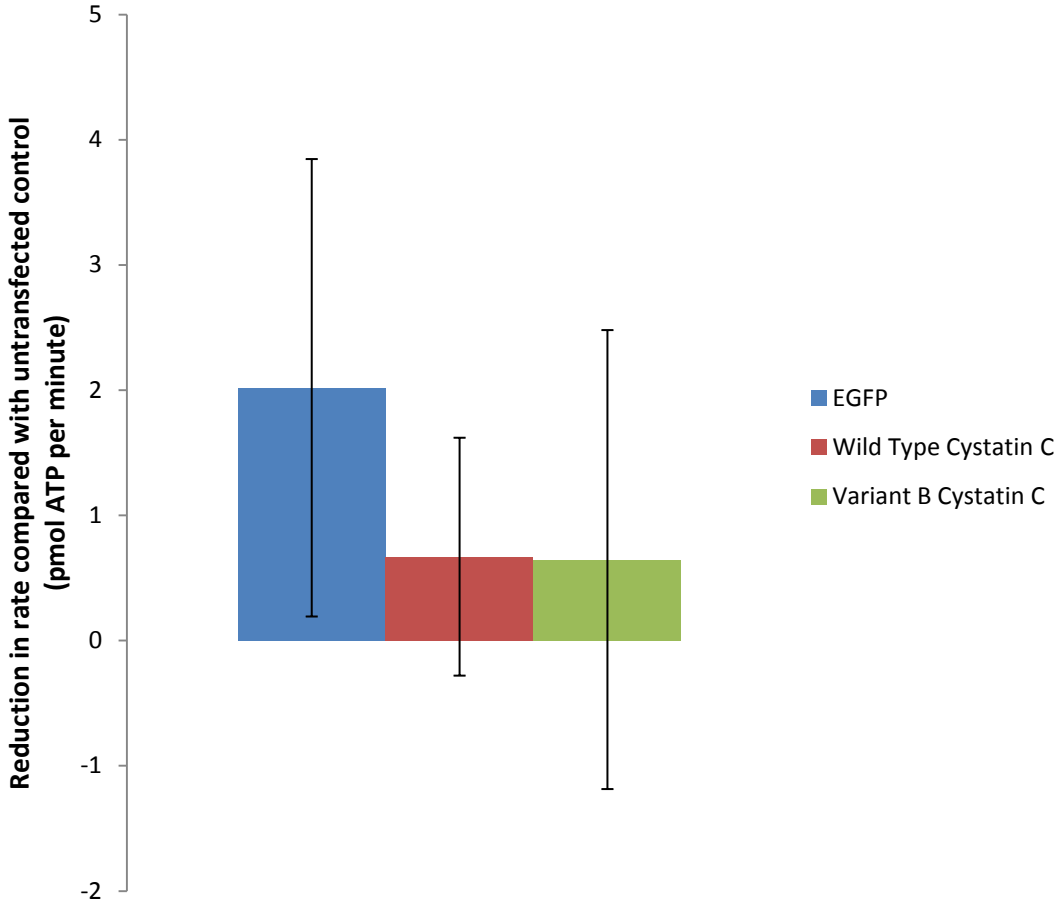

Figure 3.4 Preliminary data showing the reduction in rate of ATP production in mitochondria from ARPE19 cells transfected with pEGFP-N3 vector or pEGFP-N3 vector based cystatin C constructs. Rates were calculated from gradients of ATP concentration measurements using a bioluminescence-based ATP detection kit. Triplicate technical replicates were taken for each of 4 samples. The EGFP control demonstrated a significant difference from the untransfected control ($P<0.01$). However the wild type cystatin C and variant B cystatin C demonstrated no significant difference either from the controls or from each other. Typical transfection rates: EGFP - 35%, Wild Type Cystatin C - 15%, Variant B Cystatin C - 8%. Error bars show standard deviations.

3.3.2 Respiratory rate by oxygen depletion

The uptake of oxygen by the cells was used as an indirect measurement of the respiration rate of the cell (oxygen being a key part of the respiratory process and crucial for generation of ATP). An oxygen electrode was used to measure oxygen uptake by a discrete number of cells, normalised across samples, and the rate of uptake compared between transfected and untransfected, wild type and variant B cystatin C.

In order to ensure that the cells survived and were active for the short time of the experiment it was necessary to use an appropriate buffer that would keep the cells intact and also be compatible with the experimental system. Consequently a series of initial tests with previously used buffers were attempted, specifically a buffer previously used to assess muscle cells within the oxyprobe system. However this resulted in problems in getting the system to work as the originally recommended buffers proved to be unsuitable for RPE cells.

Subsequent testing of different buffers showed that PBS supplemented with 10 mM potassium orthophosphate and HEPES was a suitable buffer to test respiration in RPE cells. This resulted in a stable starting point and effective stable decrease in oxygen level upon the addition of cells (figure 3.5).

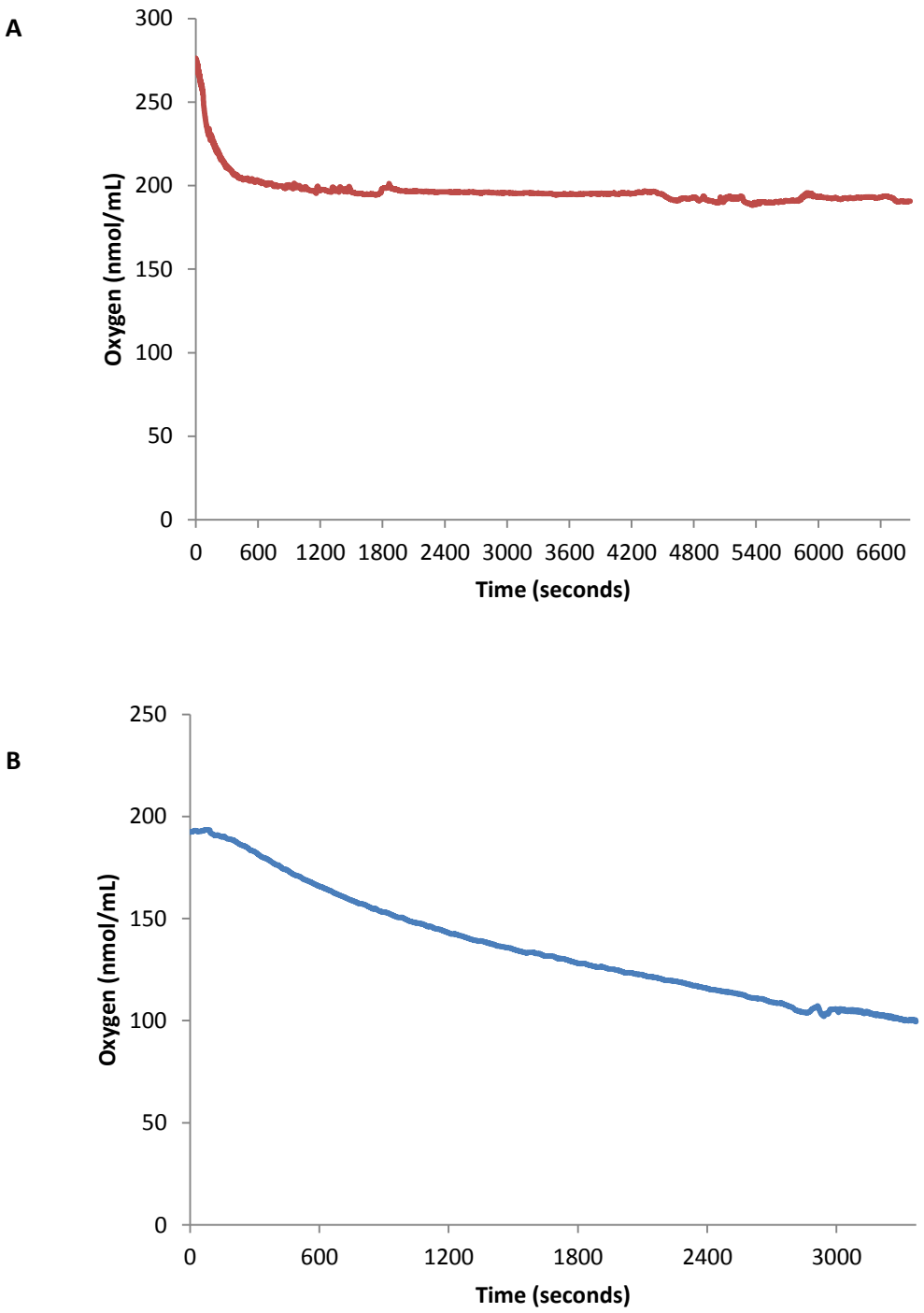

Figure 3.5 Optimisation of oxygen electrode. In **A** the establishment of a baseline for the buffer is illustrated, initially the oxygenation rate is high, however this drops to a stable level within a few minutes to around 150-200 nmol/mL. This stable level was maintained over a period of hours, confirming that any reduction in oxygen from this baseline would be due to the presence of cells. **B** illustrates the effect of adding D407 with no substrates. The rate is slower than with substrates but indicates a clear reduction in the level of oxygen present in the chamber.

This optimisation demonstrated several key factors. Firstly that the buffer allows the cells to survive in the chamber, which is a crucial step in order to conduct this experiment. Secondly that even with no supplements the cells were demonstrated to be capable of respiration. This can be attributed to reagents for the respiratory process being present within the cells already. Thirdly, that this number of cells (approximately 1 million loaded) is appropriate for producing a visible oxygen depletion readout over a short period of time. Finally that a stable rate of oxygen consumption is produced by the presence of the cells, making it suitable for comparative readings between the differentially transfected and untransfected cells. It also provides an baseline for the buffer, which is likely to vary somewhat, but can be expected to be between approximately 150 and 200 nmol/mL; with any significant departure from that baseline being indicative of a problem with the setup on any particular reading.

Trypsin harvested cells, suspended in the optimised buffer, were loaded into the oxygen probe chamber following equilibration and stabilisation of the probe. Experimental substrates glutamate, malate and ADP were added sequentially and measurements were taken over a period of no less than thirty minutes following the final addition to ensure the consistency of the decrease in oxygen concentration.

This was calculated for each sample and normalised to the untransfected control. The rate of oxygen consumption (and hence, indirectly, the rate of respiration) was expressed as a relative rate to the untransfected for each set of samples (figure 3.6). Overall very small differences were detected between the rates and no significant difference was detected between any of the samples when normalised to the untransfected control. Hence indicating that oxygen consumption is not effected as a result of either transfection or the overexpression of EGFP tag or cystatin C fusion protein constructs.

One advantage of this technique was that it allowed for whole, intact cells to be measured over time rather than isolated mitochondria, thus eliminating the difficulties of equal mitochondrial loading and improving the relevance of the measurement by using whole cells (thus preserving other intracellular processes involved). In addition it crucially allowed for the addition of supplements during the experiment, which is not possible with certain other systems (Diepart *et al.*, 2010). However there are also disadvantages of this method. As the differences themselves were very small this meant that it is quite likely that it was below the detection threshold of the sensor for significance. This is exacerbated by the fact that at least one study comparing methods of measuring consumption classified the Clark

electrode as being poor for reproducibility of results for cells, despite being a commonly used method (Diepart *et al.*, 2010). There is also the fact that Clark-type electrodes consume oxygen in the measurement process (Warkentin *et al.*, 2007), potentially effecting the results.

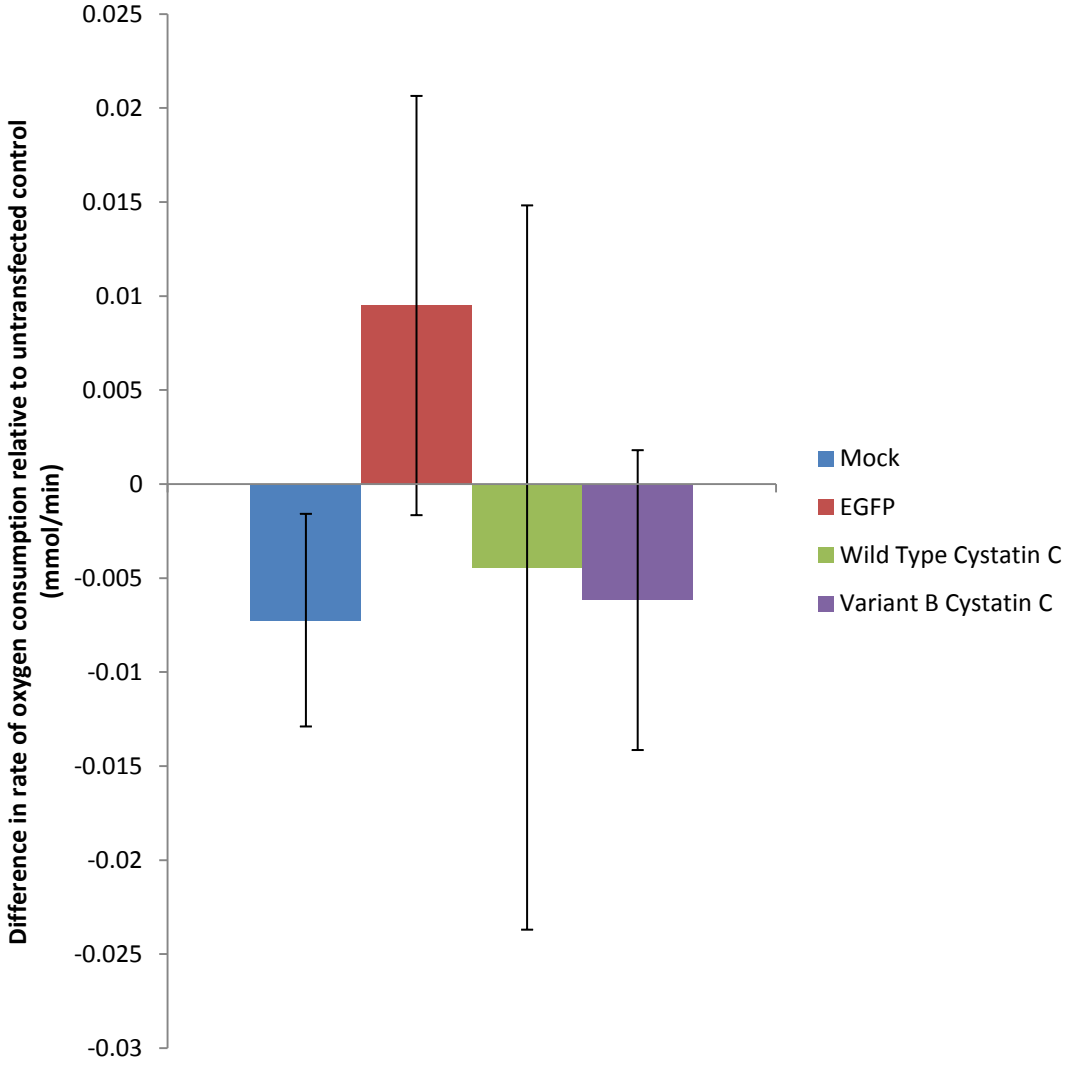

Figure 3.6 Oxygen consumption rate of D407 cells relative to untransfected control. Rate calculated from gradients of oxygen consumption following addition of all substrates. No significant difference was identified between any of the rates shown (n = 3). Mean transfection rates: EGFP - 44%, wild type cystatin C - 55%, variant B cystatin C - 53%. Error bars show standard deviations.

3.3.3 Total ATP content of cells

Total ATP content of transfected and untransfected cells was measured in order to identify the overall intracellular level of ATP as a result of overexpression of the fusion proteins. The relative amounts of ATP within the cells would indicate whether or not the ATP is being maintained within the cell at a normal level.

Optimisation of the experiment was carried out to ascertain the optimal number of cells to use (figure 3.7). Serially diluted cells were loaded into a white bottomed plate in duplicate and a Promega CellTiter-Glo ® Luminescent Cell viability assay kit was used according to the manufacturer's instructions. From this assay it was determined that approximately 40,000 cells were ideal for usage, balancing a strong signal with ease of accurate counting for loading onto the plate.

For the full experiment D407 cells were transfected with cystatin C EGFP fusion proteins and grown overnight and imaged approximately one hour before the beginning of the experiment to ensure the transfection was successful and to check the rates of transfection of each sample.

Cells were harvested utilising trypsin and counted so that a discrete number of cells could be loaded into the wells. Cells were diluted in 100 µL media and added to a 96 well white-bottomed luminescence tissue culture plates plate in triplicate for technical replicates. Relative luminescence used as a measure of relative ATP concentrations (figure 3.8).

Media by itself presented a very low level of luminescence signal, indicating negligible background to interfere with the ATP readings from the cells. No significant difference was detected between any of the transfected samples, nor was any difference detected between treated and untreated cells; indicating that the ATP levels are not significantly different under the conditions tested.

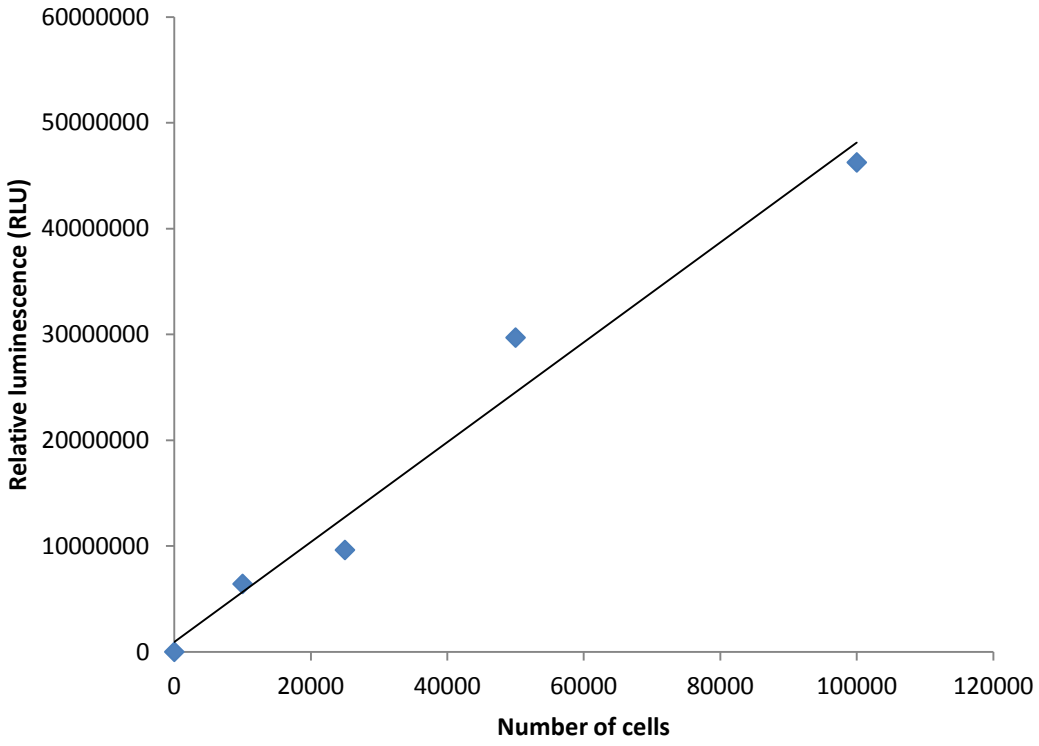

Figure 3.7 Cell number test for ATP luminescence detection. D407 cells loaded by volume after cell counting to identify concentration (n = 2). From this it was decided to load 40,000 cells per experiment. Higher numbers of cells resulted in higher readings but were more difficult to load accurately due to the limited volume of wells necessitating a very high concentration, making accurate counting difficult. Lower numbers of cells were easier to load but produced a fainter signal.

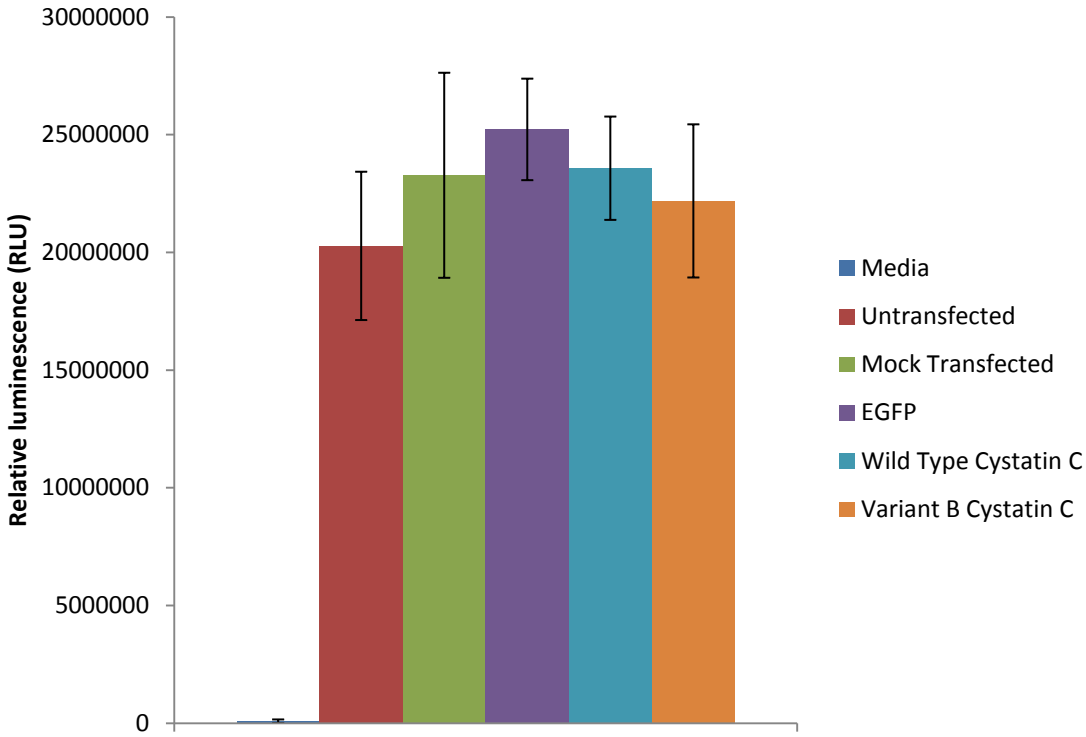

Figure 3.8 Relative luminescence for ATP content of transfected and untransfected D407 cells. Technical replicates in triplicate, n = 3. No significant difference was identified between the relative luminescence levels, and hence the relative levels of ATP in the sample, were observed between the experimental samples. Cell-free media resulted in an extremely low level of background fluorescence that is unlikely to interfere with results. Mean transfection rates for samples were: EGFP - 38%, wild type cystatin C - 31%, variant B cystatin C - 24%. Error bars are standard deviations.

3.4 Apoptosis

Prior experiments indicated that the presence of variant B protein might lead to cleavage of caspase 3 and consequently the activation of the caspase apoptotic pathway. However the visual appearance of transfected cells was healthy, not dying, which seemed to contradict this. Caspase 3 is a crucial protein in both primary caspase-based apoptotic pathways and is therefore a key point to test for general apoptotic activation.

Although there was a distinct lack of visible signs of cell death it may simply be that there is a very low level of apoptotic activation; which could potentially lead into interference with normal cell processes. Consequently western blots were carried out on transfected and untransfected samples in an attempt to confirm this prior result.

D407 cells were transfected with the pEGFP-N3 vectors and grown overnight. Cell lysates were taken and the lysates subjected to western blot analysis. Commercially purchased Jurkat cell lysates were used as controls for caspase-3 cleavage. Lysates were equally loaded by protein content and successful transfer to the membrane was confirmed by Ponceau S staining.

The transfection of D407 cells, with either construct, and the subsequent expression of cystatin C fusion proteins was not found to cause detectable levels of active caspase 3. The uncleaved pro-caspase 3 protein was clearly detectable in all samples indicating that caspase 3 was indeed present. However cleaved caspase 3 was only detectable in chloroquine-treated Jurkat cells (used as a positive control for the active form of the protein) and, as such, there is no evidence for cleaved caspase 3 in the samples.

This indicates that the caspase 3 apoptotic pathway has not been activated by the presence of the cystatin C protein. This contradicts the previous preliminary experiments however it is consistent with microscope observations of transfected cells compared with untransfected cells. Specifically there is no noticeable indications when inspected visually which would be expected from increased levels of apoptotic activity (figure 3.10). Note, however, that this experiment is specific to the involvement of caspase 3 mediated apoptotic activity.

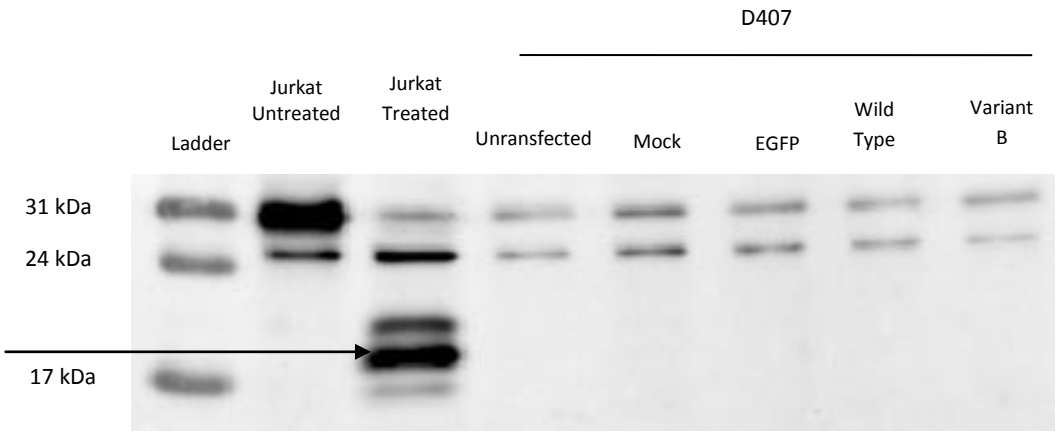

Figure 3.9 Caspase 3 probed blot of D407 lysates transfected with EGFP, wild type cystatin C fusion protein and variant B cystatin C fusion protein. Commercially available Jurkat control lysates were used as positive and negative controls (9663S, New England Biolabs). Lower molecular weight fragments (as seen for the positive control, Jurkat treated with cytochrome C to induce apoptosis) indicate the cleavage and thus activation of the apoptotic pathway. The samples lacked these low molecular weight fragments showing activated caspase 3, instead only presenting uncleaved bands similar to the negative control (untreated Jurkat cell lysate). D407 samples normalised to total protein content.

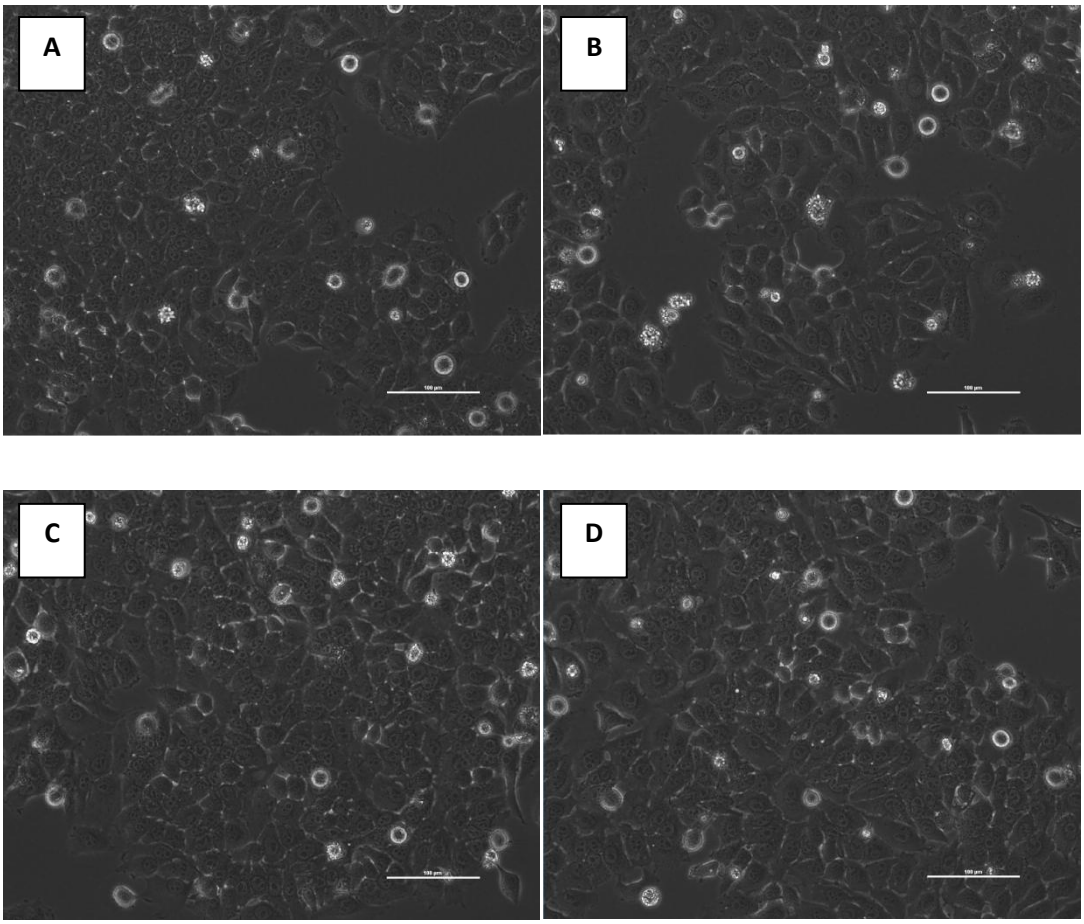

Figure 3.10 Bright field images of untransfected and transfected D407 cells. A, D407 cells seeded at the same time as **B**, **C** and **D**. **B**, D407 cells 24 hours post transfection with EGFP producing plasmid. **C**, D407 cells 24 hours post transfection with cystatin C wild type-EGFP fusion protein. **D**, D407 cells 24 hours post transfection with cystatin C variant B-EGFP fusion protein. Scale bars are 100 µm. There was no visually apparent effect of the transfection upon the cells which may indicate increased apoptosis, no obvious increase in dead cells or cell debris. Cells adhered well to the flask and grew to form the monolayer with cobblestone appearance characteristic of RPE cells (as can be seen beginning to form in patches on each image).

3.5 Autophagy

The autophagic process was assessed by use of an autophagic marker protein, the B isoform of protein Light Chain 3 (LC3B). This is a marker of autophagy due to its presence in the membrane of autophagocytes.

Specifically this protein is found within the cytosol in a particular form known as LC3B-I. Through the autophagic process LC3B-I is converted to LC3B-II via lipidation and is incorporated into the membranes of autophagic vesicles. As a result of this LC3 has been established as a marker for autophagic vesicles and the ratio between the two forms can be used as a simple indicator for changes in autophagy.

D407 cells were transfected with the EGFP plasmid constructs and grown for 24 hours. Following transfection, cells were examined by microscope for the successful uptake of plasmid, media was removed and the cells lysed for western blotting. SDS-PAGE followed by western blot analysis was carried out using an LC3B specific antibody (Cell Signalling Technologies, #2775) which detects both forms of the protein (figure 3.11).

The ratio between the two bands for each sample was calculated as an indicator of levels of autophagosomes, which acts as an indicator of disruption to the autophagic process. Although it does not indicate if this is due to increased production of autophagic vesicles or decreased clearance. These ratios were normalised to the untransfected control ratio in each set in order to correct for any variation between sets of samples resulting from any slight variations in conditions.

An increase in the number of autophagic vesicles was detected in transfected cells compared to untransfected and mock transfected cells, and for mock transfected cells compared to untransfected cells (figure 3.12). As this increase was also detected in the EGFP transfected samples and a smaller increase in the mock transfectant it appears that this increase is due to the effect of transfection on the cell and is not because of the presence of cystatin C, either wild type or variant B. Consequently this implies that under the experimental conditions tested there is no effect specific to the variant B protein on the number of autophagosomes present. Although this does not provide specific information on the rate it does highlight that there appears to be no specific disruption.

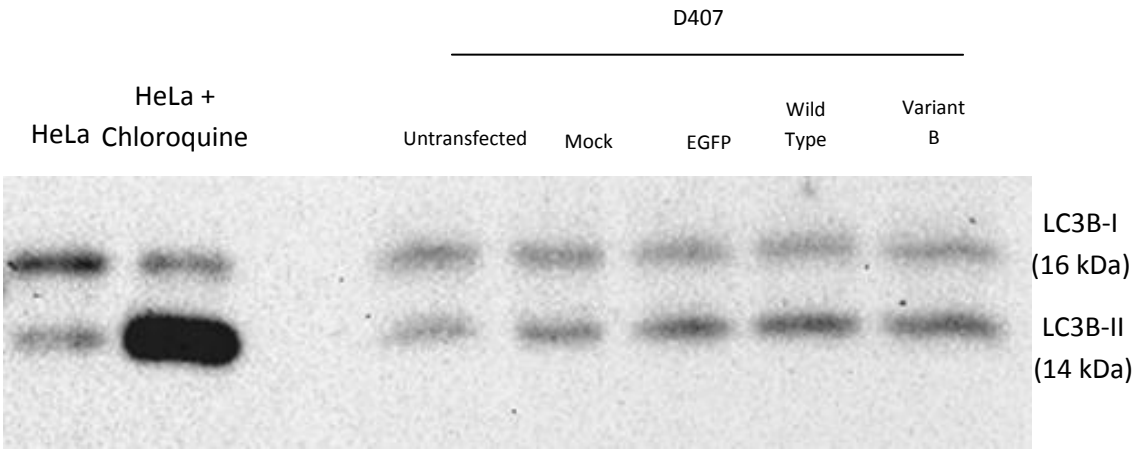

Figure 3.11 Sample western blot of autophagic marker LC3B in D407 cell lysates. HeLa was used as a control cell line, with untreated HeLa acting as a negative control and choloroquine-treated HeLa (50 µM of chloroquine overnight) used as a positive control for the LC3B-II form of the protein. An increase in the -II form was clearly visible resulting from the chloroquine treatment. Readings were taken of both the LC3B-I and LC3B-II bands and the ratio between the two calculated. The HeLa samples were valuable only as controls as their ratios could not be used to compare with the D407 ratios as LC3B ratios cannot be used to compare different cell lines since expression levels can differ greatly.

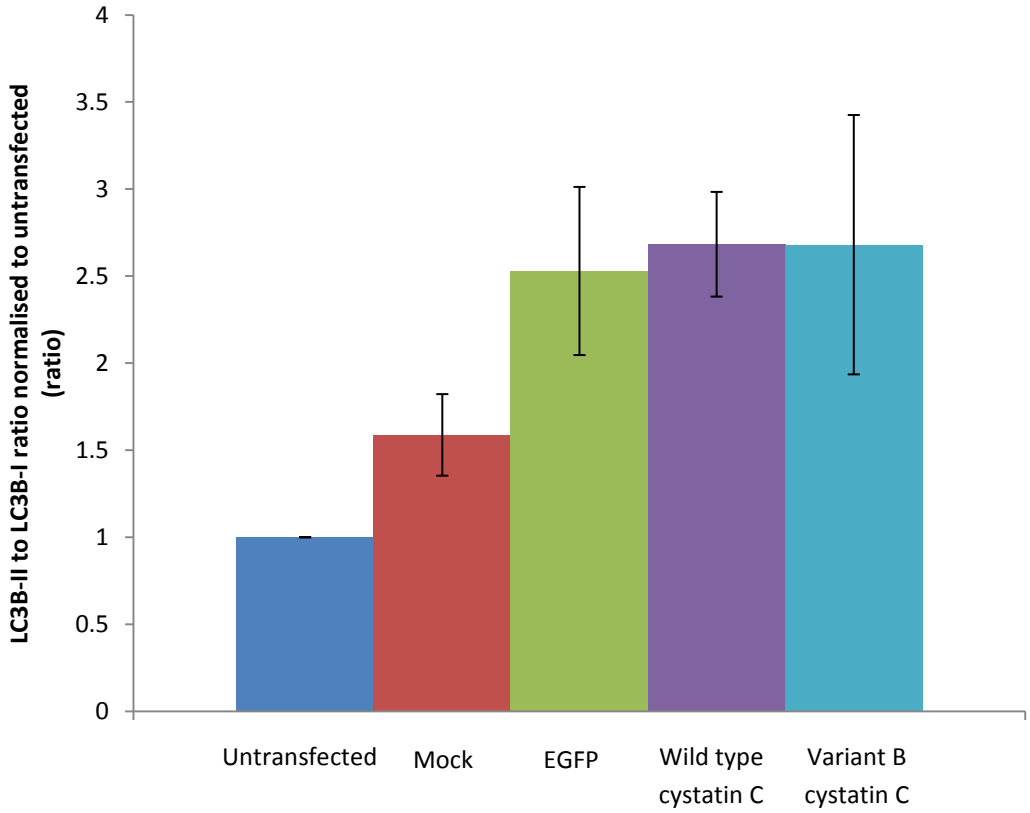

Figure 3.12 LC3B ratios as an autophagy marker for D407 transfected and untransfected cells. Ratios were normalised to untransfected sample in each experimental set in order to minimise variability between sets resulting from slight variations in conditions. Ratio is LC3B-II to LC3B-I, with a higher value indicative of increased numbers of autophagic vesicles within the cell. All samples treated with transfection reagent have statistically significantly higher ratios ($P < 0.01$) than the untransfected samples. EGFP and wild type cystatin C have statistically significantly higher ratios ($P < 0.05$) than the mock transfection, with variant B cystatin C close to significance ($P = 0.07$). Transfection rates were: EGFP - 47%, wild type cystatin C - 45%, variant B cystatin C - 24%. Error bars are standard deviations.

3.6 Oxidative stress

Oxidative stress is of great significance for cells in the eye, particularly the RPE. Oxidative stress is typically due to the production of reactive oxygen species which are highly reactive molecules with the potential to react with intracellular proteins.

Oxidative stress has a number of potential causes in cells. In particular it can be caused by the generation of reactive oxygen species by the mitochondria. The process of respiration involves the use of oxygen, resulting in significant amounts of oxygen in the cell concentrating at the mitochondria and the subsequent formation of reactive oxygen species. This results in the mitochondria themselves being particularly at risk from oxidative stress-related damage and, further, that cells with large numbers of mitochondria are at greater risk.

Consequently, analysis of the effect of variant B cystatin C protein on intracellular oxidative stress levels through reactive oxygen species measurements was a high priority for this study. CellROX® Deep Red dye combined with flow cytometry was the method selected after comparison with other techniques. This allowed for the specific selection of fluorescent cells, producing meaningful data on any relationship between the expression of the proteins and the extent of oxidative stress. It also allowed for a comparison to be drawn between the fluorescent cells in a sample and the nonfluorescent cells, thus providing a control inherent in each individual sample which helps to correct for any potential variation in uptake of the dye.

For untransfected samples, approximately 10,000 cells were measured. For transfected samples a minimum amount of transfected cells was used as a parameter for measurement; specifically this was 5,000 cells after 24 hours and 2,000 cells after five days. This difference is due to the decrease in transfection over this period of time, necessitating a smaller count due to significantly larger amounts of cells needing to be counted in order to obtain a sufficient amount of readings. The population of cells following harvesting was largely uniform and single celled, although a small population of duplets or clusters was also present, these were eliminated from the analysis. Following treatment and harvesting, cells were kept on ice suspended in PBS with 2% FCS until they could be analysed.

Untransfected cells typically clustered with very low levels of green fluorescence and a clear red fluorescence indicating that the staining was successful. In transfected samples a

substantial untransfected population displayed similar characteristics to that of untreated cells however a significant number of cells displayed green fluorescence.

A low level of increased green autofluorescence was detected in a fraction of a percentage (less than 0.1%) of the untransfected cells with corresponding increases in the oxidative stress marker, likely cellular debris. For transfected samples a significantly larger percentage of the sample displayed strong fluorescent signal.

Twenty four hours post transfection there is an increase in oxidative stress apparently resulting from the transfection reagent (figure 3.13). This can be clearly seen by comparing the statistically significantly higher red fluorescent signal of the oxidative stress dye in the mock transfectant samples with the low reading in the untransfected sample. The data from the plasmid transfectants suggests that the effect only occurs in cells which have been treated with the transfection reagent but not taken up a plasmid; although the data for this is not statistically significant for all three transfected samples there is a clear pattern visible in the readings.

Five days post transfection (four days growth in normal media with no transfection reagent) results in the loss of this increase in oxidative stress for the mock sample over the untreated sample. The presence of EGFP likewise displays no effect on the oxidative stress of the cell compared to untransfected cells from the same sample. However both wild type cystatin C and variant B cystatin C fusion protein transfectants display statistically significant increases in oxidative stress over the untransfected cells within the same sample (figure 3.14).

The advantages of this assay were that individual cells were measured to make up a population, hence providing large numbers of data points. Further given the difference in the wavelengths of the dye there was little chance of cross-contamination of signal. However disadvantages included the background level of fluorescence potentially interfering with results plus the large drop-off in transfection rate after five days. This necessitated a huge number of counts to gain sufficient transfected cell counts for analysis meaning the untransfected counts for these are significantly larger than other counts. In addition particularly low-fluorescence transfected cells may be mixed with untransfected readings.

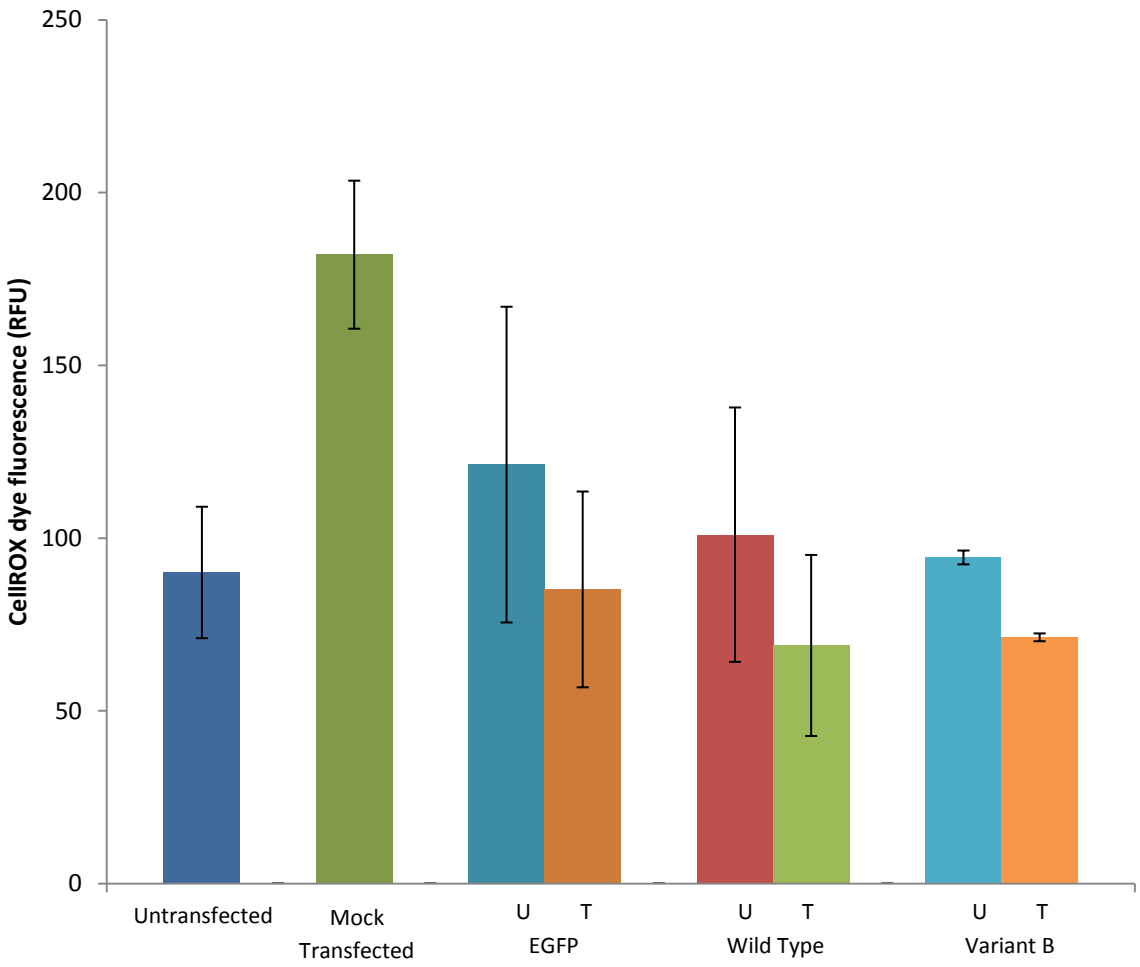

Figure 3.13 Mean oxidative stress in transfected (T) and untransfected (U) D407 cells treated with CellROX oxidative stress dye, 1 day post-transfection. Transfections either with just EGFP or with EGFP-tagged Wild Type or Variant B cystatin C. By t-test the mock transfected cells were statistically significantly more fluorescent, hence having more oxidative stress, than the untransfected cells ($P < 0.01$), as were the untransfected cells from the variant B sample compared to transfected cells from the same sample ($P < 0.01$). Approximately 5000 transfected cells were measured for each transfected count and a minimum of approximately 5000 untransfected cells for untransfected measurements. Error bars show standard deviation.

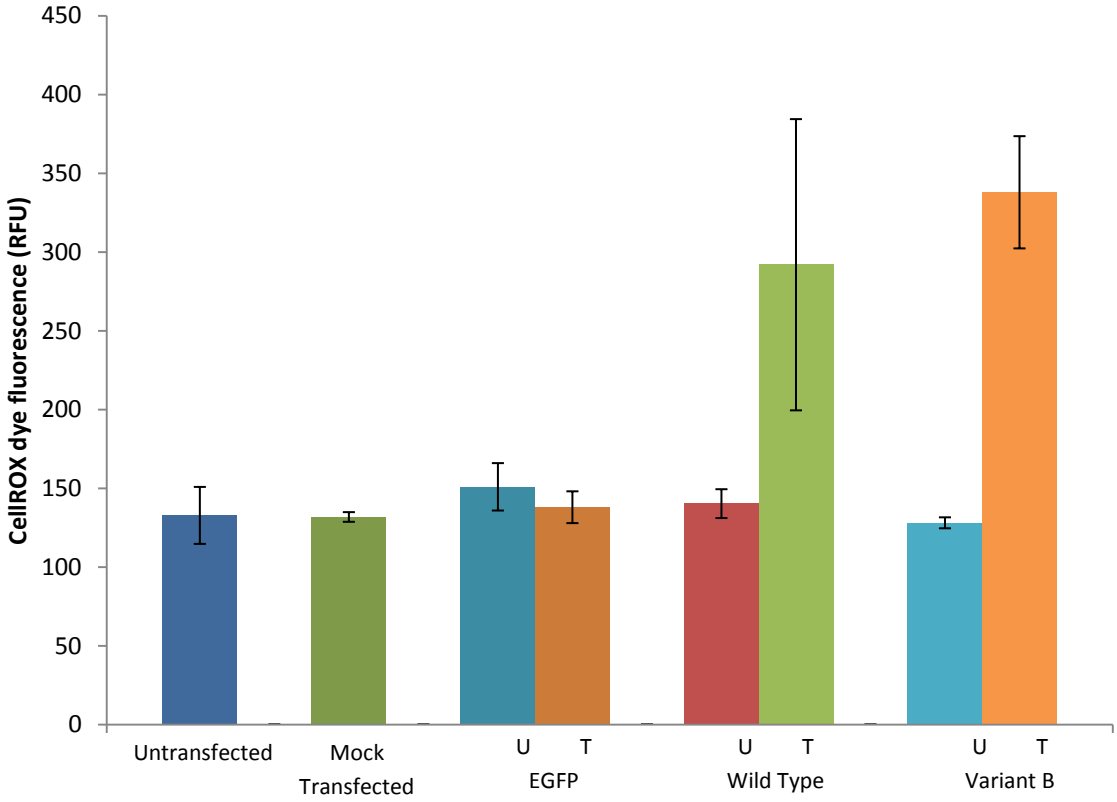

Figure 3.14 Mean oxidative stress in transfected (T) and untransfected (U) D407 cells treated with CellROX oxidative stress dye, 5 days post-transfection. By t-test the differences between the EGFP transfected and untransfected cells in the same sample are insignificant (P=0.2834), the respective differences for Wild Type (P=0.0474) and Variant B (P=0.0005) are significant, but the difference between transfected Wild Type and Variant B is not significant (P=0.4665). Approximately 2000 transfected cells were measured for each transfected count and at least approximately 10,000 cells for untransfected measurements (however many more were recorded for the untransfected cells in the transfected samples due to loss of transfection by this time). Error bars show standard error.

Chapter 4

Protein-protein interactions:

mass spectrometry analysis

4.1 Introduction

In addition to the functional tests which were used to assess possible ways in which the variant B protein could cause intracellular effects compared with wild type protein it was decided that the intracellular protein-protein binding partners of cystatin C would also be assessed. This would provide a starting point for additional future work exploring the intracellular interactions of variant B cystatin C.

Of particular interest are interacting proteins with the potential for involvement in how it is transported (if at all) to the mitochondria, how the mislocalisation with the mitochondria occurs (through any interactions with mitochondrial proteins) and how it might affect intracellular processes (thus potentially leading to the development of AMD). In order to achieve this, mass spectrometry was selected for the purpose of identifying and analysing interacting proteins.

Mass spectrometry allows for high precision identification of proteins. By utilising immunoprecipitation techniques it is possible to specifically select out a target protein and its interacting partners from a mixed solution of proteins and then to identify those interacting proteins. This has the distinct advantage over western blot screening of IP samples in that all of the proteins within a sample can be identified, without having to guess at possible interactions and subsequently probe for them.

For this study both wild type cystatin C and variant B cystatin C fusion proteins have been immunoprecipitated, HaloTag with no linked protein was used as a control for nonspecific interactions. Mass spectrometry analysis was then performed on the immunoprecipitated samples by the University of Liverpool Proteomics service.

4.2 Preparation and optimisation

4.2.1 Production of new plasmid constructs

One option for mass spectrometry analysis was to simply use the existing EGFP constructs for pull-down and isolation of cystatin C as well as any interacting proteins. However this suffered from a number of potential limitations and disadvantages.

Firstly, contamination resulting from the denaturing of antibody itself can prove to be a problem. The traditional process for protein pull-down necessitates the use of an antibody it is typically performed using an antibody for the target in combination with protein A or protein G linked to agarose beads. Specifically, incubating a sample (such as a cell lysate) with the antibody for the protein desired followed by an incubation with protein A or protein G agarose slurry which links to the first antibody and allows the protein to be pulled down by centrifugation. However this leads to large amounts of antibody fragments after elution as the antibody is released along with the proteins.

Consequently it is preferable to perform the mass spectrometry with a selection method that is directly attached to the beads or column being used. This allows for the elimination of the majority of the ligand or antibody in question. Traditionally this has involved either using antibody covalently attached to beads or by producing and using a His tag construct which is recoverable due to its affinity for certain metal ions (nickel, cobalt and copper, with cobalt being the most specific).

Secondly , contamination from the target protein can disrupt results. When attempting to identify proteins bound to a particular target proteins by this method large amounts of the target protein remain in the sample. This results in a huge signal for the target protein with the potential to interfere with the results. Further, if the target protein is capable of binding to itself this is more difficult to identify.

For the purpose of carrying out mass spectrometry analysis a new cystatin C construct was produced. To address the two disadvantages detailed above a new type of tag was selected, known as HaloTag® (Promega). HaloTag® is a versatile way to tag proteins at either terminus which forms covalent bonds with proprietary ligands which allows it to be used as a flexible and highly specific way to select for the protein in question. This results in the tagged protein becoming permanently bound to the ligand, thus preventing it from detaching upon elution in the process of immunoprecipitation. Consequently ensuring that the sample eluted consists only of those proteins that are bound to the target tagged protein and not ligand fragments or excessive amounts of tagged protein which may overwhelm the sample.

The new construct was produced by amplifying the cystatin C wild type and variant B genes out of the existing EGFP constructs using primers incorporating appropriate restriction

digest sites for its insertion into the Halotag plasmid. From there the target plasmid and the amplified cystatin C were digested to allow for insertion and ligated together (figure 4.1).

Transformation into bacteria followed by followed by colony picking on selective media allowed for the selection of bacteria containing the appropriate plasmids. Three colonies from each transformation were selected from the original agar plates and all three grew successfully when streaked onto selective media agar plates. Two of each of these three selected colonies for each clone were found to have successfully taken up the plasmid, as verified by plasmid extraction and agarose gel electrophoresis demonstrating a clear band of DNA present at the correct size (figure 4.2).

The success of the insert and the integrity of the plasmid was confirmed by restriction digest agarose DNA gels and by DNA sequencing. In addition the capability of Halotag ligands to bind to the plasmid construct and to confirm expression of the protein construct intracellularly was tested using a fluorescent TMR ligand to check for the presence of protein within transfected cells compared with untransfected cells.

HaloTag® only transfection resulted in a cell-wide glow however the plasmid constructs presented with a localised glow. Localisation for wild type and variant B constructs was as per the EGFP constructs. As with the EGFP tagged protein it was necessary to attach Halotag to the C-terminus of the protein to ensure the tag remains following cleavage of the targeting sequence at the N-terminus.

A

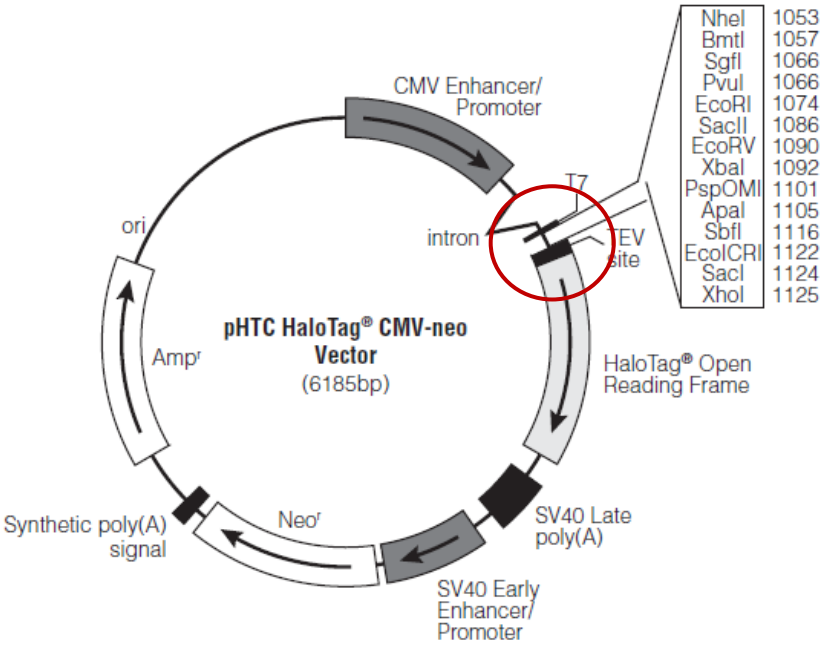

B

GCTAGCAAAGCGATCGCTTCC**GAA|TTC**CTACCGCGGATATCTAGATTTGGGCCCAATTCCT

GCAGGCGAGCT**CTC|GAG**

C

GCTAGCAAAGCGATCGCTTCC**GAATTC**ATGGCCGGGCCCCTGCGCGCCCCGCTGCTCCTGC

TGGCCATCCTGGCCGTGGCCCTGGCCGTGAGCCCCGCGGCCGGCTCCAGTCCCGGCAAGC

CGCCGCGCCTGGTGGGAGGCCCCATGGACGCCAGCGTGGAGGAGGAGGGTGTGCGGCG

TGCACTGGACTTTGCCGTCGGCGAGTACAACAAAGCCAGCAACGACATGTACCACAGCCG

CGCGCTGCAGGTGGTGCGCGCCCGCAAGCAGATCGTAGCTGGGGTGAACTACTTCTTGGA

CGTGGAGCTGGGCCGAACCACGTGTACCAAGACCCAGCCCAACTTGGACAACTGCCCCTTC

CATGACCAGCCACATCTGAAAACGAAAGCATTCTGCTCTTTCCAGATCTACGCTGTGCCTTG

GCAGGGCACAATGACCTTGTCGAAATCCACCTGTCAGGACGCC**CTCGAG**CCAACCACTGA

GGATCTGTACTTTCAGAGCGATAACGATGGATCCGAAATCGGTACTGGCTTTCCATTCGAC

CCCCATTATGTGGAAGTCCTGGGCGAGCGCATGCACTACGTCGATGTTGGTCCGCGCGAT
GGCACCCCTGTGCTGTTCCTGCACGGTAACCCGACCTCCTCCTACGTGTGGCGCAACATCAT
CCCGCATGTTGCACCGACCCATCGCTGCATTGCTCCAGACCTGATCGGTATGGGCAAATCC
GACAAACCAGACCTGGGTTATTTCTTCGACGACCACGTCCGCTTCATGGATGCCTTCATCGA
AGCCCTGGGTCTGGAAGAGGTCGTCCTGGTCATTCACGACTGGGGCTCCGCTCTGGGTTTC
CACTGGGCCAAGCGCAATCCAGAGCGCGTCAAAGGTATTGCATTTATGGAGTTCATCCGCC
CTATCCCGACCTGGGACGAATGGCCAGAATTTGCCCGCGAGACCTTCCAGGCCTTCCGCAC
CACCGACGTCGGCCGCAAGCTGATCATCGATCAGAACGTTTTTATCGAGGGTACGCTGCCG
ATGGGTGTCGTCCGCCCGCTGACTGAAGTCGAGATGGACCATTACCGCGAGCCGTTCCTG
AATCCTGTTGACCGCGAGCCACTGTGGCGCTTCCCAAACGAGCTGCCAATCGCCGGTGAGC
CAGCGAACATCGTCGCGCTGGTCGAAGAATACATGGACTGGCTGCACCAGTCCCCTGTCCC
GAAGCTGCTGTTCTGGGGCACCCCAGGCGTTCTGATCCCACCGGCCGAAGCCGCTCGCCTG
GCCAAAAGCCTGCCTAACTGCAAGGCTGTGGACATCGGCCCGGGTCTGAATCTGCTGCAA
GAAGACAACCCGGACCTGATCGGCAGCGAGATCGCGCGCTGGCTGTCTACTCTGGAGATT
TCCGGT

Figure 4.1 HaloTag® construct insert schematic. A shows the complete map of the HaloTag® plasmid used (From Promega pHTC HaloTag® CMV-neo Vector Product Information sheet, 9PIG771), the red circle highlights the multiple cloning site. **B** is the full sequence of the multiple cloning site with the EcoRI cutting site highlighted in red and the XhoI cutting site highlighted in blue. **C** is the full sequence for the multiple cloning site and HaloTag® sequence with the ligated cystatin C wild type inserted, which is highlighted by underlining. Yellow highlights the C-terminal HaloTag® sequence.

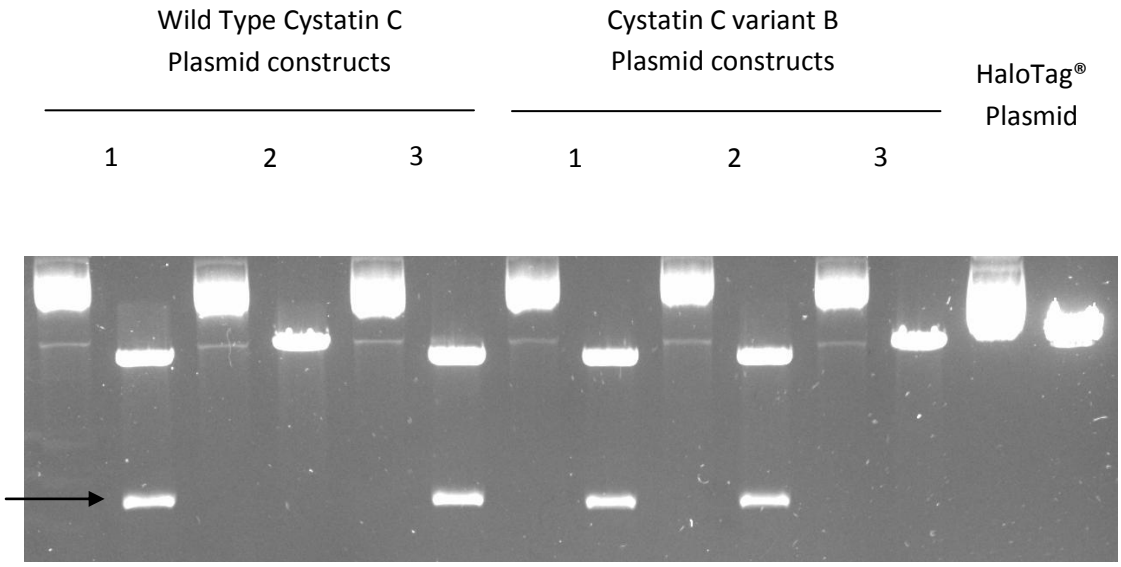

Figure 4.2 Restriction digest of Halotag constructs to confirm insert. Each sample consists of an uncut plasmid for reference and a plasmid cut with EcoRI and XhoI to demonstrate the presence of the cystatin insert. Not all plasmids successfully took up cystatin C as can be seen in wild type cystatin C sample 2 and variant B cystatin C sample 3 where only the cut band of the plasmid is visible with no insert. The cystatin C band is marked with an arrow . HaloTag® plasmid cut is provided for reference.

4.2.2 Optimisation of protein pull-down

In order to ascertain the differences and similarities between the interactions of variant B cystatin C and wild type cystatin C it was necessary to carry out a protein pull-down. This allowed for the specific isolation of cystatin C and any bound proteins from the cell lysates and consequently for the identification of said bound proteins through the use of mass spectrometry.

Protein pull-down was carried out utilising a Halotag Mammalian Pull-down kit (Promega). Attempts were made to pull-down samples from multiwell tissue culture plates. However this resulted in a relatively low amount of protein precipitated from the samples. Hence, this proved to be insufficient for our purposes and consequently experiments were scaled up significantly.

Success was eventually achieved utilising T75 flasks. These produced a large pellet of cells for lysis and processing. Subsequent protein pull-down of these optimisation samples resulted in clear protein bands on SDS polyacrylamide gels detected by silver staining which were indicative of successful pull-down of proteins. The method proved to be highly effective resulting in a sufficient amount of interacting proteins for mass spectrometry analysis.

Initially the kit was used as recommended by the manufacturer, however the elution buffer contained within the kit was SDS-based. This was judged to be inappropriate for use in a mass spectrometer as it would interfere with the column and contaminate results, potentially damaging the machine.

An alternative elution buffer, RapiGest (Waters) was tested. The results of this in comparison with SDS elution were clearly visible on silverstained SDS gels (figure 4.3). This resulted in a significantly lower amount of protein being visible, with significantly fainter bands present compared with SDS elution. However bands were still present for both samples indicating that both methods were successful in eluting protein from the beads.

Despite the lower quantity of elution of protein with RapiGest compared with an SDS buffer it was decided that it is nevertheless preferable to carry it out directly in RapiGest. This is due to the fact that SDS elution would require the sample to be cleaned of SDS, the most likely method of which would be to run the sample on an SDS-PAGE gel and extract from

said gel. By doing this there would not only be an extra, lengthy, step in the processing of the sample before the mass spectrometry itself but it is also likely that a significant amount of protein would be lost in the process. Furthermore it was possible that certain proteins would be lost due to the relatively small amounts of the protein in the sample in the first place. The consequent loss of protein through the extra steps would likely result in more lost in the extra step than gained through the more efficient elution from beads by using this buffer. As a result, although not as efficient, RapiGest elution was the best option available.

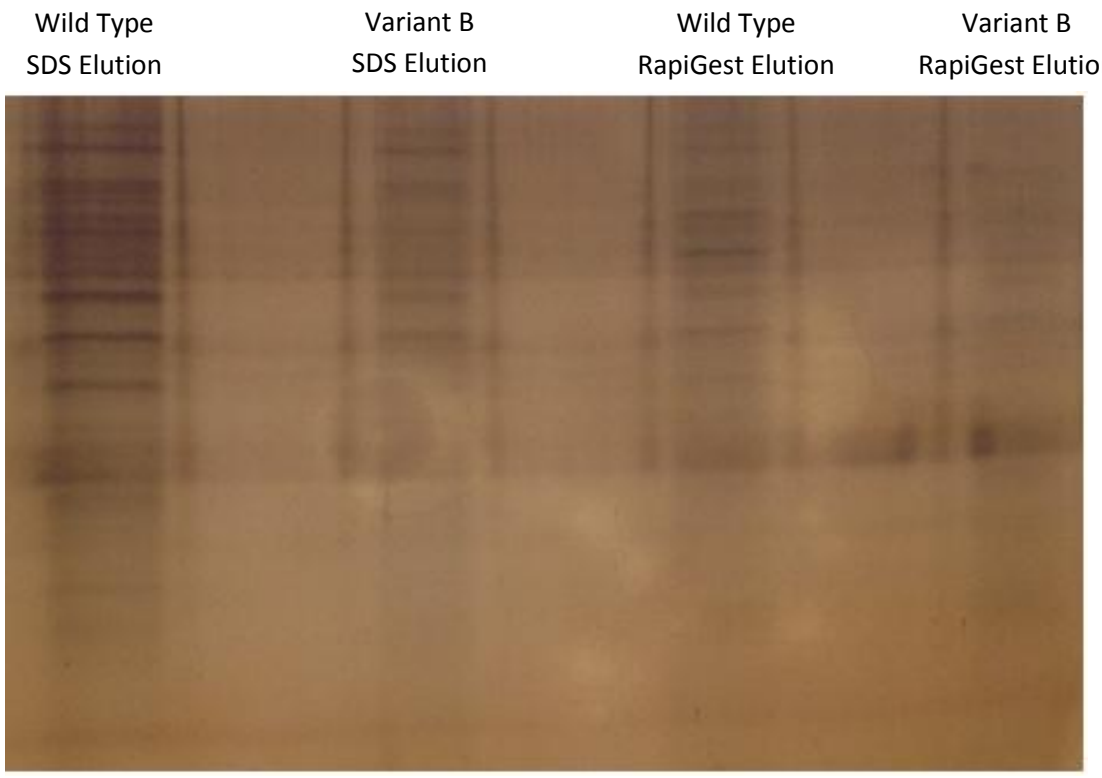

Figure 4.3 Silver stain of Halotag protein pull-downs with different elution buffers. T75 lysed and HaloTag pulled-down before resin separated into two tubes for elution by two different methods. Each lane is therefore approximately half a T75 of pulled down protein. SDS elution was more successful than RapiGest elution, however both methods presented bands for both of the constructs.

4.2.3 Preliminary mass spectrometry

An effective extraction and elution technique for the HaloTag® constructs utilising a mass spectrometry appropriate elution buffer was thus established. Following this a preliminary mass spectrometry analysis run was attempted. This was to simultaneously provide a starting point for mass spectrometry analysis and to ensure that the overall technique was capable of producing effective mass spectrometry results.

The backbone HaloTag® plasmid by itself was usedas a control for nonspecific binding of Samples were analysed by the University of Liverpool Proteomics facility and results were returned as spectral counts with associated Mascot searches for each data file (courtesy of Dr Deborah Simpson).

Mascot searches were compared to identify proteins unique to either the wild type cystatin C or variant B cystatin C as an initial mass spectrometry analysis (given the n=1 nature of this preliminary run and the sole utilisation of spectral counts it cannot be used by itself to draw conclusions on differences). These are presented in Table 4.1 with details of potential involvement in aspects of interest to this study.

This preliminary run confirmed the validity of the methods used and, more importantly, confirmed that results could be obtained even with the lower protein concentration resulting from RapiGest elution. Consequently the decision was made to continue with full mass spectrometric analysis of lysates.

Table 4.1 Preliminary mass spectrometry analysis by spectral counting, unique proteins. A complete list of all proteins identified in the preliminary mass spectrometry as only being present in either variant B cystatin C pulled-down samples or wild type cystatin C immunoprecipitated samples. Proteins which were found to be present in both were excluded, as were those proteins for which spectra were identified in the HaloTag®-only control. Included are accession numbers, name and a brief overview of potential relevance to this study.

Accession	Protein	Potential relevance to AMD/cystatin C/mitochondria	Cystatin specific to
P02774	Vitamin D-binding protein	Unknown, found on cell surfaces and associates with immunoglobulin and IgG on lymphocytes.	Variant B
P38646	Stress-70 protein, mitochondrial	Implicated in cell proliferation and ageing. May act as a chaperone.	Variant B
P05141	ADP/ATP translocase 2	Involved in exchange of ADP from cytoplasm with ATP in mitochondria across inner membrane.	Variant B
P35232	Prohibitin	DNA synthesis inhibitor, involved in cellular proliferation. May be involved in regulating mitochondrial respiration and ageing.	Variant B
P02647	Apolipoprotein A-1	Involved in protein aggregation. Associated with Alzheimer's disease.	Variant B
P53634	Dipeptidyl peptidase 1	Protease. Strongly inhibited by cystatin C.	Variant B
P07360	Complement component 8	Unknown. Involved in complement cascade. Note: Many other complement components detected in both. Likely to not be highly relevant.	Wild Type

P01023	Alpha-2-Macroglobulin	Unknown. Inhibits proteinases by a unique mechanism – a stretch of peptides containing cleavage sites for different proteinases. Protein becomes trapped when cleaves the site. Entrapped enzyme remains active against low molecular weight substrates.	Wild Type
P01019	Angiotensinogen	Unknown. Regulator of blood pressure, body fluid and electrolyte homeostasis. Serine endopeptidase inhibitor.	Wild Type
P0C0S5	Histone H2A.Z	Unknown. Chromatin structural protein. Note: Other histones detected in both. Likely to not be highly relevant.	Wild Type
Q6NXT2	Histone H3.3C	Unknown. Chromatin structural protein. Note: Other histones detected in both. Likely to not be highly relevant.	Wild Type
P08779	Keratin type I cytoskeletal 16	Unknown. Structural component of cytoskeleton. Note: Other keratins detected in both. Likely to not be highly relevant.	Wild Type
P02538	Keratin type II cytoskeletal 6A	Unknown. Structural component of cytoskeleton. Note: Other keratins detected in both. Likely to not be highly relevant.	Wild Type
P00739	Haptoglobin-related protein	Unknown. Homologous to serine proteases but has no enzymatic activity.	Wild Type

4.3 Protein interaction analysis

Following the demonstrated success of the method triplicate samples were produced and treated as for the preliminary experiment, using RapiGest buffer for elution, and transferred to the University of Liverpool Proteomics facility for analysis.

Data was returned as both spectral counts and as raw and normalised abundances subjected to ANOVA analysis. Mascot (Matrix Science) and Progenesis QI (Nonlinear Dynamics) had been used to analyse the mass spectrometry raw output. The processing of samples through mass spectrometry and the subsequent analysis of the raw data through these programs was done by Dr Deborah Simpson of the Centre for Proteome Research, University of Liverpool.

Of the two analysis methods, ion abundance is more sensitive than spectral counting (Milac *et al.*, 2012). However both have been used in the examination of the dataset and selection of proteins for discussion.

Full details of normalised abundances are presented in Appendix Table 1 along with ANOVA p-values, complete spectral counts are presented in Appendix Table 2 with confidence scores for reliability of identification. In total 185 proteins were identified as being present in the samples and those with the most significant differences were chosen as a set for further analysis.

4.3.1 Significant results by ANOVA analysis

From ANOVA analysis of the full mass spectrometry data set eight proteins appeared to have significant differences either against the control or between the wild type and variant B. These are presented in Table 4.2 with their normalised abundances in each sample. Individual unpaired t-test values for each of the three pull-downs are presented in Table 4.3.

The first three proteins listed were expected to be significant binding partners, and help to validate the approach by their presence. Cathepsins B and L along with dipeptidyl peptidase 1, also known as cathepsin C, are known inhibitory targets for cystatin C and their presence indicates the effective pull-down of cystatin C bound proteins. Each of them demonstrated

a statistically significant, or close to statistically significant, higher presence in normalised abundancy in cystatin C transfected samples compared with the HaloTag control samples. Further, spectral counts were uniformly zero for the control samples but counts were present for cystatin C samples. There was no identified difference between wild type and variant B cystatin C samples for cathepsins B and L in either spectral counts or normalised abundance. However a significant difference was detected for dipeptidyly peptidase I in the spectral counts, with a higher level detected for wild type cystatin C.

It is worth noting that for the cathepsins in each case the wild type value from set 2 that is particularly low. Eliminating that value as a potential outlier brings all three to $P < 0.05$ significance level in normalised abundance, demonstrating a statistically significantly higher level of abundance in the wild type samples.

The fourth protein is 78 kDa glucose-regulated protein, individual t-testing indicates this is significantly increased in variant B cystatin C binding compared to the control plasmid. Spectral counting indicated a significant increase for both wild type and variant, as well as a close to significant difference between the two with wild type cystatin C being higher. As for the cathepsins, eliminating the single lowest abundance from the wild type dataset resulted in a statistically significant difference in abundances between the two.

Cystatin C itself is also present on this list. Given that the fusion protein should not be able to detach from the bead based ligand it seems likely this is the result of the formation of dimers. There is a statistically significant difference ($P<0.01$) in spectral counts between wild type cystatin C and the control, but no other differences.

Prohibitin displays a very strong statistically significant normalised abundancy increase ($P < 0.01$) in variant B cystatin C compared with wild type cystatin C. Further there is a close to significant increase in binding to variant B over the control.

Both leucyl-cystinyl aminopeptidase and stress-70 protein display a similar normalised abundancy pattern to the cathpsins with respect to differences in variant B and wild type cystatin C binding. Namely elimination of an apparent outlier (all from the same set, notably) of wild type cystatin C readings results in statistically significant higher levels in the wild type form ($P < 0.05$).

Table 4.2 ANOVA significant results of mass spectrometry Halotag pull down ion abundances for Halotag, Wild Type Cystatin C-Halotag fusion and Variant B Cystatin C-Halotag fusion transfected D407. Table shows those proteins with an ANOVA P-value of <0.05. These are the normalised ion abundances from the mass spectrometry output.

Accession	Protein	Halotag Normalised abundance			Wild Type Normalised abundance			Variant B Normalised abundance			ANOVA (P=)
P07711;Q5NE16	Cathepsin L1	13113.03	48227.11	40417.78	3533291	734520.6	4277290	1098944	1036262	2798111	0.000793
P07858	Cathepsin B	86042.56	62776.73	73531.79	4362367	1006305	4940636	1435178	615334.4	2405779	0.001136
P53634	Dipeptidyl peptidase 1	27491.31	157320.1	52984.53	8593620	1301101	11220991	852512.1	285743.6	1178349	0.00384
P11021;O95399	78 kDa glucose-regulated protein	78167.37	294317.7	55676.82	7384152	911581.5	14463609	979188	637926.2	1398130	0.010751
P01034	Cystatin-C	76287.66	151379.5	86871.38	5340401	1911358	37207228	341471.9	289242.5	2858737	0.011564
P35232	Prohibitin	39491.17	60223.67	36007.04	41333.37	26046.57	35478.42	68523.07	60103.76	80632.52	0.021159
Q9UIQ6	Leucyl-cystinyl aminopeptidase	39372.51	53683.88	44553.74	3754831	99494.74	2320624	43164.89	82493.12	68016.2	0.033988
P38646	Stress-70 protein, mitochondrial	22874.29	67301.2	20673.51	900229.3	99261.2	720731.3	122446.6	242889.6	37965.08	0.048722

Table 4.3 Individual T-test values for paired comparisons between differently transfected cells for ANOVA indicated significant proteins (Table 4.2). Cathepsins found in wild type and variant B transfected samples are significantly or close to significantly higher than those found in the Halotag control sample. Prohibitin displays a very statistically significant difference between wild type and variant B cystatin C and a close to significant difference between variant B cystatin C and the control. Confidence score for the mass spectrometry result is included, indicative of reliability of identification of protein in question.

Accession	Protein	Mass Spectrometry Confidence Score	Halotag-Wild Type T-test (P=)	Halotag-Variant B T-test (P=)	Wild Type-Variant B T-test (P=)
P07711;Q5NE16	Cathepsin L1	645.5	0.059456919	0.049304905	0.380727736
P07858	Cathepsin B	784.36	0.051830837	0.052599005	0.21662346
P53634	Dipeptidyl peptidase 1	1143.68	0.078935255	0.058378623	0.10322176
P11021;O95399	78 kDa glucose-regulated protein	2620.78	0.129978739	0.02070666	0.168435252
P01034	Cystatin-C	1210.91	0.260533842	0.280220256	0.292267756
P35232	Prohibitin	199.85	0.27987545	0.063515872	0.008851566
Q9UIQ6	Leucyl-cystinyl aminopeptidase	1265.14	0.131358	0.200991494	0.134066929
P38646	Stress-70 protein, mitochondrial	1072.19	0.092001209	0.187372088	0.153761031

4.3.2 Other notable protein readings

Presented here are several observations on proteins that were not detected as significant by ANOVA analysis but may be of potential interest. The complete data set can be seen in Appendix 1, for complete ion abundance data and spectral count data.

Despite the significant difference in binding for prohibitin there was no detected corresponding difference between wild type cystatin C and variant B cystatin C in normalised abundances for prohibitin-2 ($P = 0.11$). Nor was there any detectable difference in level from the control sample.

A close to significant difference was detected between the wild type and variant B samples for voltage-dependent anion-selective channel protein 1, with variant B seeming to bind more strongly ($P = 0.067$). Removal of an apparent outlier (approximately three times higher than either of the other two) also resulted in a significant difference between the variant B sample and the HaloTag® control sample ($P < 0.05$).

Heat shock protein beta-1 is nearly absent in spectral counts from the control and variant B samples, however it is clearly present in the wild type samples. Removal of an apparent outlier (as for cathepsin) brings normalised abundance differences between wild type and variant B samples close to significance ($P = 0.062$).

Finally, calmodulin-like protein 3 is close to significantly higher in wild type samples over variant B samples ($P = 0.063$). Removing an apparent outlier from each of the control and wild type results in the wild type being significantly higher than either ($P < 0.01$).

4.3.3 Summary

Mass spectrometry analysis produced a wealth of data on potential intracellular binding partners for cystatin C. The presence of cathepsins, well known cystatin C targets, served to support the integrity of the dataset.

In particular prohibitin is a stand out result from this dataset, with a significantly higher amount of this protein bound to variant B cystatin C compared with either the control or wild type cystatin C. With its high binding capability and very high significance it appears to be an excellent candidate for future studies.

Chapter 5

Discussion

5.1 Overview of results

This study sought to address two major investigative lines, both of them relating to variant B cystatin C. First was the aim of examining some of the major intracellular processes which may be influenced by the presence of the variant B protein. Second was the nature of variant B interactions within the cell, specifically proteins it binds to and how they may relate to RPE cellular mechanisms implicated in AMD pathology.

In the first instance the processes examined were respiration, apoptosis, autophagy and oxidative stress. Respiration was assessed by total ATP content and by oxygen depletion utilising an oxygen probe to give an indirect measure of the respiratory rate of the cells. Autophagic change was assessed by quantification of relative levels of the two forms of the autophagy related protein LC3B, a change being indicative of a change in the number of autophagosomes and consequently disruption to the normal rate of autophagy. Apoptosis was assessed by the activation of caspase-3, a crucial protein in the caspase cascade and the cleavage of which is necessary for activation, based on preliminary data indicating cleavage.

Oxidative stress was measured by flow cytometry and use of the CellROX® oxidative stress indicator dye. This allowed for cell-wide levels of reactive oxygen species (ROS) to be assessed in large populations of cells, indicating the level of oxidative stress. A statistically significant increase in ROS was detected 5 days post transfection in D407 cells transfected with wild type cystatin C and variant B cystatin C as evidenced by increased fluorescence of the indicator dye.

In the second instance the protein interactions were assessed by mass spectrometry of protein pull-downs. The proteins specifically bound to cystatin C (both wild type and variant B) constructs were isolated and assessed for significant differences in rate of binding to the two forms of the protein as well as compared to a background level of nonspecific binding. A number of significant proteins were identified as binding partners specifically for wild type cystatin C, variant B cystatin C or both. Some of these, such as prohibitin, are of particular interest and may prove to be starting points for very valuable future work.

5.2 Respiration

5.2.1 Overexpression of EGFP or cystatin C-EGFP fusion protein does not significantly affect the rate of respiration

It was of significant importance to check whether the simple act of overexpressing cystatin C would result in changes by itself. The constructs available all overexpress the fusion proteins by means of the CMV promoter in order to guarantee large amounts of the protein in question in an attempt to trigger any effects associated with their expression. This overexpression results in a significant amount of cystatin C being present within the cell, in excess of normal physiological conditions.

Oxygen is used at a specific rate in the respiratory process as the final acceptor for the electrons from the electron transport chain. Consequently it can be used as an indirect measure of the respiratory process. Specifically by measuring the decreasing level of oxygen within a chamber it is possible to indirectly compare the relative rate of respiration between samples.

This oxygen probe data for the overexpression of wild type cystatin C, chapter 3.3.2, presented no significant change in the rate of depletion of oxygen, indicating no increase or decrease in rate of respiration, compared with untransfected samples. Consequently neither the vector itself, nor the overexpression of cystatin C causes an effect on the rate of production of ATP.

This was an expected outcome given the nature of the constructs. The wild type form of cystatin C enters the secretory pathway and is passed out of the cell (Paraoan *et al.*, 2001), it is not known for being specfically mitochondrially localised and as such it seemed unlikely that even high levels of the protein would result in blocking of this specific process. Further, the EGFP protein by itself is distributed throughout the cytoplasm upon expression; again, giving no reason to expect any effect upon the mitochondria.

It is worth noting that, although this data indicates that cystatin C has no direct regulatory involvement in the respiratory process in cells, there is some evidence in published studies to suggest that there is an indirect link between cystatin C and the respiratory processes. More specifically it has been noted that growing cancer cells in hypoxic conditions (1% oxygen) leads to the down-regulation of cystatin C and an elevated level of cathepsin B,

with the effect being greater in metastatic tumour cells (Wickramasinghe *et al.*, 2005), linking cystatin C with hypoxia-enhanced tumour progression. Consequently it is possible that disruption of respiration, and thus alteration of normal oxygen levels, could result in the normal cellular responses being altered by the presence of the variant B gene, given the apparent link between oxygen levels and cystatin C expression.

5.2.2 Rate of respiration is not significantly altered by variant B cystatin C

Given the association with the mitochondria the respiratory process was one possibility by which the protein could interfere with normal cellular processes; with the protein mislocalisation having the potential for interactions with one or more of the proteins involved in the process such as ATP synthase or part of the electron transport chain. Alternatively, assuming no direct interaction with the proteins, the increased concentration of protein around the mitochondria might itself interfere with the process.

The reduction of ATP production capacity in the presence of an age-related protein has precedent in the form of A2E, a well established component of lipofuscin which is itself a hallmark of ageing (Lamb & Simon, 2004). Recent studies have established that growing cells in the presence of A2E inhibits the production of ATP (Saadat *et al.*, 2014).

Using this method no significant difference was identified in the rate of respiration between cells transfected with wild type protein or variant B protein. Further, as for the wild type cystatin C and EGFP proteins, no significant difference was found between transfected and untransfected cells. This indicates two major points.

Firstly it indicates that the variant B cystatin C protein does not interfere with the respiratory process. This is key, as it provides evidence against respiration being the a major source of disruption in the RPE, or indeed in other cells, contributing to disease resulting from variant B cystatin C. Given the high energy requirements of RPE cells it would be expected that degradation of respiration would result in significant negative effects on the cells. The apparent lack of such effects is unsurprising and supportive of a more subtle effect on the cellular functions.

Secondly, it suggests that variant B cystatin C does not bind with part of the respiratory pathway to an extent sufficient to have a detrimental effect to the process. The variant B

protein is highly mitochondrially located, however it is not known how this occurs. If it were to be via the proteins of the respiratory process it might be expected that there would be a detrimental effect on the normal functioning of this process given the presence of the variant B protein. Since this is evidently not the case it suggests that this is unlikely to be the primary way by which variant B protein associates with the mitochondria.

In summary these results indicate that although reduced ATP production is a feature of ageing in cells, variant B cystatin C does not appear to induce a change on the respiratory process of RPE cells. Nor does it seem that binding to parts of the respiratory pathway the cause of variant B's mislocalisation to the mitochondria.

5.2.3 Total cellular ATP content is not significantly altered by cystatin C wild type or cystatin C variant B overexpression

In addition to the rate of ATP production, data on the total ATP content of cells was presented in chapter 3.3.3. Although the rate of production is important and more informative with respect to the effect of variant B cystatin C protein given its mitochondrial localisation it was also desirable to take distinct measurements of cellular ATP content. This allows for the overall state of ATP within the cell to be monitored. More specifically although the oxygen depletion may indicate whether or not it is being produced at the same rate, only direct ATP measurements can inform whether it is also being consumed at the same rate.

Overall no significant difference was demonstrated between any of the treated samples or the controls, indicating that the ATP content within the cells is stable. These findings support the previous observation that there is no change in rate whilst simultaneously indicating that there is no effect on the usage of ATP, or at least not one that could be detected with luciferase assay.

Given the variety of cellular processes that use ATP this is crucial. Further it has recently been established that a decrease in the cellular levels of ATP (such as occurs with ageing) can result in increase vulnerability of the cells to damage (Schütt *et al.*, 2012). As the levels are not altered as the result of cystatin C variant B protein expression this provides evidence to help rule this out as a method of action.

5.3 Apoptosis

5.3.1 Caspase 3 is not activated by the presence of cystatin C variant B

Despite indications of involvement of cystatin C in apoptosis from the literature, the variant B cystatin C protein does not appear to result in increased levels of caspase 3 activation. The RPE cells were not noticeably unhealthy from visual inspection of transfected cells and were not dying off in a way that suggested a pro-apoptotic role for the variant.

Further there was no indication of activation of the caspase 3 protein as a result of the overexpression of cystatin C or of the expression of variant B cystatin C. Cleavage of pro-caspase 3 to its active form is a crucial linked step in the process of activation of the apoptotic pathway by both intrinsic and extrinsic pathways. If there were any activation of the apoptotic machinery through these pathways it would therefore be expected to result in the activation of caspase-3.

Overall these results seem to preclude the involvement of variant B cystatin C in the induction of apoptosis as a key process by which it could be acting. It is unknown why preliminary results indicated that this might be the case but the results presented here appear to be more expected in light of the variant B involvement in AMD as a progressive degenerative disease rather than an acute disease involving mass cell death.

To clarify AMD is characterised by the degradation of the retina with a build up of deposits and neovascularisation through Bruch's membrane and into the photoreceptor layer, largely limited to the macular region. It does not involve mass cell death of RPE cells and consequently it would seem unlikely that mass triggering of apoptosis as a result of a faulty gene product would be the cause.

Although this experiment indicates that there is no activation of caspase-3 in this incidence it does not contradict indications that apoptosis may be a contributory process for the progression of degenerative disease. This experiment has focussed specifically on whether variant B triggers apoptosis in a healthy cell line, however it may be that apoptosis is a late event in such degeneration and thus is outside the scope of this experiment.

5.4 Autophagy

5.4.1 Levels of autophagosomes are not changed by the presence of variant B cystatin C

Our data indicates that cystatin C does not appear to induce autophagic change in the RPE cells of the eye. However this method of autophagy detection has its limitations. Optimally for autophagy the autophagic flux should be measured. Although LC3B ratios can inform that there is a change in autophagy it provides no information specific to the rate (and, indeed, may miss a rate change if both production and clearance are changed to the same degree).

However this result is indicative that there is no disruption to the overall process as a whole which would lead to increased numbers or a build up of autophagosomes. Consequently this suggests that variant B does not influence autophagy within RPE cells.

This is perhaps somewhat surprising. Autophagy is a crucial process in the RPE, disruption of which has been associated with processes such as damage by A2E (Saadat *et al.*, 2014) and increased susceptibility to oxidative stress (Mitter *et al.*, 2014). Further, cystatin C has recently been implicated in having a protective role in autophagy in neuronal cells (Tizon *et al.*, 2010; Gauthier *et al.*, 2011) .

It may be theorised that although there is no overall change in levels of autophagosomes indicating the disruption of specific stages of the process resulting in autophagy imbalance, there may be an effect on the rate of the process as a whole, without creating an imbalance within said process. Given the implication of cystatin C in mTOR signalling by Tizon *et al.* (2010) it cannot be ruled out that disruption of normal cystatin C levels could lead to effects upon autophagy overall, without changing the number of autophagosomes.

Given the lack of flux data autophagy cannot totally be ruled out as a contributory process. However the data presented here indicate that its involvement is less likely than the literature on cystatin C and autophagy would imply. Consequently although it is not to be ruled out, this study suggests that autophagy may not be the most valuable line of investigation.

5.5 Oxidative stress

5.5.1 Overexpression of wild type cystatin C and variant B cystatin C results in an increase in oxidative stress within the cell

The overexpression of cystatin C results in a significant increase in oxidative stress in the D407 RPE cell line over untransfected cells. This effect was not observed with either mock transfected cells or EGFP only transfected cells, consequently indicating that the effect is due specifically to cystatin C and not in response to the transfection reagent or to the EGFP tag (or, by association, by the simple act of protein overexpression with this vector).

There was no indication of a significant difference between the variant B and wild type forms of the protein. This seems to indicate that the presence of cystatin C within the cell is sufficient in itself to cause the increase in oxidative stress; which implies that this is a simple artefact of overexpression of cystatin C.

However, it is important to note is that the plasmid constructs lead to the overexpression of the proteins in question. As a result there is a far higher concentration of even the wild type protein compared with in vivo conditions. Hence this simple explanation may not be indicative of what is occurring.

More specifically, the high level of expression results in a high concentration of cystatin C intracellularly; from western blots on cell lysates it is known that there is a large amount of cystatin C fusion protein within the cells even with the wild type cystatin C construct as a result of the CMV promoter. Consequently even without the mitochondria specific localisation it seems highly possible that the very high levels of wild type cystatin C have resulted in a build up within the cell, the secretory mechanisms unable to clear the protein as effectively.

This results in a potential explanation and avenue worthy of further examination. Specifically that the intracellular accumulation of cystatin C over time can result in increased levels of oxidative stress. In the case of variant B cystatin C its impaired secretion results in this accumulation occurring more rapidly and increasing risk of degeneration resulting in the association with AMD as reported by Zurdel *et al.* (2001).

Although speculative, this hypothesis matches both the oxidative stress results in this study and with literature on both cystatin C variant B and with oxidative stress in relation to

ageing and AMD. There is evidence throughout the literature to suggest that cystatin C has a protective role in oxidative stress induced cell death in neuronal cells (Nishio *et al.*, 2000; Nishiyama *et al.*, 2005) and that it is regulated by oxidative stress in the RPE (Alizadeh *et al.*, 2006) suggesting its role as an oxidative stress response. Consequently the suggestion that inappropriate cellular processing and retention within the cell of cystatin C, such as in the case of variant B cystatin C, could result in disruption ofoxidative stress regulation is highly plausible.

Further work is needed to confirm or refute this hypothesis. However it represents an intriguing proposal with the potential to go some way to explaining how variant B cystatin C leads to increased levels of oxidative stress in RPE cells. A process which has been implicated in AMD.

5.6 Mass Spectrometry

5.6.1 General observations on results

One of the immediately obvious patterns in the mass spectrometry data is the significant number of different keratins within the sample. Which may lead to the conclusion that keratins are of particular importance, however that would be in error. Keratins are a very common contaminant of mass spectrometry samples, typically resulting from skin and hair. More specifically dust in a laboratory is likely to be keratin and it can settle from the atmosphere onto glassware and plasticware consequently resulting in contamination. Every effort was made in this procedure to avoid this form of contamination, minimising it, however this results in the keratins present in the sample being unlikely to be of any experimental interest.

Variation between replicate samples is difficult to avoid, even with every care being taken to ensure that samples have been produced identically. Indeed, due to inherent variability in the process samples measured multiple times on an instrument in the same way each time can vary noticeably. Samples were run sequentially through the same column on the same day in order to minimise any difference however there is still a significant amount of variation, enough to call into question certain individual readings. This means that it has been essential to individually examine proteins of interest to check for outliers and to compare individual values. A limitation of this is that this analysis may miss a potential protein of interest, although care has been taken to select a number of the most crucial results for discussion.

Finally, both the spectral counts and normalised abundances are of value for analysis. Although the normalised abundance is the more sensitive of the two (Milac *et al.*, 2012) the spectral counts are also useful both for comparison and to draw attention to proteins which have been overlooked in abundance, as determined by ANOVA analysis, due to outlying values.

5.6.2 Cathepsins are bound at an increased level by wild type cystatin C compared with variant B cystatin C

Cathepsins are well established as inhibitory targets for cystatin C, in particular cathepsins B, H, L and S (Barret, 1986; Turk & Bode, 1991) as well as dipeptidyl peptidase I, also known as cathepsin C (Nicklin & Barrett, 1984). Cathepsins are proteases which have been linked with aggregation based age related diseases including age related macular degeneration (Im & Kazlauskas, 2007) and Alzheimer's disease (Kaur & Levy, 2012; Yamashima, 2013). As a specific example, cathepsin B is known to degrade human amyloid-β in mice, amyloid-β being a key (Wang *et al.*, 2012).

Mass spectrometry confirms the interaction of wild type cystatin C protein with cathepsins B, L and C; this serves both as a confirmation that the fusion protein can effectively bind to its normal target and demonstrates that the mass spectrometry process is working appropriately. Further, the variant B form of the protein also binds to the cathepsins to a statistically significant extent, demonstrating that despite the difference in amino acid sequence it is still capable of activity. Which is to be expected as the secretion is only reduced as a result of the mutation, not eliminated (Paraoan *et al.*, 2004) and the change is within the targeting sequence, not within the mature protein.

After removing an apparent outlier there is also a statistically significant difference in the level of binding to cathepsins between variant B cystatin C and wild type cystatin C. It is difficult to say, however, whether this difference is due to an instability in binding (which seems unlikely as the amino acid change is in the targeting sequence, not in the mature protein) or due to its misassociation with other proteins and the mitochondria. This reduced binding seems to be consistent with the expected characteristics of the fusion proteins. Specifically wild type cystatin C passes through normal processing pathways within the cell and binds with cathepsins. Variant B cystatin C passes through this route at a reduced level as a result of its retention and localisation to the mitochondria.

Consequently although the level is reduced it seems unlikely that this is a result of disrupted ability of the mature form of each protein to bind. Instead it is more likely that the difference in level of binding is simply due to more wild type cystatin C being processed appropriately and thus more cystatin C is present in locations where it can bind with cathepsins than variant B cystatin C which has reduced processing given the mislocalisation.

5.6.3 Prohibitin

5.6.3A Overview

Prohibitin is a widely expressed protein known to be translated from chromosome 17q21 (Sato *et al.*, 1992). It consists of a 272 amino acid protein chain which associates with prohibitin-2 protein. It has been found in a wide variety of species, with homologues of the gene present in mammals, *Drosophila*, *C. elegans*, plants and yeast (Coates *et al.*, 1997).

Originally the protein was thought to be of significance in cellular proliferation as a suppressor protein and in tumour suppression as well as potential roles in cell senescence (Nuell *et al.*, 1991; Liu *et al.*, 1994; McClung, 1995). However it was later demonstrated that its antiproliferative activity appears to be localised to the 3' UTR of the gene and consequently it is believed that the RNA, rather than the protein, acts as a regulatory element. The protein itself has been implicated in processes such as apoptosis (Fusaro *et al.*, 2003) and as a molecular chaperone (Nijtmans *et al.*, 2000)

Prohibitin was found to be mitochondrially localised, originally this was identified using immunofluorescence on tagged protein expressed in hamster kidney cells as far back as 1995 (Ikonen *et al.*). It is found in the mitochondria as a large complex consisting of two subunits with a ring-like structure located at the mitochondria's inner membrane, targeted there by noncleavable targeting sequences in the N-terminal of the proteins (Tatsuta *et al.*, 2005). It seems to be of importance in both the production of new mitochondria and the normal metabolic functions of mitochondria as well as acting as a molecular scaffold (Nijtmans *et al.*, 2000; Tatsuta *et al.*, 2005).

In addition prohibitin has become known as being involved in oxidative stress. Most relevant for our purposes is the recent discovery of its involvement in oxidative stress in the eye. More specifically it has been found that prohibitin is translocated between mitochondria and the nucleus and consequently it seems to be an early signalling event for oxidative stress in the RPE and the retina (Lee *et al.*, 2010).

As a result of the above, prohibitin seems a plausible candidate for involvement with variant B cystatin C protein. Its involvement with the mitochondria, as well as numerous processes implicated in the disease, make it highly relevant to this study.

5.6.3B Variant B Cystatin C interacts with Prohibitin protein significantly more than wild type cystatin C does

From the mass spectrometry analysis it is apparent that the variant B form of cystatin C interacts with prohibitin to a statistically significantly higher level than the wild type form. This is the singular most striking result from the whole of the mass spectrometry dataset, with a very strong statistical significance level.

This presents numerous implications for the understanding of variant B cystatin C. Firstly, as a mitochondrial-associated protein the high level of binding of the variant to it immediately suggests that this is a possible cause of the mitochondrial localisation. In addition it has been established that prohibitin can be found and bind to proteins within the nucleus (Wang *et al.*, 2002; Fusaro *et al.*, 2003). This, combined with its mitochondrial specific targeting sequence, raises the intriguing possibility that it is the binding of variant B cystatin C with this protein that leads to the mitochondrial targeting resulting from the mutation. This hypothesis is speculative, but it provides a potential explanation for both the mistrafficking to the mitochondria and its apparent retention there.

5.6.3C Variant B Cystatin C does not interact with Prohibitin-2 at a significant level

In contrast with its partner protein, the mass spectrometry data does not indicate a statistically significant difference between the interactions of variant B cystatin C and wild type cystatin C with respect to their interaction with prohibitin-2. The lack of binding suggests that the binding is specific to the prohibitin subunit and may even inhibit the formation of the complex. This is a potential explanation for a way in which variant B protein disrupts normal cellular functioning however there is no additional data available to draw a conclusion from these observations.

5.6.4 Voltage-dependent anion-selective channel protein 1

Voltage-dependent anion-selective channel protein 1 is a protein found in the outer mitochondrial membrane and also in the plasma membrane of cells (Lawen *et al.*, 2005). In mitochondria it provides a channel through which small molecules can diffuse (Colombini, 1979) and is the major pore-forming protein (Lawen *et al.*, 2005). In particular it is a major pathway through which metabolites including ADP/ATP, succinate and citrate are exchanged (Benz, 1994).

The higher rate detected in binding of the variant B cystatin C and wild type cystatin C as well as the statistically significant difference from the HaloTag® control suggests that this may be another mitochondrial protein responsible for variant B's localisation. Extensive binding of cystatin C to a crucial pore protein such as this might be assumed to block its function. However our findings on respiration suggest that this is unlikely, as restricted exchange of crucial metabolites would be expected to lead to a disruption of the respiratory process.

Interestingly VDAC has recently been implicated in superoxide diffusion from the mitochondrial intermembrane space and consequently in the role of oxidative stress in relation to the mitochondria. Specifically dihydroetheidium oxidation was observed to be slowed in muscle fibre cells following antimycin A treatment when VDAC inhibitors were present (Sakellariou *et al.*, 2013). Further it has been demonstrated that reduced levels of VDAC1 result in significantly reduced levels of lipid peroxidation in a VDAC1 +/- mouse model in comparison to VDAC1 +/+ mice (Manczak *et al.*, 2013); which appears to be further evidence of VDAC1's involvement in increasing levels of reactive oxygen species within the intracellular environment.

Taken together with the above oxidative stress data this is highly suggestive of an effect of intracellularly retained cystatin C having an effect on oxidative stress through its mitochondrial association.

5.6.5 Other mass spectrometry implicated cystatin C binding partners

5.6.5A 78 kDa glucose-regulated protein

This protein is believed to be involved in correct folding of proteins via interaction with DNAJC10 (Uniprot P11021) in the endoplasmic reticulum. Consequently the statistically significant binding rate with wild type cystatin C is easy to understand as, presumably, the interaction comes about through the processing steps. Although it does not seem significant with respect to the effect of variant B cystatin C this result supports the wild type cystatin C construct being properly processed by the secretory pathway and thus is perhaps noteworthy as an additional point of evidence in favour of the quality of the mass spectrometry dataset.

5.6.5B Leucyl-cystinyl aminopeptidase

Significantly binds to wild type cystatin C. Also known as oxytocinase it is involved in the release of N-terminal amino acids (Uniprot Q9UIQ6). It is believed to be the angiotensin IV receptor in the brain (Gard, 2008) with angiotensin IV having links with Alzheimer's disease through being a potential treatment target (Wright & Harding, 2008).

5.6.5C Mitochondrial stress-70 protein

A heat shock protein localised to mitochondria but also found in the endoplasmic reticulum, plasma membrane and cytoplasmic vesicles. Plays a role in cell proliferation, stress response and maintenance of the mitochondria (NCBI Gene database). The mass spectrometry data indicates it binds significantly with wild type cystatin C which is unusual given its mitochondrial localisation, however given that it is also found in parts of the secretory pathway it is difficult to determine how significant this finding is.

5.6.5E Heat shock protein beta-1

Also known as HSP27 (Uniprot P04792) and appears to be significantly bound to wild type cystatin C. Known to be involved in stress resistance and actin organisation and has been implicated as a mediator of oxidative injury to the RPE cells (Pons *et al.*, 2010) and is highly

expressed in the RPE (Strunnikova *et al.*, 2001). May be involved in coping with the stress of the internal overexpression of cystatin C.

5.6.5F Calmodulin-like protein 3

Believed to compete with calmodulin for cellular substrates, calmodulin is a messenger protein for the transduction of calcium signals and is involved in control of a number of enzymes and ion channels. Implicated in Alzheimer's disease (Min *et al.*, 2013). Appears to bind significantly with wild type cystatin C but the effect of this on intracellular processes and how this relates to the RPE cells is unknown.

5.7 Future work

For each of the two main lines of work in this study, one result stands out in particular from the rest as being particularly worthy of further investigation. The most promising step onwards from the mass spectrometry results is for additional follow up work to be carried out on the subject of prohibitin's potential interaction with variant B cystatin C. Following analysis of the mass spectrometry results an attempt was made to confirm the prohibitin result using western blot analysis, as well as to measure the relative levels of prohibitin in transfected cell lysates. Unfortunately due to time limitations it was not possible to optimise and complete these experiments in time for this study. However this is a key step to further future work. It may be necessary to carry out an ELISA to quantify the level of prohibitin, there are a number of commercial prohibitin ELISA kits that could fulfil this purpose.

Voltage-dependent anion-selective channel protein 1 appears to also be a protein of interest and would also benefit from additional experiments. Papers published within the past few years link this protein to Alzheimer's disease and to oxidative stress, therefore it seems quite possible that it is also involved with variant B cystatin C mediated AMD. However prohibitin appears to be the better candidate of the two (if one is to be chosen) for immediate follow up research given its potential to be both the cause of the mitochondrial targeting and the reason for its localisation there whilst also being linked to oxidative stress in the RPE.

In addition to the above, immunofluorescence in live cells could be used to monitor the localisation of cystatin C with these potential bound proteins. This is significantly simplified due to the work done in this study to create the HaloTag® construct. As HaloTag® itself is not intrinsically fluorescent there is great flexibility in experimental design, meaning that producing good quality images should be possible. In the case of prohibitin in particular this will provide information about where in the cell variant B cystatin C is bound to prohibitin and whether prohibitin is acting as an anchor to the mitochondria or variant B cystatin C is being transported there by prohibitin, or perhaps both. An more informative approach might be to attempt to monitor fluorescence via a time course.

Following this there are a number of experiments that could be carried out. The interactions between prohibitin and prohibitin 2 as a result of the presence of cystatin C variant B would be a valuable piece of information. Ideally the effect of cystatin C variant B

on mitochondrial biogenesis would be measured, given the that prohibitin is implicated in the process. Perhaps through visualisation and measurement of mitochondria using mitochondrial dyes on samples (Medeiros, 2008).

Assuming that prohibitin is indeed confirmed as a binding partner for variant B cystatin C it would be valuable to use protein interaction modelling in an attempt to specifically identify how this interaction occurs. If it is due to the targeting sequence of variant B cystatin C this would explain exactly why this amino acid substitution results in the mislocalisation.

For the functional assays the oxidative stress measurements are of greatest interest and warrant additional work. The great importance of oxidative stress in AMD pathology coupled with the link between variant B, mitochondria and AMD suggests that this could be a method of action for the variant B protein if it can be verified.

Unfortunately the constructs used to date all rely on the CMV promoter which massively overexpresses the protein. This is an effective way to exaggerate a response for measurement, however it means the protein is present at non-physiological levels compared *in vivo* RPE cells. The consequence being in this case that potentially the level of wild type cystatin C within the cell is inadvertently leading to a phenotype similar to that of variant B cystatin C being retained within the cell.

The solution to this is the production of constructs utilising the normal promoter for human cystatin C. By expressing with the normal promoter and regulatory elements it is expected that cystatin C would be produced at normal cellular levels for RPE cells and thus this would be a much more accurate reflection of the effects *in vivo*. One disadvantage of this approach, however, is that effects may be masked by the endogenous cystatin C.

In addition, this construct could be used to examine other processes perhaps to re-examine those already studied here but under a physiologically-relevant concentration. Given the low level of response likely from low levels of protein it is likely even more sensitive assays would be needed. Nevertheless a plasmid construct with the human promoter would be a very valuable research tool and would be an excellent next step.

5.8 Concluding remarks

A number of progressive steps in our understanding of variant B cystatin C have resulted from this study. Firstly, the apparent increase in oxidative stress resulting from high levels of intracellular cystatin C is of potentially great importance to the understanding of variant B cystatin C's effect on RPE cells. If this is indeed the method of action for variant B cystatin C then it once again raises the question of to what extent is oxidative stress a central cause of AMD and ageing in general. Verifying that this occurs as a result of cystatin C intracellular build up is an extremely important next step.

In addition two mitochondrial based proteins which appear to interact with variant B cystatin C have been identified, opening up new lines of investigation with the potential to push forward our understanding of this mislocalisation. If a variant B cystatin C protein interaction at the mitochondria were to be confirmed this will provide a clear avenue of further investigation for the effects of variant B on the RPE cells and the integration of that into the larger picture of AMD pathogenesis.

Finally a potential explanation for how variant B cystatin C's mislocalisation to the mitochondria occurs in the form of prohibitin has been identified. If this is validated as the pathway (or at least a pathway) by which variant B is mislocalised then the long standing question of precisely how the single base mutation in the targeting sequence of cystatin C causes intracellular retention and mitochondrial mislocalisation may finally be answered.

References

Ablonczy, Z., Dahrouj, M., Tang, P. H., Liu, Y., Sambamurti, K., Marmorstein, A. D. & Crosson, C. E. (2011). Human retinal pigment epithelium cells as functional models for the RPE in vivo. Invest Ophthalmol Vis Sci., 52, 8614-8620.

Abrahamson, M., Barrett, A. J., Salvesen, G. & Grubb, A. (1986). Isolation of six cysteine proteinase inhibitors from human urine. Their physicochemical and enzyme kinetic properties and concentrations in biological fluids. J Biol Chem., 261, 11282-11289.

Abrahamson, M., Grubb, A., Olafsson, I. & Lundwall, A. (1987a). Molecular cloning and sequence analysis of cDNA coding for the precursor of the human cysteine proteinase inhibitor cystatin C. FEBS Lett., 216, 229-233.

Abrahamson, M., Ritonja, A., Brown, M. A., Grubb, A., Machleidt, W. & Barrett, A. J. (1987b). Identification of the probable inhibitory reactive sites of the cysteine proteinase inhibitors human cystatin C and chicken cystatin. J Biol Chem., 262, 9688-9694.

Abrahamson, M., Islam, M. Q., Szpirer, J., Szpirer, C. & Levan, G. (1989). The human cystatin C gene (CST3), mutated in hereditary cystatin C amyloid angiopathy, is located on chromosome 20. Hum Genet., 82, 223-226.

Abrahamson, M., Olafsson, I., Palsdottir, A., Ulvsbäck, M., Lundwall, A., Jensson, O. & Grubb, A. (1990). Structure and expression of the human cystatin C gene. Biochem J., 268, 287-294.

Abrahamson, M. & Grubb, A. (1994). Increased body temperature accelerates aggregation of the Leu-68->Gln mutant cystatin C, the amyloid-forming protein in hereditary cystatin C amyloid angiopathy. Proc. Natl. Acad. Sci. USA, 91, 1416-1420.

Adamis, A. P., Shima, D. T., Yeo, K. T., Yeo, T. K., Brown, L. F., Berse, B., D'Amore, P. A. & Folkman, J. (1993). Synthesis and secretion of vascular permeability factor/vascular endothelial growth factor by human retinal pigment epithelial cells. Biochem Biophys Res Commun., 193, 631-638.

Ahuja, S., Ahuja-Jensen, P, Johnson, L. E., Caffé, A. R., Abrahamson, M., Ekström, P. A. & van Veen, T. (2008). Invest Ophthalmol Vis Sci., 49, 1089-1096.

Alizadeh, P., Smit-McBride, Z., Oltjen, S. L. & Hjelmeland, L. M. (2006). Regulation of cysteine cathepsin expression by oxidative stress in the retinal pigment epithelium/choroid of the mouse. Exp Eye Res., 83, 679-687.

Angelidis, C., Deftereos, S., Giannopoulos, G., Anatoliotakis, N., Bouras, G., Hatzis, G., Panagopoulou, V., Pyrgakis, V. & Cleman, M. W. (2013). Cystatin C: an emerging biomarker in cardiovascular disease. Curr Top Med Chem., 13, 164-179.

Ardeljan, C. P., Ardeljan, D., Abu-Asab, M. & Chan, C. C. (2014). Inflammation and Cell Death in Age-Related Macular Degeneration: An Immunopathological and Ultrastructural Model. J Clin Med., 3, 1542-1560.

Ban, Y. & Rizzolo, L. J. (2000). Regulation of glucose transporters during development of the retinal pigment epithelium. Brain Res., 121, 89-95.

Barja, G. (2013). Updating the mitochondrial free radical theory of aging: an integrated view, key aspects, and confounding concepts. Antioxid Redox Signal., 19, 1420-1445.

Barka, T. & van der Noen, H. (1994). Expression of the cysteine proteinase inhibitor cystatin C mRNA in rat eye. Anat Rec., 239, 343-348.

Barrett, A. J., Davies, M. E. & Grubb, A. (1984). The place of human gamma-trace (cystatin C) amongst the cysteine proteinase inhibitors. Biochem Biophys Res Commun., 120, 631-6.

Barrett, A. J. (1986). The cystatins: a diverse superfamily of cysteine peptidase inhibitors. Biomed Biochim Acta., 45, 1363-1374.

Beatty, S., Koh, H, Phil, M., Henson, D. & Boulton, M. (2000). The role of oxidative stress in the pathogenesis of age-related macular degeneration. Surv Ophthalmol., 45, 115-134.

Bengtsson, E., Nilsson, J. & Jovinge, S. (2008). Cystatin C and cathepsins in cardiovascular disease. Front Biosci., 13, 5780-5786.

Benussi, L., Ghidoni, R., Steinhoff, T., Alberici, A., Villa, A., Mazzoli, F., Nicosia, F., Barbiero, L., Broglio, L., Feudatari, E., Signorini, S., Finckh, U., Nitsch, R. M. & Binetti, G. (2003). Alzheimer disease-associated cystatin C variant undergoes impaired secretion. Neurobiol Dis., 13, 15-21.

Benz, R. (1994). Permeation of hydrophilic solutes through mitochondrial outer membranes: Review on mitochondrial porins. Biochim Biophys Acta., 1197, 167-196.

Bergmann, M., Schütt, F., Holz, F. G. & Kopitz, J. (2004). Inhibition of the ATP-driven proton pump in RPE lysosomes by the major lipofuscin fluorophore A2-E may contribute to the pathogenesis of age-related macular degeneration. FASEB J., 18, 562-564.

Bhattacharya, S., Chaum, E., Johnson, D. A. & Johnson, L. R. (2012). Age-related susceptibility to apoptosis in human retinal pigment epithelial cells is triggered by disruption of p53-Mdm2 association. Invest Ophthalmol Vis Sci., 53, 8350-8366.

Bhutto, I. & Lutty, G. (2012). Understanding age-related macular degeneration (AMD): relationships between the photoreceptor/retinal pigment epithelium/Bruch's membrane/choriocapillaris complex. Mol Aspects Med., 33, 295-317.

Blasiak, J., Petrovski, G., Veréb, Z., Facskó, A. & Kaarniranta, K. (2014). Oxidative stress, hypoxia, and autophagy in the neovascular processes of age-related macular degeneration. Biomed Res Int., Epub 2014:768026.

Bode, W., Engh, R., Musil, D., Thiele, U., Huber, R., Karshikov, A., Brzin, J., Kos, J. & Turk, V. (1988). The 2.0 Å X-ray crystal structure of chicken egg white cystatin and its possible mode of interaction with cysteine proteinases. EMBO J., 7, 2593-2599.

Bok, D. (1993). The retinal pigment epithelium: a versatile partner in vision. J Cell Sci Suppl., 17, 189-195.

Bonilha, V. L. (2008). Age and disease-related structural changes in the retinal pigment epithelium. Clin Ophthalmol,. 2, 413-424.

Booij, J. C., Baas, D. C., Beisekeeva, J., Gorgels, T. G. & Bergen, A. A. (2010). The dynamic nature of Bruch's membrane. Prog Retin Eye Res., 29, 1-18.

Boulton, M. & Dayhaw-Barker, P. (2001). The role of the retinal pigment epithelium: topographical variation and ageing changes. Eye (Lond)., 15, 384-389.

Brown, P. K. & Wald, G. (1964). Visual pigments in single rods and cones of the human retina. Direct measurements reveal mechanisms of human night and color vision. Science, 144, 45-52.

Brunk, U. T. & Terman, A. (2002). Lipofuscin: mechanisms of age-related accumulation and influence on cell function. Free Radic Biol Med., 33, 611-619.

Brzin, J., Popvic, T., Turk, V., Borchart, U. & Machleidt, W. (1984). Human cystatin, a new protein inhibitor of cysteine proteinases. Biochem Biophys Res Commun, 118, 103-109.

Burgansky-Eliash, Z., Barash, H., Nelson, D., Grinvald, A., Sorkin, A., Loewenstein, A. & Barak, A. (2014). Retinal Blood Flow Velocity in Patients with Age-Related Macular Degeneration. Curr Eye Res., 39, 304-311.

Butler, E. A. & Flynn, F. V (1961). The occurrence of post-gamma protein in urine: a new protein abnormality. J Clin Pathol., 14, 172-178.

Butler, J. M., Sharif, U., Ali, M., McKibbin, M., Thompson, J. P., Gale, R., Yang, Y. C., Inglehearn, C. & Paraoan, L. (2015). A missense variant in *CST3* exerts a recessive effect on susceptibility to age-related macular degeneration resembling its association with Alzheimer's disease. Hum Genet., Epub ahead of print.

Cano, M., Wang, L., Wan, J., Barnett, B. P., Ebrahimi, K., Qian, J. & Handa, J. T. (2014). Oxidative stress induces mitochondrial dysfunction and a protective unfolded protein response in RPE cells. Free Radic Biol Med., 69, 1-14.

Chapman Jr., H. A., Reilly Jr., J. J., Yee, R. & Grubb, A. (1990). Identification of cystatin C, a cysteine proteinase inhibitor, as a major secretory product of human alveolar macrophages in vitro. Am Rev Respir Dis, 141, 698-705.

Chistiakov, D. A., Sobenin, I. A., Revin, V. V., Orekhov, A. N. & Bobryshev, Y. V. (2014). Mitochondrial aging and age-related dysfunction of mitochondria. Biomed Res Int., Epub 2014:238463.

Chong, E. W., Simpson, J. A., Robman, L. D., Hodge, A. M., Aung, K. Z., English, D. R., Giles, G. G. & Guymer, R. H. (2009). Red meat and chicken consumption and its association with age-related macular degeneration. Am J Epidemiol.. 169, 867-876.

Clarke, P. & Tyler, K. L. (2009). Apoptosis in animal models of virus-induced disease. Nat Rev Microbiol., 7, 144-155.

Coates, P. J., Jamieson, D. J., Smart, K., Prescott, A. R. & Hall, P. A. (1997). The prohibitin family of mitochondrial proteins regulate replicative lifespan. Curr Biol., 7, 607-610.

Cohen, D. H., Feiner, H., Jensson, O. & Frangione, B. (1983). Amyloid fibril in hereditary cerebral hemorrhage with amyloidosis (HCHWA) is related to the gastroentero-pancreatic neuroendocrine protein, gamma trace. J Exp Med., 158, 623-628.

Colombini, M. (1979). A candidate for the permeability pathway of the outer mitochondrial membrane. Nature, 279, 643-645.

Coria, F., Castaño, E. M. & Frangione, B. (1987). Brain amyloid in normal aging and cerebral amyloid angiopathy is antigenically related to Alzheimer's disease beta-protein. Am J Pathol., 129, 422-428.

Couch, S. M. & Bakri, S. J. (2011). Review of combination therapies for neovascular age-related macular degeneration. Semin Ophthalmol., 26, 114-120.

Curcio, C. A., Sloan, K. R., Kalina, R. E. & Hendrickson, A. E. (1990). Human photoreceptor topography. J Comp Neurol., 292, 497-523.

Curcio, C. A. & Johnson, M. (2013). Structure, Function and Pathology of Bruch's membrane. In Retina Vol. 1 Part 2, 466-481, ed. Ryan, S. J., Schachat, A. P., Wilkinson, C. P., Hinton, D. R., Sadda, S. & Wiedemann, P.; Elsevier, London.

Davis, A. A., Bernstein, P. S., Bok, D., Turner, J., Nachtigal, M. & Hunt, R. C. (1995). A Human Retinal Pigment Epithelial Cell Line That Retains Epithelial Characteristics After Prolonged Culture. Invest Ophthalmol Vis Sci., 35, 955-964.

Davis, W. L., Jones, R. G. & Hagler, H. K. (1981). An electron microscopic histochemical and analystical X-ray microprobe study of calcification in Bruch's membrane from human eyes. J. Histochem. Cytochem., 29, 601-608.

De La Paz, M. A., Pericak-Vance, M. A., Lennon, F., Haines, J. L. & Seddon, J. M. (1997). Exclusion of TIMP3 as a candidate locus in age-related macular degeneration. Invest Ophthalmol Vis Sci., 38, 1060-1065.

Dhanasekaran, D. N. & Reddy, E. P. (2008). JNK signaling in apoptosis. Oncogene 27, 6245-6251.

Diepart, C., Verrax, J., Calderon, P. B., Feron, O. & Jordan, B. F. (2010). Comparison of methods for measuring oxygen consumption in tumor cells in vitro. Analytical Biochemistry 396(2), 250-256

Drenser, K. A., Trese, M. T., Capone Jr., A., Hartzer, M. & Dailey, W. (2007). Elevated levels of cystatin C and tenascin-C in schisis cavities of patients with congenital X-linked retinoschisis. Retina, 27, 1086-1089.

Du, H., Sun, X., Guma, M., Luo, J., Ouyang, H., Zhang, X., Zeng, J., Quach, J., Nguyen, D. H., Shaw, P. X., Karin, M. & Zhang, K. (2013). JNK inhibition reduces apoptosis and neovascularization in a murine model of age-related macular degeneration. Proc Natl Acad Sci USA., 110, 2377-2382.

Dunn, K. C., Aotaki-Keen, A. E., Putkey, F. R. & Hjelmeland, L. M. (1996). ARPE-19, a human retinal epithelial cell line with differentiated properties. Exp. Eye Res 62, 155-169.

Edrey, Y. H. & Salmon, A. B. (2014). Revisiting an age-old question regarding oxidative stress. Free Radic Biol Med., 71, 368-378.

Ellis, C. J. (1981). The pupillary light reflex in normal subjects. Br J Ophthalmol. 65, 754-759.

Emeterio Nateras, O. S., Harrison, J. M., Muir, E. R., Zhang, Y., Peng, Q., Chalfin, S., Gutierrez, J. E., Johnson, D. A., Kiel, J. W. & Duong, T. Q. (2014). Choroidal Blood Flow Deacreases with Age: An MRI Study. Curr Eye Res., 39, 1059-1067.

Euler, T., Haverkamp, S., Schubert, T. & Baden, T. (2014). Retinal bipolar cells: elementary building blocks of vision. Nat Rev Neurosci., 15, 507-519.

Filler, G., Bökenkamp, A., Hofmann, W., Le Bricon, T., Martínez-Brú, C. & Grubb, A. (2005). Cystatin C as a marker of GFR – history, indications, and future research. Clin Biochem., 38, 1-8.

Fleming, J. E., Miquel, J., Cottrell, S. F., Yengoyan, L. S. & Economos, A. C. (1982). Is cell aging caused by respiration-dependent injury to the mitochondrial genome? Gerontology, 28, 44-53.

Fusaro, G., Dasgupta, P., Rastog, S., Joshi, B. & Chellappan, S. (2003). Prohibitin induces the transcriptional activity of p53 and is exported from the nucleus upon apoptotic signaling. J Biol Chem., 278, 47853-47861.

Gard, P. R. (2008). Cognitive-enhancing effects of angiotensin IV. BMC Neurosci., 9, S15.

Garron, L. K. (1963). The Ultrastructure of the Retinal Pigment Epithelium with Observations on the Choriocapillaris and the Bruch's Membrane. Trans. Am. Ophthalmol. Soc., 61, 545-588.

Gauthier, S., Kaur, G., Mi, W., Tizon, B. & Levy, E. (2011). Protective mechanisms by cystatin C in neurodegenerative diseases. Front Biosci., 3, 541-554.

Gehrs, K. M., Anderson, D. H., Johnson, L. V. & Hageman, G. S. (2006). Age-related macular degeneration - emerging pathogenetic and therapeutic concepts. Ann. Med., 38, 450-471.

Ghiso, J., Pons-Estel, B. & Frangione, B. (1986). Hereditary cerebral amyloid angiopathy: the amyloid fibrils contain a protein which is a variant of cystatin C, an inhibitor of lysosomal cysteine proteases. Biochem Biophys Res Commun., 136, 548-554.

Glenn, J. V., Mahaffy, H., Wu, K., Smith, G., Nagai, R., Simpson, D. A., Boulton, M. E. & Stitt, A. W. (2009). Advanced glycation end product (AGE) accumulation on Bruch's membrane: links to age-related RPE dysfunction. Invest Ophthalmol Vis Sci., 50, 441-451.

Grubb, A. & Löfberg, H. (1982). Human γ-trace, a basic microprotein: Amino acid sequence and presence in the adenohypophysis. Proc Natl Acad Sci USA., 79, 3024-3027.

Grubb, A. O., Weiber, H. & Löfberg, H. (1983). The gamma-trace concentration of normal human seminal plasma is thirty-six times that of normal human blood plasma. Scand J Clin Lab Invest., 43, 421-425.

Haines, J. L., Hauser, M. A., Schmidt, S., Scott, W. K., Olson, L. M., Gallins, P., Spencer, K. L., Kwan, S. Y., Noureddine, M., Gilbert, J. R., Schnetz-Boutaud, N., Agarwal, A., Postel, E. A. & Pericak-Vance, M. A. (2005). Complement factor H variant increases the risk of age-related macular degeneration. Science, 308, 419-421.

Hanout, M., Ferraz, D., Ansari, M., Magsood, N., Kherani, S., Sepah, Y. J., Rajagopalan, N., Ibrahim, M., Do, D. V. & Nguyen, Q. D. (2013). Therapies for neovascular age-related

macular degeneration: current approaches and pharmacologic agents in development. Biomed Res Int., 2013, Epub 830837.

Hargrave, P. A. (2001). Rhodopsin Structure, Function, and Topography The Friedenwald Lecture. Invest Ophthalmol Vis Sci., 41, 3-9.

Harman, D. (1956). Aging: a theory based on free radical and radiation chemistry. J Gerontol., 11, 298-300.

Hartong, D. T., Berson, E. L. & Dryja, T. P. (2006). Retinitis pigmentosa. The Lancet, 360, 1795-1809.

He, Y. & Tombran-Tink, J. (2010). Mitochondrial decay and impairment of antioxidant defenses in aging RPE cells. Adv Exp Med Biol., 664, 165-183.

Heriot, W. J., Henkind, P., Bellhorn, R. W. & Burns, M. S. (1984). Choroidal neovascularization can digest Bruch's membrane. A prior break is not essential. Ophthalmology, 91, 1603-1608.

Hogan, M. J., Alvarado, J. A. & Weddell, J. E. (1971). Histology of the human eye; an atlas and textbook. Saunders, Philadelphia.

Ikonen, E., Fiedler, K., Parton, R. G. & Simons, K. (1995). Prohibitin, an antiproliferative protein, is localized to mitochondria. FEBS Lett., 358, 273-277.

Ikram, M. K., Mitchell, P., Klein, R., Sharrett, A. R., Couper, D. J. & Wong, T. Y. (2012). Age-related macular degeneration and long-term risk of stroke subtypes. Stroke, 43, 1681-1683.

Iloki Assanga, S. B., Gil-Salido, A. A., Lewis Luján, L. M., Rosas-Durazo, A., Acosta-Silva, A. L., Rivera-Castañeda, E. G. & Rubio-Pino, J. L. (2013). Cell growth curves for different cell lines and their relationship with biological activities. Int J Biotechnol Mol Biol Res., 4, 60-70.

Im, E. & Kazlauskas, A. (2007). The role of cathepsins in ocular physiology and pathology. Exp Eye Res., 84, 383-388.

Jackson, T. L., Chakravarthy, U., Slakter, J. S., Muldrew, A., Shusterman, E. M., O'Shaughnessy, D., Arnoldussen, M., Gertner, M. E., Danielson, L., Moshfeghi, D. M. & INTREPID Study Group. Stereotactic Radiotherapy for Neovascular Age-Related Macular Degeneration: Year 2 Results of the INTREPID Study. Ophthalmology. Epub ahead of print.

Jacobs, H. T. (2003). The mitochondrial theory of aging: dead or alive? Aging Cell, 2, 11-17.

Janowski, R., Kozak, M., Jankowska, E., Grzonka, Z., Grubb, A., Abrahamson, M & Jaskolski, M. (2001). Human cystatin C, an amyloidogenic protein, dimerizes through three-dimensional domain swapping. Nat Struct Biol., 8, 316-320.

Jaskólski, M. (2001). 3D domain swapping, protein oligomerization and amyloid formation. Acta Biochim Pol., 48, 807-827.

Jensson, O., Gudmundsson, G., Amason, A., Blöndal, H., Petursdottir, I., Throsteinsson, L., Grubb, A., Löfberg, A., Cohen, D. & Frangione, B. (1987). Hereditary cystatin C (gamma-trace) amyloid angiopathy of the CNS causing cerebral hemorrhage. Acta Neurol Scand., 76, 102-114.

Joshi, M. M., Drenser, K., Hartzer, M., Dailey, W., Capone Jr., A. & Trese, M. E. (2006). Intraschisis cavity fluid composition in congenital X-linked retinschisis. Retina, 26, S57-60.

Kaarniranta, K. (2010). Autophagy -- hot topic in AMD. Acta Ophthalmol., 88, 387-388.

Kaarniranta, K., Sinha, D., Blasiak, J., Kauppinen, A., Veréb, Z., Salminen, A., Boulton, M. E. & Petrovski, G. (2013). Autophagy and heterophagy dysregulation leads to retinal pigment epithelium dysfunction and development of age-related macular degeneration. Autophagy 9, 973-984.

Kaeser, S. A., Herzig, M. C., Coomaraswamy, J., Kilger, E., Selenica, M. L., Winkler, D. T., Staufenbiel, M., Levy, E., Grubb, A. & Jucker, M. (2007). Cystatin C modulates cerebral beta-amyloidosis. Nat Genet., 39, 1437-1439.

Kaur, G. & Levy, E. (2012). Cystatin C in Alzheimer's disease. Front Mol Neurosci, 5, 79.

Kawamura, S. & Tachibanaki, S. (2008). Rod and cone photoreceptors: Molecular basis of the difference in their physiology. Comp Biochem Physiol. 150, 369-377.

Kay, P., Yang, Y. C., Hiscott, P., Gray, D., Maminishkis, A. & Paraoan, L. (2014). Age-related changes of cystatin C expression and polarized secretion by retinal pigment epithelium: potential age-related macular degeneration links. Invest Ophthalmol Vis Sci., 55, 926-934.

Klaver, C. C., Kliffen, M., van Duijin, C. M., Hofman, A., Cruts, M., Grobbee, D. E., van Broeckhoven, C. & de Jong, P. T. (1998). Genetic association of apolipoprotein E with age-related macular degeneration. Am J Hum Genet.., 63, 200-206.

Klein, R., Cruickshanks, K. J., Myers, C. E., Sivakumaran, T. A., Iyenger, S. K., Meuer, S. M., Schubert, C. R., Gangnon, R. E. & Klein, B. E. (2013). The relationship of atherosclerosis to the 10-year cumulative incidence of age-related macular degeneration: the Beaver Dam studies. Ophthalmology, 120, 1012-1019.

Komai, Y. & Ushiki, T. (1991). The three-dimensional organization of collagen fibrils in the human cornea and sclera. Invest Ophthalmol Vis Sci., 32, 2244-2258.

La Vail, M. M. (1976). Rod outer segment shedding in rat retina: relationship to cyclic lighting. Science, 194, 1071-1074.

Lally, D. R., Gerstenblith, A. T. & Regillo, C. D. (2012). Preferred therapies for neovascular age-related macular degeneration. Curr Opin Ophthalmol., 23, 182-188.

Lamb, L. E. & Simon, J. D. (2004). A2E: a component of ocular lipofuscin. Photochem Photobiol., 79, 127-136.

Laskowski Jr., M. & Kato, I. (1980). Protein inhibitors of proteinases. Ann Rev Biochem., 49, 593-626.

Lawen, A., Ly, J. D., Lane, D. J, Zarschler, K., Messina, A. & De Pinto, V. (2005). Voltage-dependent anion-selective channel 1 (VDAC1)--a mitochondrial protein, rediscovered as a novel enzyme in the plasma membrane. Int J Biochem Cell Biol., 37, 277-282.

Lee, H., Arnouk, H., Sripathi, S., Chen, P., Zhang, R., Bartoli, M, Hunt, R. C., Hrushesky, W. J., Chung, H., Lee, S. H. & Jahng, W. J. (2010). Prohibitin as an oxidative stress biomarker in the eye. Int J Biol Macromol., 47, 685-690.

Levy, E., Jaskolski, M. & Grubb, A. (2006). The role of cystatin C in cerebral amyloid angiopathy and stroke: cell biology and animal models. Brain Pathol., 16, 60-70.

Liang, X., Nagai, A., Terashima, M., Sheikh, A. M., Shiota, Y., Mitaki, S., Kim, S. U. & Yamaguchi, S. (2011). Cystatin C induces apoptosis and tyrosine hydroxylase gene expression through JNK-dependent pathway in neuronal cells. Neurosci Lett., 496, 100-105.

Lindahl, P., Abrahamson, M. & Björk, I. (1992). Interaction of recombinant human cystatin C with the cysteine proteinases papain and actinidin. Biochem J., 281, 49-55.

Liu, X. T., Stewart, C. A., King, R. L., Danner, D. A., Dell'Orco, R. T. & McClung, J. K. (1994). Prohibitin expression during cellular senescence of human diploid fibroblasts. Biochem Biophys Res Commun., 201, 409-414.

Liu, Y., Hart, P. J., Schlunegger, M. P. & Eisenberg, D. (1998). The crystal structure of a 3D domain-swapped dimer of RNase A at a 2.1-Å resolution. Proc. Natl. Acad. Sci USA 95, 3437-3442.

Liu, Y., Cai, H., Wang, Z., Li, J., Wang, K., Yu, Z. & Chen, G. (2013). Induction of autophagy by cystatin C: a potential mechanism for prevention of cerebral vasospasm after experimental subarachnoid hemorrhage. Eur J Med Res., 18, 21.

Löfberg, H., Grubb, A. O., Sveger, T. & Olsson, J. E. (1980). The cerebrospinal fluid and plasma concentrations of gamma-trace and beta2-microglobulin at various ages and in neurological disorders. J Neurol., 223, 159-170.

Löfberg, H., Grubb, A., Davidsson, L., Kjellander, B., Strömblad, L. G., Tibblin, S. & Olsson, S. O. (1983). Occurrence of gamma-trace in the calcitonin-producing C-cells of simian thyroid gland and human medullary thyroid carcinoma. Acta Endocrinol. (Copenh), 104, 69-76.

Logue, M. W., Schu, M., Vardarajan, B. N., Farrell, J., Lunetta, K. L., Jun, G., Baldwin, C. T., Deangelis, M. M. & Farrer, L. A. (2014). A search for age-related macular degeneration risk variants in Alzheimer disease genes and pathways. Neurobiol Aging., 35, 1510.e7-18.

Machalińska, A., Kawa, M. P., Marlicz, W. & Machalińska B. (2012). Complement system activation and endothelial dysfunction in patients with age-related macular degeneration (AMD): possible relationship between AMD and atherosclerosis. Acta Ophthalmol. 90, 695-703.

Manczak, M., Sheiko, T., Craigen, W. J. & Reddy, P. H. (2013). Reduced VDAC1 protects against Alzheimer's disease, mitochondria, and synaptic deficiencies. J Alzheimers Dis., 37, 679-690.

Mao, H., Seo, S. J., Biswal, M. R., Li, H., Conners, M., Nandyala, A., Jones, K., Le, Y. Z. & Lewin, A. S. (2014). Mitochondrial oxidative stress in the retinal pigment epithelium leads to localized retinal degeneration. Invest Ophthalmol Vis Sci., 55, 4613-4627.

Mares, J. A., Voland, R. P., Sondel, S. A., Millen, A. E., Larowe, T., Moeller, S. M., Klein, M. L., Blodi, B. A., Chappell, R. J., Tinker, L., Ritenbaugh, C., Gehrs, K. M., Sarto, G. E., Johnson, E., Snodderly, D. M. & Wallace, R. B. (2011). Healthy lifestyles related to subsequent prevalence of age-related macular degeneration. Arch Ophthalmol., 129, 470-480.

Maritim, A. C., Sanders, R. A. & Watkins, J. B. (2003). Diabetes, oxidative stress, and antioxidants: a review. J Biochem Mol Toxicol., 17, 24-38.

Marmor, M. F. (1990). Control of subretinal fluid: experimental and clinical studies. Eye (Lond)., 4, 340-344.

Marmorstein, A. D. (2001). The Polarity of the Retinal Pigment Epithelium. Traffic, 2, 867-872.

McClung, J. K., Jupe, E. R., Liu, X. T. & Dell'Orco, R. T. (1995). Prohibitin: potential role in senescence, development, and tumor suppression. Exp Gerontol., 30, 99-124.

McLeod, D. S., Grebe, R., Bhutto, I., Merges, C., Baba, T. & Lutty, G. A. (2009). Relationship between RPE and choriocapillaris in age-related macular degeneration. Invest Ophthalmol Vis Sci. 50, 4982-4991.

Medeiros, D. M. (2007). Assessing mitochondria biogenesis. Methods, 46, 288-294.

Mi, W., Pawlik, M., Sastre, M., Jung, S. S., Radvinsky, D. S., Klein, A. M., Sommer, J., Schmidt, S. D., Nixon, R. A., Mathews, P. M. & Levy, E. Cystatin C inhibits amyloid-beta deposition in Alzheimer's disease mouse models. Nat Genet., 39, 1440-1442.

Miceli, M. V., Liles, M. R. & Newsome, D. A. (1994). Evaluation of Oxidative Processes in Human Pigment Epithelial Cells Associated with Retinal Outer Segment Phagocytosis. Exp Cell Res., 214, 242-249.

Milac, T. I., Randolph, T. W. & Wang, P. (2012). Analyzing LC-MS/MS data by spectral count and ion abundance: two case studies. Stat Interface., 5, 75-87.

Min, D., Guo, F., Zhu, S., Xu, X., Mao, X., Cao, Y., Lv, X Gao, Q., Wang, L., Chen, T., Shaw, C., Hao, L. & Cai, J. (2013). The alterations of Ca2+/calmodulin/CaMKII/CaV1.2 signaling in experimental models of Alzheimer's disease and vascular dementia. Neurosci Lett., 538, 60-65.

Miller, J. W. (2011). Treatment of age-related macular degeneration: beyond VEGF. Jpn J Ophthalmol., 54, 523-528.

Miquel, J. & Fleming, J. E. (1984). A two-step hypothesis on the mechanisms of in vitro cell aging: cell differentiation followed by intrinsic mitochondrial mutagenesis. Exp Gerontol., 19, 31-36.

Miquel, J. (1991). An integrated theory of aging as the result of mitochondrial-DNA mutation in differentiated cells. Arch Gerontol Geriatr., 12, 99-117.

Mitsuda, S., Yoshii, C., Ikegami, Y. & Araki, M. (2005). Tissue interaction between the retinal pigment epithelium and the choroid triggers retinal regeneration of the newt *Cynops pyrrhogaster*. Dev Biol. 280, 122-132.

Mitter, S. K., Song, C., Qi, X., Mao, H., Rao, H., Akin, D., Lewin, A., Grant, M., Dunn Jr., W., Ding, J., Rickman, C. B. & Boulton, M. (2014). Dysregulated autophagy in the RPE is associated with increased susceptibility to oxidative stress and AMD. Autophagy, 10, 1989-2005.

Mullins, R. F., Russell, S. R., Anderson, D. H. & Hageman, G. S. (2000). Drusen associated with aging and age-related macular degeneration contain proteins common to extracellular deposits associated with atherosclerosis, elastosis, amyloidosis, and dense deposit disease. FASEB J., 14, 835-846.

Nagai, A., Terashima, M., Sheikh, A. M., Notsu, Y., Shimode, K., Yamaguchi, S., Kobayashi, S. Kim, S. U. & Masuda, J. (2008). Involvement of cystatin C in pathophysiology of CNS diseases. Front Biosci., 13, 3470-3479.

Navarro, A. & Boveris, A.(2010). Brain mitochondrial dysfunction in aging, neurodegeneration, and Parkinson's disease. Front Aging Neurosci., 2, 34.

Newsome, D. A., Huh, W. & Green, W. R. (1987). Bruch's membrane age-related changes vary by region. Curr Eye Res., 6, 1211-1221.

Nickla, D. L. & Wallman, J. (2010). The multifunctional choroid. Prog Retin Eye Res., 29, 144-168.

Nicklin, M. J. & Barrett, A. J. (1984). Inhibition of cysteine proteinases and dipeptidyl peptidase I by egg-white cystatin. Biochem J., 223(1), 245-253.

Nijtmans, L. G., de Jong, L., Artal Sanz, M., Coates, P. J., Berden, J. A., Back, J. W., Muijsers, A. O., van der Spek, H. & Grivell, L. A. (2000). Prohibitins act as a membrane-bound chaperone for the stabilization of mitochondrial proteins. EMBO J., 19, 2444-2451.

Nilsson, M., Wang, X., Rodziewicz-Motowidlo, S., Janowski, R., Lindström, V, Onnerfjord, P., Westermark, G., Grzonka, Z., Jaskolski, M. & Grubb, A. (2004). Prevention of domain swapping inhibits dimerization and amyloid fibril formation of cystatin C: use of engineered disulfide bridges, antibodies, and carboxymethypapain to stabilize the monomeric form of cystatin C. J Biol Chem., 279, 24236-24245.

Nishio, C., Yoshida, K., Nishiyama, K., Hatanaka, H. & Yamada, M. (2000). Involvement of cystatin C in oxidative stress-induced apoptosis of cultured rat CNS neurons. Brain Res., 873, 252-262.

Nishiyama, K., Konishi, A., Nishio, C., Araki-Yoshida, K., Hatanaka, H., Kojima, M., Ohmiya, Y., Yamada, M. & Koshimizu, H. (2005). Expression of cystatin C prevents oxidative stress-induced death in PC12 cells. Brain Res Bull., 67, 94-99.

Nuell, M. J., Stewart, D. A., Walker, L., Friedman, V., Wood, C. M., Owens, G. A., Smith, J. R., Schneider, E. L., Dell'Orco, R., Lumpkin, C. K., Danner, D. B. & McClung, J. K. (1991). Prohibitin, an evolutionarily conserved intracellular protein that blocks DNA synthesis in normal fibroblasts and HeLa cells. Mol Cell Biol., 11, 1372-1381.

Ohno-Matsui, K. (2011). Parallel findings in age-related macular degeneration and Alzheimer's disease. Prog Retin Eye Res., 30, 217-238.

Pak, J. W., Herbst, A., Bua, E., Gokey, N., McKenzie, D. & Aiken, J. M. (2003). Rebuttal to Jacobs: the mitochondrial theory of aging: alive and well. Aging Cell, 2, 9-10.

Papadaki, T., Tsilimbaris, M., Pallikaris, I. & Thermos, K. (2010). Somatostatin receptor activation (sst_1-sst_5) differentially influences human retinal pigmenmt epithelium cell viability. Acta Ophthalmologica 88(6), e228-e233.

Paraoan, L., Girerson, I. & Maden, B. E. (2000). Analysis of expressed sequence tags of retinal pigment epithelium: cystatin C is an abundant transcript. Int J Biochem Cell Biol., 32, 417-426.

Paraoan, L., White, M. R., Spiller, D. G., Grierson, I. & Maden, B. E. (2001). Precursor cystatin C in cultured retinal pigment epithelium cells: evidence for processing through the secretory pathway. Mol Membr Bio.l, 18, 229-236.

Paraoan, L., Grierson, I. & Maden, B. E. (2003). Fate of cystatin C lacking the leader sequences in RPE cells. Exp Eye Res., 76, 753-756.

Paraoan, L., Ratnayaka, A., Spiller, D. G., Hiscott, P., White, M. R. & Grierson, I. (2004). Unexpected intracellular localization of the AMD-associated cystatin C variant. Traffic, 5, 884-895.

Paraoan, L. & Grierson, I. (2007) Focus on molecules: cystatin C. Exp Eye Res., 84, 1019-1020.

Parfitt, M., Crook, R., Rogues, P., Rossor, M. & Chartier-Harlin, M. C. (1993). The Cystatin-C gene is not linked to early onset familial Alzheimer's disease. Neurosci Lett., 154, 81-83.

Parver, L. M. (1991). Temperature Modulating Action of Choroidal Blood Flow. Eye, 5, 181-185.

Pons, M., Cousins, S. W., Csaky, K. G., Striker, G. & Marin- Castaño, M. E. (2010). Cigarette smoke-related hydroquinone induces filamentous actin reorganization and heat shock protein 27 phosphorylation through p38 and extracellular signal-regulated kinase 1/2 in retinal pigment epithelium: implications for age-related macular degeneration. Am J Pathol., 177, 1198-1213.

Pouranaras, C. J., Rungger-Brändle, E., Riva, C. E., Hararson, S. H. & Stefansson, E. (2008). Regulation of retinal blood flow in health and disease. Prog Retin Eye Res., 27, 284-330.

Ratnayaka, A., Paraoan, L., Spiller, D. G., Hiscott, P., Nelson, G., White, M. R. & Grierson, I. (2007). A dual Golgi- and mitochondria-localised Ala25Ser precursor cystatin C: an additional tool for characterising intracellular mis-localisation leading to increased AMD susceptibility. Exp Eye Res., 84, 1135-1139.

Rizzolo, L. J. (2007). Development and Role of Tight Junctions in the Retinal Pigment Epithelium. Int Rev Cytol., 258, 195-234.

Rozzini, L., Riva, M., Ghilardi, N., Facchinetti, P., Forbice, E., Semeraro, F. & Padovani, A. (2014). Cognitive dysfunction and age-related macular degeneration. Am J Alzheimers Dis Other Demen., 29, 256-262.

Roberts, J. M. & Forrester, J. V. (1990). Factors affecting the migration and growth of endothelial cells from microvessels of bovine retina. Exp Eye Res., 50, 165-172.

Saadat, K. A., Murakami, Y., Tan, X., Nomura, Y., Yasukawa, T., Okada, E., Ikeda, Y. & Yanagi, Y. (2014). Inhibition of autophagy induces retinal pigment epithelial cell damage by the lipofuscin fluorophore A2E. FEBS Open Bio., 4, 1007-1014.

Saitoh, E., Sabatini, L. M., Eddy, R. L., Shows, T. B., Azen, E. A., Isemujra, S. & Sanada, K. (1989). The human cystatin C gene (CST3) is a member of the cystatin gene family which is localized on chromosome 20. Biochem Biophys Res Commun., 162, 1324-1331.

Sakellariou, G. K., Vasilaki, A., Palomero, J., Kayani, A., Zibrik, L., McArdle, A. & Jackson, M. J. (2013). Studies of mitochondrial and nonmitochondrial sources implicate nicotinamide adenine dinucleotide phosphate oxidase(s) in the increased skeletal muscle superoxide generation that occurs during contractile activity. Antioxid Redox Signal., 18, 603-621

Sanz, A. & Stefanatos, R. K. (2008). The mitochondrial free radical theory of aging: a critical view. Curr Aging Sci., 1, 10-21.

Sato, T., Saito, H., Swensen, J., Olifant, A., Wood, C., Danner, D., Sakamoto, T., Takita, K., Kasumi, F., Miki, Y., Skolnick, M. & Nakamura, Y. (1992). The human prohibitin gene located on chromosome 17q21 is mutated in sporadic breast cancer. Cancer Res., 52, 1643-1646.

Schütt, F., Aretz, S., Auffarth, G. U.& Kopitz, J. (2012). Moderately reduced ATP levels promote oxidative stress and debilitate autophagic and phagocytic capacities in human RPE cells. Invest Ophthalmol Vis Sci., 53, 5354-5361.

Seddon, J. M., George, S. & Rosner, B. (2006). Cigarette smoking, fish consumption, omega-3 fatty acid intake, and associations with age-related macular degeneration: the US Twin Study of Age-Related Macular Degeneration. Arch Ophthalmol., 124, 995-1001.

Sena, L. A. & Chandel, N. S. (2012). Physiological roles of mitochondrial reactive oxygen species. Mol Cell., 48, 158-167.

Shen, J., Yang, X., Dong, A., Petters, R. M., Peng, Y. W., Wong, F. & Campochiaro, P. A. (2005). Oxidative damage is a potential cause of cone cell death in retinitis pigmentosa. J Cell Physiol., 203, 457-464.

Shlipak, M. G., Mattes, M. D. & Peralta, C. A. (2013). Update on cystatin C: incorporation into clinical practice. Am J Kidney Dis., 62, 595-603.

Shokolenko, I. N., Wilson, G. L. & Alexeyev, M. F. (2014). Aging: A mitochondrial DNA perspective, critical analysis and an update. World J Exp Med., 4, 46-57.

Simonsen, O., Grubb, A. & Thysell, H. (1985). The blood serum concentration of cystatin C (gamma-trace) as a measure of the glomerular filtration rate. Scand J Clin Lab Invest., 45, 97-101.

Slee, E. A., Adrain, C. & Martin, S. J. (1999). Serial killers: ordering caspase activation events in apoptosis. Cell Death Differ., 6, 1067-1074.

Solomon, S. D., Lindsley, K., Vedula, S. S., Krzystolik, M. G. & Hawkins, B. S. (2014). Anti-vascular endothelial growth factor for neovascular age-related macular degeneration. Cochrane Database Syst Rev., 8, CD005139.

Spector, A. (1995). Oxidative stress-induced cataract: mechanism of action. FASEB J., 9, 1173-1182.

Stone, E. M., Braun, T. A., Russell, S. R., Kuehn, M. H., Lotery, A. J., Moore, P. A., Eastman, C. G., Casavant, T. L. & Sheffield, V. C. (2004). Missense variations in the fibulin 5 gene and age-related macular degeneration. N Engl J Med., 351, 346-353.

Strauss, O. (2005). The retinal pigment epithelium in visual function. Physiol Rev., 85, 845-881.

Strunnikova, N., Baffi, J., Gonzalez, A., Silk, W., Cousins, S. W. & Csaky, K. G. (2001). Regulated heat shock protein 27 expression in human retinal pigment epithelium. Invest Ophthalmol Vis Sci., 42, 2130-2138.

Sung, C. H. & Chuang, J. Z. (2010). The cell biology of vision. J Cell Biol. 190, 953-963.

Suzuki, Y., Jin, C. & Yazawa, I. (2014). Cystatin C triggers neuronal degeneration in a model of multiple system atrophy. Am J Pathol., 184, 790-799.

Tang, P. H., Kono, M., Koutalos, Y., Ablonczy, Z. & Crouch, R. K. (2013). New insights into retinoid metabolism and cycling within the retina. Prog Retin Eye Res., 32, 48-63.

Tatsuta, T., Model, K. & Langer, T. (2005). Formation of membrane-bound ring complexes by prohibitins in mitochondria. Mol Biol Cell., 16, 248-259.

Thanan, R., Oikawa, S., Hiraku, Y., Ohnishi, S., Ma, N., Pinlaor, S., Yongvanit, P., Kawanishi, S. & Murata, M. (2014). Oxidative Stress and Its Significant Roles in Neurodegenerative Diseases and Cancer. Int J Mol Sci., 16, 193-217.

Tizon, B., Sahoo, S., Yu, H., Gauthier, S., Kumar, A. R., Mohan, P., Figliola, M., Pawlik, M., Grubb, A., Uchiyama, Y., Bandyopadhyay, U., Cuervo, A. M., Nixon, R. A. & Levy E. (2010). Induction of autophagy by cystatin C: a mechanism that protects murine primary cortical neurons and neuronal cell lines. PLoS One, 5, e9819.

Turk, V. & Bode, W. (1991). The cystatins: protein inhibitors of cysteine proteinases. FEBS Lett., 2895, 213-219.

van der Merwe, E. L. & Kidson, S. H. (2010). Advances in imaging the blood and aqueous vessels of the ocular limbus. Exp Eye Res., 91, 118-126.

Virgili, G. & Bini, A. (2007). Laser photocoagulation for neovascular age-related macular degeneration. Cochrane Database Syst Rev., 3, CD004763.

Wang, A. L., Lukas, T. J., Yuan, M., Du, N., Tso, M. O. & Neufeld, A. H. (2009). Autophagy, exosomes and drusen formation in age-related macular degeneration. Autopagy, 5, 563-564.

Wang, C., Sun, B., Zhou, Y, Grubb, A. & Gan, L. (2012). Cathepsin B degrades amyloid-β in mice expressing wild-type human amyloid precursor protein. J Biol Chem., 287, 39834-39841.

Wang, S., Fusaro, G., Padmanabhan, J. & Chellappan, S. P. (2002). Prohibitin co-localizes with Rb in the nucleus and recruits N-CoR and HDAC1 for transcriptional repression. Oncogene, 21, 8388-8396.

Warkentin, M., Freese, H. M., Karsten, U. & Schumann, R. (2007). New and Fast Method To Quantify Respiration Rates of Bacterial and Plankton Communities in Freshwater Ecosystems by Using Optical Oxygen Sensor Spots. Applied and Environmental Microbiology 73(21), 6722-6729.

Wassélius, J., Håkansson, K., Johansson, K., Abrahamson, M. & Ehinger, B. (2001). Identification and localization of retinal cystatin C. Invest Ophthalmol Vis Sci., 42, 1901-1906.

Wassélius, J., Håkansson, K., Abrahamson, M. & Ehinger, B. (2004). Cystatin C in the anterior segment of rat and mouse eyes. Acta Ophthalmol Scand., 82, 68-75.

Wassélius, J., Johansson, K., Håkansson, K., Abrahamson, M. & Ehinger, B. (2005). Cystatin C uptake in the eye. Graefes Arch Clin Exp Ophthalmol., 243, 583-592.

Wickramasinghe, N. S., Banerjee, K., Nagaraj, N. S., Vigneswaran, N. & Zacharias, W. (2005). Hypoxia alters cathepsin B / inhibitor profiles in oral carcinoma cell lines. AntiCancer Res., 25, 2841-2849.

Williams, M. A., Silvestri, V., Craig, D., Passmore, A. P. & Silvestri, G. (2014). The prevalence of age-related macular degeneration in Alzheimer's disease. J Alzheimers Dis., 42, 909-914.

Wright, J. W. & Harding, J. W. (2008). The angiotensin AT4 receptor subtype as a target for the treatment of memory dysfunction associated with Alzheimer's disease. J Renin Angiotensin Aldosterone Syst., 9, 226-237.

Yamashima, T. (2013). Reconsider Alzheimer's disease by the 'calpain-cathepsin hypothesis'--a perspective review. Prog Neurobiol., 105, 1-23.

Yan, L. J. (2014). Positive oxidative stress in aging and aging-related disease tolerance. Redox Biol., 2C, 165-269.

Zanon-Moreno, V., Marco-Ventura, P., Lleo-Perez, A., Pons-Vazquez, S., Garcia-Medina, J.J., Vinuesa-Silva, I., Moreno-Nadal, M. A. & Pinazo-Duran, M. D. (2008). Oxidative stress in primary open-angle glaucoma. J Glaucoma., 17, 263-268.

Zhao, S., Thornguist, S. C. & Barnstable, C. J. (1995). In vitro transdifferentiation of embryonic rat retinal pigment epithelium to neural retina. Brain Res. 677, 300-310.

Zhang, C., Rissman, R. A. & Feng, J. (2014). Characterization of ATP Alternations in an Alzheimer's Disease Transgenic Mouse Model. J Alzheimers Dis., Epub ahead of print.

Zurdel, J., Finckh, U., Menzer, G., Nitsch, R. M. & Richard, G. (2002). CST3 genotype associated with exudative age related macular degeneration. Br J Ophthalmol., 86(2), 214-219.

Appendix 1:

Complete Mass Spectrometry Data

Appendix Table 1: Complete ion abundance data for mass spectrometry experiment. ANOVA values for significance are included.

Accession	Protein	Halotag Normalised abundance			Wild Type Normalised abundance			Variant B Normalised abundance			ANOVA (P=)
P07711;Q5NE16	Cathepsin L1 OS=Homo sapiens GN=CTSL PE=1 SV=2	13113.03	48227.11	40417.78	3533291	734520.6	4277290	1098944	1036262	2798111	0.000793
P07858	Cathepsin B OS=Homo sapiens GN=CTSB PE=1 SV=3	86042.56	62776.73	73531.79	4362367	1006305	4940636	1435178	615334.4	2405779	0.001136
P53634	Dipeptidyl peptidase 1 OS=Homo sapiens GN=CTSC PE=1 SV=2	27491.31	157320.1	52984.53	8593620	1301101	11220991	852512.1	285743.6	1178349	0.00384
P11021;O95399	78 kDa glucose-regulated protein OS=Homo sapiens GN=HSPA5 PE=1 SV=2	78167.37	294317.7	55676.82	7384152	911581.5	14463609	979188	637926.2	1398130	0.010751
P01034	Cystatin-C OS=Homo sapiens GN=CST3 PE=1 SV=1	76287.66	151379.5	86871.38	5340401	1911358	37207228	341471.9	289242.5	2858737	0.011564
P35232	Prohibitin OS=Homo sapiens GN=PHB PE=1 SV=1	39491.17	60223.67	36007.04	41333.37	26046.57	35478.42	68523.07	60103.76	80632.52	0.021159
Q9UIQ6	Leucyl-cystinyl aminopeptidase OS=Homo sapiens GN=LNPEP PE=1 SV=3	39372.51	53683.88	44553.74	3754831	99494.74	2320624	43164.89	82493.12	68016.2	0.033988

P38646	Stress-70 protein, mitochondrial OS=Homo sapiens GN=HSPA9 PE=1 SV=2	22874.29	67301.2	20673.51	900229.3	99261.2	720731.3	122446.6	242889.6	37965.08	0.048722
P10620	Microsomal glutathione S-transferase 1 OS=Homo sapiens GN=MGST1 PE=1 SV=1	1641.517	3141.681	433.8308	10914.03	1798.646	2841.203	12411.44	20345.96	6111.78	0.058656
P62937;Q9Y536	Peptidyl-prolyl cis-trans isomerase A OS=Homo sapiens GN=PPIA PE=1 SV=2	29470.73	162034.3	12643.23	292088.5	97330.7	263163.1	315751.9	498830.2	152595	0.07311
P05141;P12235	ADP/ATP translocase 2 OS=Homo sapiens GN=SLC25A5 PE=1 SV=7	9393.296	39520.21	13843.83	145886.5	32156.45	67251.9	38041.04	92643.51	63980.06	0.080526
P27348	14-3-3 protein theta OS=Homo sapiens GN=YWHAQ PE=1 SV=1	0	20706.29	0	2856.544	1263.53	1177.183	0	0	0	0.082311
P08107;P17066;P48741	Heat shock 70 kDa protein 1A/1B OS=Homo sapiens GN=HSPA1A PE=1 SV=5	7479.263	29820.18	4588.248	254641.1	24926.59	151876.9	26550.67	65418.14	10251.86	0.094093
P06899;Q6DN03	Histone H2B type 1-J OS=Homo sapiens GN=HIST1H2BJ PE=1 SV=3	245.1087	2899.985	380.4734	2616.036	25814.98	2339.599	123.3444	152.0741	1849.241	0.10787

P53999	Activated RNA polymerase II transcriptional coactivator p15 OS=Homo sapiens GN=SUB1 PE=1 SV=3	532.7164	1707.237	35.01324	2937.899	5459.864	1685.558	6111.674	12202.11	1039.289	0.124139
P11142;P54652	Heat shock cognate 71 kDa protein OS=Homo sapiens GN=HSPA8 PE=1 SV=1	75182.39	235862.4	39617.75	1519797	155003.8	786293.8	135869.4	323164.2	66244.67	0.126988
P62979	Ubiquitin-40S ribosomal protein S27a OS=Homo sapiens GN=RPS27A PE=1 SV=2	155769.6	246037.2	40204.98	649273.1	334605	612750.7	82389.5	521172.7	109571	0.147286
Q99623	Prohibitin-2 OS=Homo sapiens GN=PHB2 PE=1 SV=2	30298.4	64060.42	31402.53	43260.65	24924.31	28322.11	96167.18	38163.75	70684.28	0.165195
P31151	Protein S100-A7 OS=Homo sapiens GN=S100A7 PE=1 SV=4	0	171.4909	0	160.8923	166.4249	21031.89	0	0	488.73	0.171072
Q15149	Plectin OS=Homo sapiens GN=PLEC PE=1 SV=3	1727.877	15092.12	541.861	8798.345	120412.7	11130.47	3437.309	7242.767	1855.088	0.173123
P23396	40S ribosomal protein S3 OS=Homo sapiens GN=RPS3 PE=1 SV=2	24620.44	91909.58	13473.82	394026.6	89002.09	70539.27	115645.2	219705.2	48929.75	0.178646
P12236	ADP/ATP translocase 3 OS=Homo sapiens GN=SLC25A6 PE=1 SV=4	4217.865	9195.174	4589.295	52767.26	5581.639	10046.29	16882.42	25974.56	15182.11	0.188879

P62249	40S ribosomal protein S16 OS=Homo sapiens GN=RPS16 PE=1 SV=2	11865.3	11898.78	4949.291	40992.88	39464.68	8171.663	23403.1	50393.92	15593.7	0.189398
P22314	Ubiquitin-like modifier-activating enzyme 1 OS=Homo sapiens GN=UBA1 PE=1 SV=3	9.665088	1212.953	0	141.5592	636.5612	3.198	2749.157	8714.175	349.511	0.2036
Q06830;P32119;Q13162	Peroxiredoxin-1 OS=Homo sapiens GN=PRDX1 PE=1 SV=1	144872.8	231173.1	135787.2	309433.2	110144.7	203966.5	243880.6	288676.1	362547.5	0.209532
A8MT79	Putative zinc-alpha-2-glycoprotein-like 1 OS=Homo sapiens PE=5 SV=2	2896.413	4525.868	2524.937	4446.255	9383.985	22808.24	3778.97	28742.47	7448.632	0.221211
P21796	Voltage-dependent anion-selective channel protein 1 OS=Homo sapiens GN=VDAC1 PE=1 SV=2	14616	72965.27	23301.79	37358.05	25176.97	47344.92	51902.55	65224.53	86685.09	0.222051
P06748	Nucleophosmin OS=Homo sapiens GN=NPM1 PE=1 SV=2	11372.25	31949.59	20361.11	27868.83	194008.8	67152.13	15039.27	83673.06	18390.76	0.227452
P84095	Rho-related GTP-binding protein RhoG OS=Homo sapiens GN=RHOG PE=1 SV=1	483.5288	7328.744	992.581	25731.42	846.2422	13003.81	0	24795.77	0	0.228527

Q8NC51	Plasminogen activator inhibitor 1 RNA-binding protein OS=Homo sapiens GN=SERBP1 PE=1 SV=2	358.3373	1093.083	0	2268.619	1331.332	2000.049	984.067	3407.9	1054.015	0.229626
P07437;A6NKZ8;A6NNZ2;Q13885;Q9BUF5;Q9H4B7	Tubulin beta chain OS=Homo sapiens GN=TUBB PE=1 SV=2	20800.08	133209.6	10379.49	650494.6	52869.02	80925.95	110260	255439.5	104260.9	0.235618
P62913	60S ribosomal protein L11 OS=Homo sapiens GN=RPL11 PE=1 SV=2	5020.837	29654.06	3145.072	65063.15	53135.43	10502.11	20538.64	42587.06	12411.1	0.242398
P04792	Heat shock protein beta-1 OS=Homo sapiens GN=HSPB1 PE=1 SV=2	19868.11	113933.4	3033.569	204276.6	63841.02	160007	55391.6	81426.75	11965.35	0.246318
Q08211	ATP-dependent RNA helicase A OS=Homo sapiens GN=DHX9 PE=1 SV=4	0	682.7522	0	1016.908	11053.31	0	2901.396	12533.72	425.837	0.247831
P62888	60S ribosomal protein L30 OS=Homo sapiens GN=RPL30 PE=1 SV=2	4257.212	10560.23	2341.326	6144.587	24108.8	10867.94	10394.13	19381.69	6434.29	0.260156
P61978	Heterogeneous nuclear ribonucleoprotein K OS=Homo sapiens GN=HNRNPK PE=1 SV=1	3132.741	25100.79	971.9891	21463.29	15637.07	26927.3	29709.15	85925.56	4873.354	0.266266

P27482	Calmodulin-like protein 3 OS=Homo sapiens GN=CALML3 PE=1 SV=2	960.7899	84307.5	2738.187	44016.62	12494.79	54986.75	4989.855	5222.784	3835.266	0.285151
P62847	40S ribosomal protein S24 OS=Homo sapiens GN=RPS24 PE=1 SV=1	5073.946	9157.179	2860.024	3136.422	1854.097	0	12018.56	6139.535	2040.283	0.288213
P60660;P14649	Myosin light polypeptide 6 OS=Homo sapiens GN=MYL6 PE=1 SV=2	11149.72	36550.49	6835.172	23800.85	6778.879	8479.292	6093.078	8747.523	2741.108	0.290053
P62826	GTP-binding nuclear protein Ran OS=Homo sapiens GN=RAN PE=1 SV=3	10445.95	17961.89	2402.434	29265.26	16870.28	5708.014	21725.66	62419.21	14447.84	0.292968
P10809	60 kDa heat shock protein, mitochondrial OS=Homo sapiens GN=HSPD1 PE=1 SV=2	37350.48	66434.41	23919.51	104997.2	58268.29	227482.7	41123.83	195472.1	33581.87	0.295966
P52597	Heterogeneous nuclear ribonucleoprotein F OS=Homo sapiens GN=HNRNPF PE=1 SV=3	8267.865	27194.76	1302.397	6983.572	24541.33	5961.129	46233.86	51344.79	11365.8	0.297689
P10599	Thioredoxin OS=Homo sapiens GN=TXN PE=1 SV=3	13650.61	37740.69	6719.273	74121.18	20447.47	52042.63	10265.46	43718.98	21538.24	0.30109

P09211	Glutathione S-transferase P OS=Homo sapiens GN=GSTP1 PE=1 SV=2	0	19277.34	46.13795	1636.873	1431.456	3464.013	8505.175	25609.23	823.8745	0.306923
P23528;Q9Y281	Cofilin-1 OS=Homo sapiens GN=CFL1 PE=1 SV=3	6634.527	65469.18	1248.369	108995.2	20454.09	102909.5	4167.226	70063.04	8908.491	0.31484
Q71UM5	40S ribosomal protein S27-like OS=Homo sapiens GN=RPS27L PE=1 SV=3	736.453	4563.391	590.1875	8982.777	4453.93	3027.23	3277.199	5939.755	546.8993	0.322134
Q00839	Heterogeneous nuclear ribonucleoprotein U OS=Homo sapiens GN=HNRNPU PE=1 SV=6	14990.55	18616.81	8271.909	14884.28	76009.78	21253.33	17887.64	34015.32	17794.25	0.32766
P01876;P01877	Ig alpha-1 chain C region OS=Homo sapiens GN=IGHA1 PE=1 SV=2	66.54413	61437.61	1369.187	4.72617	0	3726.004	278.4505	553.6813	190.4825	0.327777
P13639	Elongation factor 2 OS=Homo sapiens GN=EEF2 PE=1 SV=4	243.5559	18716.73	138.5916	10423.14	3872.681	18768.43	62.65754	10644.71	306.8015	0.3292
P49411	Elongation factor Tu, mitochondrial OS=Homo sapiens GN=TUFM PE=1 SV=2	9742.697	5588.227	1234.161	30663.94	5120.173	10669.3	5400.737	14222.45	13288.8	0.331268
P06702	Protein S100-A9 OS=Homo sapiens GN=S100A9 PE=1 SV=1	2067.364	57554.1	4848.434	3408.474	1133.391	642.8835	885.2019	2273.055	13834.02	0.335502

P14324	Farnesyl pyrophosphate synthase OS=Homo sapiens GN=FDPS PE=1 SV=4	96.38554	984.0768	0	363.4856	342.179	569.5343	1388.981	3126.383	86.77479	0.359523
P09651;Q32P51	Heterogeneous nuclear ribonucleoprotein A1 OS=Homo sapiens GN=HNRNPA1 PE=1 SV=5	2242.632	18877.84	2400.424	5525.261	62586.75	12117.28	1125.025	25181.18	280.4879	0.365303
P80723	Brain acid soluble protein 1 OS=Homo sapiens GN=BASP1 PE=1 SV=2	12327.93	8362.618	7286.852	28633.12	9385.827	21438.68	1939.989	30757.18	2739.034	0.366128
P61353	60S ribosomal protein L27 OS=Homo sapiens GN=RPL27 PE=1 SV=2	1909.413	1085.983	91.62424	901.3417	3852.167	869.1463	3067.026	3072.597	1172.556	0.368767
P08195	4F2 cell-surface antigen heavy chain OS=Homo sapiens GN=SLC3A2 PE=1 SV=3	391.0046	1752.731	1277.137	8271.972	481.0362	1520.28	2625.718	10668.16	1845.617	0.370272
P67936	Tropomyosin alpha-4 chain OS=Homo sapiens GN=TPM4 PE=1 SV=3	252.5539	4579.481	0	6638.003	711.4677	759.4386	0	3633.434	0	0.372536
P60174	Triosephosphate isomerase OS=Homo sapiens GN=TPI1 PE=1 SV=3	3165.724	24508.6	18.81876	14045.74	6742.03	6628.407	2.602118	9364.669	170.1631	0.374694

P05090	Apolipoprotein D OS=Homo sapiens GN=APOD PE=1 SV=1	2816.893	5727.335	2945.705	3333.823	130789.6	2503.882	4604.506	2184.671	534.3652	0.378556
P31944	Caspase-14 OS=Homo sapiens GN=CASP14 PE=1 SV=2	4906.257	7900.542	832.8636	13084.5	2050.713	52519.21	8758.059	11210.49	12662.07	0.384554
P62263	40S ribosomal protein S14 OS=Homo sapiens GN=RPS14 PE=1 SV=3	2727.655	8302.627	243.3454	9411.487	10376.53	2887.308	9300.896	15266.35	2176.115	0.390748
Q8NHW5	60S acidic ribosomal protein P0-like OS=Homo sapiens GN=RPLP0P6 PE=5 SV=1	5436.534	6458.15	1411.768	4671.192	10255.2	5241.744	10032.82	26944.21	3371.657	0.394854
Q07021	Complement component 1 Q subcomponent-binding protein, mitochondrial OS=Homo sapiens GN=C1QBP PE=1 SV=1	9078.38	22206.35	3235.061	68611.6	9560.322	52240.08	6564.714	65212.99	8315.135	0.398124
P61604	10 kDa heat shock protein, mitochondrial OS=Homo sapiens GN=HSPE1 PE=1 SV=2	6739.212	19096.77	0	43172.5	14551.5	60542.9	77.89647	51337.46	146.1069	0.398934
P26373	60S ribosomal protein L13 OS=Homo sapiens GN=RPL13 PE=1 SV=4	10338.08	10562.39	3148.34	8662.245	31878.02	3108.51	22512.42	26961.51	10471.05	0.402434

P49207	60S ribosomal protein L34 OS=Homo sapiens GN=RPL34 PE=1 SV=3	1819.8	5616.845	286.3723	3121.448	2022.631	1820.933	6233.019	6402.552	2124.724	0.407152
P07737	Profilin-1 OS=Homo sapiens GN=PFN1 PE=1 SV=2	26961.97	121406.3	1303.885	49181.99	60096.36	19019.5	113664.2	334842.1	27684.14	0.408074
Q00325	Phosphate carrier protein, mitochondrial OS=Homo sapiens GN=SLC25A3 PE=1 SV=2	7071.125	18819.97	9941.442	44403.4	7537.672	42831.11	16791.26	41920.6	14213.43	0.414779
P60709;A5A3E0;P0CG38;P0CG39;P62736;P68032;Q6S8J3;Q9BYX7	Actin, cytoplasmic 1 OS=Homo sapiens GN=ACTB PE=1 SV=1	401348.1	1953730	572655.6	1922138	957543.5	1375907	506634.5	1225998	679480.5	0.415423
P62701;P22090	40S ribosomal protein S4, X isoform OS=Homo sapiens GN=RPS4X PE=1 SV=2	1457.84	5890.872	282.0348	2823.683	7602.5	707.4862	7116.985	9160.099	2301.909	0.422125
P62857	40S ribosomal protein S28 OS=Homo sapiens GN=RPS28 PE=1 SV=1	11059.83	11922.6	13765.26	33287.41	11703.02	23794.85	9938.27	30059.18	9958.472	0.424428

P07910;O60812	Heterogeneous nuclear ribonucleoproteins C1/C2 OS=Homo sapiens GN=HNRNPC PE=1 SV=4	4074.201	11667.58	1750.584	5141.099	172959.6	8437.719	3097.848	12790.72	12842.36	0.425924
P36578	60S ribosomal protein L4 OS=Homo sapiens GN=RPL4 PE=1 SV=5	2362.119	4118.333	1460.461	2047.396	7623.146	354.7611	5455.221	11736.33	2651.7	0.428325
P43307	Translocon-associated protein subunit alpha OS=Homo sapiens GN=SSR1 PE=1 SV=3	260.4053	2186.581	1808.172	7558.485	357.9385	0	4233.107	1552.53	3008.035	0.4436
P00338;P07864	L-lactate dehydrogenase A chain OS=Homo sapiens GN=LDHA PE=1 SV=2	16664.91	115136.1	2687.722	49607.02	67065.22	38362.23	141829.2	356046.4	12968.7	0.44495
P45880	Voltage-dependent anion-selective channel protein 2 OS=Homo sapiens GN=VDAC2 PE=1 SV=2	25877.63	95260.99	36281.23	79523.78	27589.69	46828.6	65727.87	61315.97	108887.5	0.445276
P30041	Peroxiredoxin-6 OS=Homo sapiens GN=PRDX6 PE=1 SV=3	1651.658	3492.913	0	7001.628	3187.642	455.5918	3136.161	10486.73	831.8769	0.450808

Q71U36;A6NHL2;Q13748;Q6PEY2;Q9BQE3;Q9H853;Q9NY65	Tubulin alpha-1A chain OS=Homo sapiens GN=TUBA1A PE=1 SV=1	373.5554	13735.16	592.4726	44122.03	8203.964	1385.242	11766.08	23254.9	1136.386	0.472955
P06576	ATP synthase subunit beta, mitochondrial OS=Homo sapiens GN=ATP5B PE=1 SV=3	19425.95	37605.08	14872.18	43301.08	18279.83	62815.81	21745.72	36689.39	20921.04	0.474901
Q15366	Poly(rC)-binding protein 2 OS=Homo sapiens GN=PCBP2 PE=1 SV=1	1191.138	7758.481	892.8504	5791.138	3298.22	8855.575	7884.038	14276.1	1144.96	0.480621
P07339	Cathepsin D OS=Homo sapiens GN=CTSD PE=1 SV=1	1629.477	7784.662	147.3561	5149.49	1910.249	8604.697	3162.118	5205.398	1850.577	0.490568
P02795	Metallothionein-2 OS=Homo sapiens GN=MT2A PE=1 SV=1	689.9888	2596.554	390.3806	6916.828	663.4322	730.9614	211.0675	6685.829	0	0.497726
Q9NQ39	Putative 40S ribosomal protein S10-like OS=Homo sapiens GN=RPS10P5 PE=5 SV=1	2498.518	7035.834	3184.254	19681.32	7489.932	4033.077	6469.173	19365.37	2630.515	0.498639
P01834	Ig kappa chain C region OS=Homo sapiens GN=IGKC PE=1 SV=1	6698.851	806784.5	12122.91	12953.67	9096.575	13563.39	10128.99	14447.26	5702.405	0.499237
P08779;O76013;P35900;Q7Z3Y9;Q8N1A0;Q99456	Keratin, type I cytoskeletal 16 OS=Homo sapiens GN=KRT16 PE=1 SV=4	125026.3	599418.8	984697.5	130458.2	37737.3	131975.3	30922.44	6738021	244082.8	0.506047

P07195	L-lactate dehydrogenase B chain OS=Homo sapiens GN=LDHB PE=1 SV=2	3046.033	11001.4	15.00021	17095.79	12874.32	2067.125	53172.54	120395.2	240.6979	0.512072
Q07020	60S ribosomal protein L18 OS=Homo sapiens GN=RPL18 PE=1 SV=2	19733.87	30072.5	10580.05	17706.16	44386.48	26052.6	27111.27	59060.38	17845.3	0.516548
P63244	Guanine nucleotide-binding protein subunit beta-2-like 1 OS=Homo sapiens GN=GNB2L1 PE=1 SV=3	1551.193	9931.967	1678.968	14960.98	4047.999	6672.025	17633.27	38628.25	1293.234	0.51998
P56134	ATP synthase subunit f, mitochondrial OS=Homo sapiens GN=ATP5J2 PE=1 SV=3	807.9087	3159.532	3169.689	4501.577	1076.231	0	0	835.6917	517.7817	0.521545
P50914	60S ribosomal protein L14 OS=Homo sapiens GN=RPL14 PE=1 SV=4	5876.198	13819.55	1149.515	5385.463	18036.49	77.86273	12147.71	20782.82	6539.508	0.525109
P58107	Epiplakin OS=Homo sapiens GN=EPPK1 PE=1 SV=2	0	3453.648	0	0	46789.19	9091.431	0	717.3711	0	0.526173

P63313;P62328	Thymosin beta-10 OS=Homo sapiens GN=TMSB10 PE=1 SV=2	23868.98	26125.81	92.97859	42556.9	22969.9	11972.37	1064.096	35588.5	679.3189	0.528163
P06454	Prothymosin alpha OS=Homo sapiens GN=PTMA PE=1 SV=2	18142.65	27937.88	266.9306	52397.24	20873.81	10527.19	449.8733	51977.36	1325.289	0.53063
P14174	Macrophage migration inhibitory factor OS=Homo sapiens GN=MIF PE=1 SV=4	10066.68	54659.69	0	10234.79	6663.247	4782.534	22836.77	35757.75	9271.517	0.538645
P25705	ATP synthase subunit alpha, mitochondrial OS=Homo sapiens GN=ATP5A1 PE=1 SV=1	7687.852	64209.52	10179.84	60049.3	26886.67	48474.09	56595.39	116291.5	8715.265	0.53875
P06733;P09104;P13929	Alpha-enolase OS=Homo sapiens GN=ENO1 PE=1 SV=2	28387.61	219189	10378.08	225835	52236.8	133274.5	10156.21	262590.2	12282.86	0.542443
P02787	Serotransferrin OS=Homo sapiens GN=TF PE=1 SV=3	7702.333	427471.1	10408.13	14044.93	9315.036	10087.34	7964.094	14995.64	12010.22	0.546749
P46781	40S ribosomal protein S9 OS=Homo sapiens GN=RPS9 PE=1 SV=3	936.6739	5538.217	1685.502	2457.664	14288.61	0	3587.775	5810.468	5936.071	0.547514
P05387	60S acidic ribosomal protein P2 OS=Homo sapiens GN=RPLP2 PE=1 SV=1	28941.27	41479.41	17539.35	93423.33	69486.42	16906.97	33189.22	80257.65	35721.22	0.549169

P67809	Nuclease-sensitive element-binding protein 1 OS=Homo sapiens GN=YBX1 PE=1 SV=3	29104.21	27814.39	708.2476	32309.05	34289.42	13413.7	26583.68	53153.2	10720.73	0.555374
P01024	Complement C3 OS=Homo sapiens GN=C3 PE=1 SV=2	288.8026	22785.59	262.4533	374.5839	387.4936	129.8754	536.2411	1388.435	183.1002	0.556237
P05787;P41219;Q9NSB2	Keratin, type II cytoskeletal 8 OS=Homo sapiens GN=KRT8 PE=1 SV=7	56816.26	76031.42	130976.5	92059.94	1003372	75296.89	152862.5	317300.7	80579.09	0.56276
Q02543	60S ribosomal protein L18a OS=Homo sapiens GN=RPL18A PE=1 SV=2	2121.809	7853.826	1028.439	1869.95	9267.594	1871.917	4424.423	11780.31	3370.751	0.571105
P04075	Fructose-bisphosphate aldolase A OS=Homo sapiens GN=ALDOA PE=1 SV=2	1096.848	17471.61	28.46111	5667.587	3625.861	10396.37	4265.032	13591.01	265.1161	0.57518
P11940;Q13310	Polyadenylate-binding protein 1 OS=Homo sapiens GN=PABPC1 PE=1 SV=2	1558.714	8375.323	401.3618	2840.421	2652.093	83.08612	11820.35	21058.62	403.9738	0.581635
P01040	Cystatin-A OS=Homo sapiens GN=CSTA PE=1 SV=1	40725.67	18192.86	7288.105	35814.88	10864.33	162392.2	27613.55	69229.96	22216.42	0.582273
P62854	40S ribosomal protein S26 OS=Homo sapiens GN=RPS26 PE=1 SV=3	4878.606	16275.42	881.5713	5026.293	24180.55	0	11488.58	18888.64	1836.998	0.590484

P52272	Heterogeneous nuclear ribonucleoprotein M OS=Homo sapiens GN=HNRNPM PE=1 SV=3	830.964	8751.501	232.7231	2810.502	4960.433	3047.123	1224.993	6026.763	322.5909	0.600057
P05109	Protein S100-A8 OS=Homo sapiens GN=S100A8 PE=1 SV=1	1396.355	102872.8	3861.255	3598.724	12714.44	17954.13	582.3346	4240.464	7953.874	0.602569
P02538	Keratin, type II cytoskeletal 6A OS=Homo sapiens GN=KRT6A PE=1 SV=3	20491.93	466684.9	26902.18	17231.9	10401.13	38038.5	17234.57	314479.7	15820.24	0.604325
P61204	ADP-ribosylation factor 3 OS=Homo sapiens GN=ARF3 PE=1 SV=2	2367.579	10552.16	3673.112	24158.51	4840.484	2271.675	14872.35	17984.94	3907.449	0.607161
P49327	Fatty acid synthase OS=Homo sapiens GN=FASN PE=1 SV=3	0	401.7261	0	0	0	0	0	10852.16	0	0.609864
P39023	60S ribosomal protein L3 OS=Homo sapiens GN=RPL3 PE=1 SV=2	20179.67	8184.007	4957.924	8987.695	12750.92	17908.41	11128.26	30030.24	10254.13	0.611026
Q5VTE0;Q05639	Putative elongation factor 1-alpha-like 3 OS=Homo sapiens GN=EEF1A1P5 PE=5 SV=1	112144.4	412166.9	73970.76	534362.5	193367.9	220420.7	299041.7	674546	95133.82	0.613994

P10412;P16401	Histone H1.4 OS=Homo sapiens GN=HIST1H1E PE=1 SV=2	27545.82	52912.74	7402.685	42354.49	143536.8	15941.64	59993.74	35341.3	22184.68	0.625423
P63104;P31946	14-3-3 protein zeta/delta OS=Homo sapiens GN=YWHAZ PE=1 SV=1	1472.992	92383.51	738.4746	15160.38	5135.734	22309.96	1136.585	16774.55	1165.305	0.629559
P05783	Keratin, type I cytoskeletal 18 OS=Homo sapiens GN=KRT18 PE=1 SV=2	24576.93	74024.65	100180.8	68676.76	544200.8	49888.73	90672.6	144697.2	34130.77	0.631979
P0CG05;A0M8Q6;B9A064; P0CF74	Ig lambda-2 chain C regions OS=Homo sapiens GN=IGLC2 PE=1 SV=1	1164.994	286471.1	3465.277	2654.196	1015.606	23238.53	2587.999	4815.269	785.6186	0.637634
Q8TF72	Protein Shroom3 OS=Homo sapiens GN=SHROOM3 PE=1 SV=2	76986.94	61357.16	241747.3	60204.6	149584	4445.949	88473.13	12793.43	193243.8	0.639565
P15924	Desmoplakin OS=Homo sapiens GN=DSP PE=1 SV=3	18801.19	90955.64	22653.06	41356.89	30639.71	156048.5	7477.322	94659.72	26147.94	0.64436
P68371;P04350;Q3ZCM7	Tubulin beta-4B chain OS=Homo sapiens GN=TUBB4B PE=1 SV=1	4618.243	23070.81	776.7972	93453.58	5544.078	8354.55	15814.1	56595.09	0	0.651163
Q14240	Eukaryotic initiation factor 4A-II OS=Homo sapiens GN=EIF4A2 PE=1 SV=2	2548.159	10989.92	337.1176	10398.54	5804.373	17408.82	22702.59	44010.35	176.7467	0.654634

P40926	Malate dehydrogenase, mitochondrial OS=Homo sapiens GN=MDH2 PE=1 SV=3	1523.516	5643.847	30.67288	3961.957	578.8155	3840.861	569.1368	410.3102	1232.411	0.657407
P13647;P12036;Q3SY84;Q7RTS7;Q8N1N4	Keratin, type II cytoskeletal 5 OS=Homo sapiens GN=KRT5 PE=1 SV=3	413683	3937016	488241.9	391047.3	142925	1081675	163574.7	2108789	420446.5	0.685838
Q01105	Protein SET OS=Homo sapiens GN=SET PE=1 SV=3	2861.33	5634.572	0	15164.88	331.7298	2994.625	0	19737.76	205.1547	0.692603
Q6UWP8	Suprabasin OS=Homo sapiens GN=SBSN PE=2 SV=2	345.9268	270.8905	1.519573	1240.296	0	11417.14	963.7798	489.8891	636.9261	0.695154
P02545	Prelamin-A/C OS=Homo sapiens GN=LMNA PE=1 SV=1	3018.527	45461.41	604.2104	7850.691	13391.43	14664.21	9467.699	12563.26	793.4076	0.699725
P27797	Calreticulin OS=Homo sapiens GN=CALR PE=1 SV=1	1192.036	7712.166	100.5758	2580.641	2026.206	5846.044	6455.253	5827.351	252.7025	0.701805
P14618	Pyruvate kinase PKM OS=Homo sapiens GN=PKM PE=1 SV=4	10748.6	75509.63	4852.821	59629.69	10431.19	71195.93	32037.48	128631.3	8934.718	0.705312
P62241	40S ribosomal protein S8 OS=Homo sapiens GN=RPS8 PE=1 SV=2	13888.75	16250.76	6787.4	6164.958	48131.6	797.0242	15150.91	33028.96	6469.94	0.713601
Q9NZT1	Calmodulin-like protein 5 OS=Homo sapiens GN=CALML5 PE=1 SV=2	8406.135	20745.07	6014	7029.994	10318.11	9272.46	7630.094	11954.81	19567.56	0.714545

P07900;Q58FG0	Heat shock protein HSP 90-alpha OS=Homo sapiens GN=HSP90AA1 PE=1 SV=5	21019.14	47817.02	4445.832	43552.82	28961.39	20390.58	114867.1	235021.3	3530.226	0.715104
P08238;P14625;Q12931;Q14568;Q58FF6;Q58FF7;Q58FF8;Q58FG1	Heat shock protein HSP 90-beta OS=Homo sapiens GN=HSP90AB1 PE=1 SV=4	41521.21	169098.9	13615.85	130119.3	71851.6	63033.97	311576.4	639716.5	9534.223	0.728856
P08729	Keratin, type II cytoskeletal 7 OS=Homo sapiens GN=KRT7 PE=1 SV=5	23280.59	53992.57	123935.2	44906.93	833311.9	39746.02	61344.4	125216.6	57415.39	0.730575
P01857	Ig gamma-1 chain C region OS=Homo sapiens GN=IGHG1 PE=1 SV=1	8801.351	467659.5	7951.57	13612.72	15529.91	23605.49	13268.27	24006.16	6782.882	0.731568
Q5D862	Filaggrin-2 OS=Homo sapiens GN=FLG2 PE=1 SV=1	25719.3	4377.761	21244.5	35758.98	5783.139	52408.35	8856.693	56159.14	33708.16	0.736403
Q09666	Neuroblast differentiation-associated protein AHNAK OS=Homo sapiens GN=AHNAK PE=1 SV=2	2904.817	27721.94	3747.15	5926.702	5373.386	10775.62	13106.53	18450.4	5435.196	0.736814

Q9H299	SH3 domain-binding glutamic acid-rich-like protein 3 OS=Homo sapiens GN=SH3BGRL3 PE=1 SV=1	3097.22	10066.28	772.144	845.145	3984.025	1265.775	2747.309	3215.829	1235.886	0.755944
P04264;P14136	Keratin, type II cytoskeletal 1 OS=Homo sapiens GN=KRT1 PE=1 SV=6	7423208	4515086	7433954	18168975	3790973	15476437	2732453	29096210	12138436	0.75666
P22528	Cornifin-B OS=Homo sapiens GN=SPRR1B PE=1 SV=2	10657.89	68705.62	27356.95	9017.234	13910.02	38882.64	11685	35199.05	25571	0.761439
P31947	14-3-3 protein sigma OS=Homo sapiens GN=SFN PE=1 SV=1	924.247	74450.71	549.4839	1076.331	612.6374	20620.52	138.5136	2316.762	2639.381	0.762458
Q5QNW6;Q96A08	Histone H2B type 2-F OS=Homo sapiens GN=HIST2H2BF PE=1 SV=3	760.478	4445.975	232.3265	513.5778	52045.58	788.9898	563.865	2184.215	3474.237	0.763936
P61313	60S ribosomal protein L15 OS=Homo sapiens GN=RPL15 PE=1 SV=2	3503.387	5714.089	1427.433	2056.115	9058.696	2636.095	4745.326	8504.931	2550.601	0.766472
P84098	60S ribosomal protein L19 OS=Homo sapiens GN=RPL19 PE=1 SV=1	9065.292	17386.33	2402.36	6039.592	22037.71	6091.797	15255.84	26783.25	4607.735	0.771892
P05386	60S acidic ribosomal protein P1 OS=Homo sapiens GN=RPLP1 PE=1 SV=1	11015.78	33544.88	10858.37	22407.79	31025.93	2480.73	41541.94	51001.01	5963.199	0.772699

P62269	40S ribosomal protein S18 OS=Homo sapiens GN=RPS18 PE=1 SV=3	11966.33	33729.73	18572.21	48386.09	69173.34	6202.017	66856.88	13555.08	44102.57	0.773293
P61247	40S ribosomal protein S3a OS=Homo sapiens GN=RPS3A PE=1 SV=2	2881.599	5120.366	619.9012	2985.944	3103.45	0	9244.09	9100.004	0	0.77942
Q71DI3;Q6NXT2	Histone H3.2 OS=Homo sapiens GN=HIST2H3A PE=1 SV=3	4388.865	112550.8	3297.113	3390.002	365064.9	7602.819	3057.545	2877.722	36995.27	0.800062
P12273	Prolactin-inducible protein OS=Homo sapiens GN=PIP PE=1 SV=1	2158.034	9179.554	13797.89	12653.84	93322.87	0	2607.488	3986.798	4815.484	0.800156
P02647	Apolipoprotein A-I OS=Homo sapiens GN=APOA1 PE=1 SV=1	14311.65	10378.71	14145.1	7112.624	13772.92	13215.11	14655.41	8503.208	13497.4	0.801811
P00558	Phosphoglycerate kinase 1 OS=Homo sapiens GN=PGK1 PE=1 SV=3	4008.709	40544.61	7250.183	18455.13	10039.11	5047.955	12625.64	37174	8047.947	0.804669
Q04695;Q9C075	Keratin, type I cytoskeletal 17 OS=Homo sapiens GN=KRT17 PE=1 SV=2	125803.2	5845811	201455.7	131431.3	703295.2	164032.2	140255.9	1198750	121878.3	0.805953
P0C0S8;P0C0S5;P16104;Q8IUE6	Histone H2A type 1 OS=Homo sapiens GN=HIST1H2AG PE=1 SV=2	25031.24	66147.68	19891.1	27759.74	2041711	9318.63	17380.13	24358.42	135516.3	0.807671

P08670;P17661	Vimentin OS=Homo sapiens GN=VIM PE=1 SV=4	22918.43	106483.9	20117.72	17560.03	514558	27432.11	16797.4	66753.18	34166.33	0.80971
Q86YZ3	Hornerin OS=Homo sapiens GN=HRNR PE=1 SV=2	122244.7	64468.22	106605.5	1128266	14679.55	25930.83	42987.26	325298.8	333359.7	0.813217
P20930	Filaggrin OS=Homo sapiens GN=FLG PE=1 SV=3	2698.692	365.5888	874.9889	5679.155	255.9236	7314.339	121.5561	2757.68	4299.466	0.81408
P04406	Glyceraldehyde-3-phosphate dehydrogenase OS=Homo sapiens GN=GAPDH PE=1 SV=3	55906.18	226887.3	37108.67	171400.9	65860.63	50515.39	138131.7	303116.8	38367.95	0.838443
P04259	Keratin, type II cytoskeletal 6B OS=Homo sapiens GN=KRT6B PE=1 SV=5	2507.352	367922.1	39268.18	3284.98	49679.51	16850.71	897.3722	397521.9	3040.705	0.840814
P32969	60S ribosomal protein L9 OS=Homo sapiens GN=RPL9 PE=1 SV=1	1309.008	1588.781	33.18558	586.1056	4679.631	1689.072	4476.501	19479.02	0	0.846589
P62805	Histone H4 OS=Homo sapiens GN=HIST1H4A PE=1 SV=2	3848.651	74773.82	7019.555	6363.047	948587.1	6268.303	5473.953	15910.27	80823.97	0.847091
P02533	Keratin, type I cytoskeletal 14 OS=Homo sapiens GN=KRT14 PE=1 SV=4	193056.1	1955687	329664	281183.4	116630.6	589917.6	87283.16	2981932	267688.3	0.848782
Q01469;A8MUU1	Fatty acid-binding protein, epidermal OS=Homo sapiens GN=FABP5 PE=1 SV=3	18012.9	76813.97	16865.42	18644.29	4808.732	235026.5	7017.771	44044.41	14823.78	0.86254

P62917	60S ribosomal protein L8 OS=Homo sapiens GN=RPL8 PE=1 SV=2	5081.717	30496	1150.857	6891.367	12530.19	5881.426	8934.193	15331.15	4802.554	0.864042
P35908;Q7Z794;Q9NY12	Keratin, type II cytoskeletal 2 epidermal OS=Homo sapiens GN=KRT2 PE=1 SV=2	2984712	968491.8	1314173	1634245	615762.1	2228992	701661.7	2515707	3182074	0.866968
P68363;P68366	Tubulin alpha-1B chain OS=Homo sapiens GN=TUBA1B PE=1 SV=1	13911.5	40506.74	3868.38	158004.2	36791.43	2749.39	32900.08	94724.78	3751.137	0.873579
P62753	40S ribosomal protein S6 OS=Homo sapiens GN=RPS6 PE=1 SV=1	2921.725	12258.03	994.2008	1977.526	13879.55	2699.157	9823.868	19705.91	970.6267	0.876743
P13645;Q2M2I5;Q7Z3Y7;Q7Z3Y8;Q7Z3Z0	Keratin, type I cytoskeletal 10 OS=Homo sapiens GN=KRT10 PE=1 SV=6	6259208	2718063	4178041	3889563	1162828	17004314	2139016	15043749	6437534	0.888102
P02768	Serum albumin OS=Homo sapiens GN=ALB PE=1 SV=2	44583.34	1831823	43685.77	96105.55	132177.8	65761.94	64014.96	428187.7	24607.51	0.889284
P62258	14-3-3 protein epsilon OS=Homo sapiens GN=YWHAE PE=1 SV=1	217.3708	6382.742	221.6579	5710.076	3.830082	588.1143	1982.067	6178.039	0	0.908319
P46777	60S ribosomal protein L5 OS=Homo sapiens GN=RPL5 PE=1 SV=3	546.6267	2017.195	428.5844	103.5458	11379.6	1155.419	801.9743	2578.33	1023.638	0.915129

P35579	Myosin-9 OS=Homo sapiens GN=MYH9 PE=1 SV=4	9071.562	67019.56	8963.336	30052.37	12382.2	33919.59	21859.35	33766.72	10006.08	0.915708
P43243	Matrin-3 OS=Homo sapiens GN=MATR3 PE=1 SV=2	97.2118	538.3257	0	0	7126.344	0	592.6074	598.0563	0	0.916634
P06744	Glucose-6-phosphate isomerase OS=Homo sapiens GN=GPI PE=1 SV=4	48.99844	14145.94	336.7758	3301.665	1538.335	0	4638.143	24414.88	0	0.922983
P14923	Junction plakoglobin OS=Homo sapiens GN=JUP PE=1 SV=3	4595.261	17305.98	8493.698	11672.82	4154.028	28187.35	2983.452	20381.24	10802.39	0.929144
P22531;P22532;P35326;Q96RM1	Small proline-rich protein 2E OS=Homo sapiens GN=SPRR2E PE=2 SV=2	21009.65	119250.5	17405.85	28432.34	5211.722	495161.9	12689.97	45621.56	31413.47	0.930886
Q5T749	Keratinocyte proline-rich protein OS=Homo sapiens GN=KPRP PE=1 SV=1	31231.93	13013.56	20721.04	43418.62	5102.596	100450.7	8470.032	76524.55	28711.55	0.932265
Q02878	60S ribosomal protein L6 OS=Homo sapiens GN=RPL6 PE=1 SV=3	8878.81	36929.11	3982.445	9162.326	23007.35	4376.562	16764.46	21764.96	5715.915	0.935026
P61626	Lysozyme C OS=Homo sapiens GN=LYZ PE=1 SV=1	8502.997	6345.146	12078.92	9764.04	2079.935	52947.44	3482.597	28288.74	18027.42	0.938852
Q02413	Desmoglein-1 OS=Homo sapiens GN=DSG1 PE=1 SV=2	15660.97	11692.87	9869.008	18601.2	4308.103	42725.27	8280.715	28297.91	10978.8	0.945703

P07355;A6NMY6	Annexin A2 OS=Homo sapiens GN=ANXA2 PE=1 SV=2	9529.432	109926.5	16669.45	23831.14	18106.68	75118.09	19589.64	47262.77	33388.74	0.952358
P47929	Galectin-7 OS=Homo sapiens GN=LGALS7 PE=1 SV=2	13147.89	450977.1	9743.681	19463.48	4392.767	256844.9	14740.58	20916.29	52204.98	0.953288
P81605	Dermcidin OS=Homo sapiens GN=DCD PE=1 SV=2	111809.2	206853.6	317877.7	185714.4	429345.9	132552.5	112249.3	303902.5	265801.4	0.965283
P01859	Ig gamma-2 chain C region OS=Homo sapiens GN=IGHG2 PE=1 SV=2	0	297517	230.336	1457.426	876.7175	115.55	100.0228	3836.654	129.6759	0.98862
P31949	Protein S100-A11 OS=Homo sapiens GN=S100A11 PE=1 SV=2	5110.838	26112.9	1525.049	9276.506	3579.061	5141.155	2293.57	10059.24	6199.379	0.98909
P35527	Keratin, type I cytoskeletal 9 OS=Homo sapiens GN=KRT9 PE=1 SV=3	5635874	3685903	4766344	22308840	3364919	1490963	1695094	8030866	9989666	0.991245

Appendix Table 2: Complete spectral count data for mass spectrometry experiment.

Accession	Protein	Confidence score	Halotag Spectral Count			Wild Type Spectral Count			Variant B Spectral Count		
P07711;Q5NE16	Cathepsin L1 OS=Homo sapiens GN=CTSL PE=1 SV=2	645.5	0	0	0	9	3	9	8	8	9
P07858	Cathepsin B OS=Homo sapiens GN=CTSB PE=1 SV=3	784.36	0	0	0	9	8	12	8	7	10
P53634	Dipeptidyl peptidase 1 OS=Homo sapiens GN=CTSC PE=1 SV=2	1143.68	0	0	0	17	14	15	9	3	8
P11021;O95399	78 kDa glucose-regulated protein OS=Homo sapiens GN=HSPA5 PE=1 SV=2	2620.78	0	5	0	35	23	39	21	13	21
P01034	Cystatin-C OS=Homo sapiens GN=CST3 PE=1 SV=1	1210.91	0	0	0	19	12	23	8	1	16
P35232	Prohibitin OS=Homo sapiens GN=PHB PE=1 SV=1	199.85	1	2	3	2	0	1	5	1	5
Q9UIQ6	Leucyl-cystinyl aminopeptidase OS=Homo sapiens GN=LNPEP PE=1 SV=3	1265.14	0	0	0	17	2	18	0	0	0

P38646	Stress-70 protein, mitochondrial OS=Homo sapiens GN=HSPA9 PE=1 SV=2	1072.19	0	0	0	16	6	12	4	9	0
P10620	Microsomal glutathione S-transferase 1 OS=Homo sapiens GN=MGST1 PE=1 SV=1	28.73	0	0	0	1	0	0	0	0	0
P62937;Q9Y536	Peptidyl-prolyl cis-trans isomerase A OS=Homo sapiens GN=PPIA PE=1 SV=2	319.29	1	6	0	3	2	1	7	6	0
P05141;P12235	ADP/ATP translocase 2 OS=Homo sapiens GN=SLC25A5 PE=1 SV=7	216.31	0	1	1	0	1	2	1	1	1
P27348	14-3-3 protein theta OS=Homo sapiens GN=YWHAQ PE=1 SV=1	157.56	0	1	0	0	0	0	0	0	0
P08107;P17066;P48741	Heat shock 70 kDa protein 1A/1B OS=Homo sapiens GN=HSPA1A PE=1 SV=5	701.23	0	1	0	3	1	3	1	2	0
P06899;Q6DN03	Histone H2B type 1-J OS=Homo sapiens GN=HIST1H2BJ PE=1 SV=3	216.99	0	0	0	0	1	0	0	0	0

P53999	Activated RNA polymerase II transcriptional coactivator p15 OS=Homo sapiens GN=SUB1 PE=1 SV=3	75.6	0	0	0	0	0	0	0	1	0
P11142;P54652	Heat shock cognate 71 kDa protein OS=Homo sapiens GN=HSPA8 PE=1 SV=1	1084.76	2	2	1	10	6	7	5	6	0
P62979	Ubiquitin-40S ribosomal protein S27a OS=Homo sapiens GN=RPS27A PE=1 SV=2	204.67	3	2	1	3	4	2	4	1	2
Q99623	Prohibitin-2 OS=Homo sapiens GN=PHB2 PE=1 SV=2	219.67	3	3	3	2	2	3	4	3	5
P31151	Protein S100-A7 OS=Homo sapiens GN=S100A7 PE=1 SV=4	44.96	0	0	0	0	0	1	0	0	0
Q15149	Plectin OS=Homo sapiens GN=PLEC PE=1 SV=3	543.17	0	1	0	0	11	0	0	0	0
P23396	40S ribosomal protein S3 OS=Homo sapiens GN=RPS3 PE=1 SV=2	356.31	2	1	0	6	5	2	5	6	2
P12236	ADP/ATP translocase 3 OS=Homo sapiens GN=SLC25A6 PE=1 SV=4	202.83	0	0	1	0	0	0	1	1	1

P62249	40S ribosomal protein S16 OS=Homo sapiens GN=RPS16 PE=1 SV=2	54.53	1	1	0	1	1	1	1	1	1
P22314	Ubiquitin-like modifier-activating enzyme 1 OS=Homo sapiens GN=UBA1 PE=1 SV=3	47.35	0	0	0	0	0	0	1	1	0
Q06830;P32119;Q13162	Peroxiredoxin-1 OS=Homo sapiens GN=PRDX1 PE=1 SV=1	350.39	5	5	6	5	3	4	6	4	8
A8MT79	Putative zinc-alpha-2-glycoprotein-like 1 OS=Homo sapiens PE=5 SV=2	34.96	1	0	0	0	0	1	0	0	0
P21796	Voltage-dependent anion-selective channel protein 1 OS=Homo sapiens GN=VDAC1 PE=1 SV=2	211.38	0	3	1	0	0	1	2	2	2
P06748	Nucleophosmin OS=Homo sapiens GN=NPM1 PE=1 SV=2	157.99	0	1	0	0	3	1	0	1	0
P84095	Rho-related GTP-binding protein RhoG OS=Homo sapiens GN=RHOG PE=1 SV=1	74.95	0	0	0	1	0	0	0	0	0

Q8NC51	Plasminogen activator inhibitor 1 RNA-binding protein OS=Homo sapiens GN=SERBP1 PE=1 SV=2	29.1	0	0	0	1	0	0	0	0	0
P07437;A6NKZ8;A6NNZ2;Q13885;Q9BUF5;Q9H4B7	Tubulin beta chain OS=Homo sapiens GN=TUBB PE=1 SV=2	840.05	1	1	0	2	2	1	3	1	0
P62913	60S ribosomal protein L11 OS=Homo sapiens GN=RPL11 PE=1 SV=2	110.4	0	0	0	1	2	0	0	2	0
P04792	Heat shock protein beta-1 OS=Homo sapiens GN=HSPB1 PE=1 SV=2	315.84	0	1	0	3	2	5	1	1	0
Q08211	ATP-dependent RNA helicase A OS=Homo sapiens GN=DHX9 PE=1 SV=4	57.52	0	0	0	0	1	0	0	1	0
P62888	60S ribosomal protein L30 OS=Homo sapiens GN=RPL30 PE=1 SV=2	48.31	1	1	0	0	1	0	0	1	0
P61978	Heterogeneous nuclear ribonucleoprotein K OS=Homo sapiens GN=HNRNPK PE=1 SV=1	187.71	0	0	0	0	1	0	2	3	0

P27482	Calmodulin-like protein 3 OS=Homo sapiens GN=CALML3 PE=1 SV=2	176.92	0	3	0	0	0	1	0	0	0
P62847	40S ribosomal protein S24 OS=Homo sapiens GN=RPS24 PE=1 SV=1	36.11	0	1	0	0	0	0	1	1	0
P60660;P14649	Myosin light polypeptide 6 OS=Homo sapiens GN=MYL6 PE=1 SV=2	93.31	0	2	1	2	1	0	1	0	1
P62826	GTP-binding nuclear protein Ran OS=Homo sapiens GN=RAN PE=1 SV=3	83.1	0	0	0	1	1	1	2	2	0
P10809	60 kDa heat shock protein, mitochondrial OS=Homo sapiens GN=HSPD1 PE=1 SV=2	363.43	0	3	0	5	3	3	4	6	0
P52597	Heterogeneous nuclear ribonucleoprotein F OS=Homo sapiens GN=HNRNPF PE=1 SV=3	82.54	0	0	0	0	0	0	1	1	0
P10599	Thioredoxin OS=Homo sapiens GN=TXN PE=1 SV=3	32.36	0	0	0	1	0	0	0	0	0

P09211	Glutathione S-transferase P OS=Homo sapiens GN=GSTP1 PE=1 SV=2	59.2	0	1	0	0	0	0	0	1	0
P23528;Q9Y281	Cofilin-1 OS=Homo sapiens GN=CFL1 PE=1 SV=3	86.37	0	1	0	0	0	0	0	1	0
Q71UM5	40S ribosomal protein S27-like OS=Homo sapiens GN=RPS27L PE=1 SV=3	29.45	0	0	0	0	1	0	0	0	0
Q00839	Heterogeneous nuclear ribonucleoprotein U OS=Homo sapiens GN=HNRNPU PE=1 SV=6	178.67	0	0	0	0	3	1	0	1	1
P01876;P01877	Ig alpha-1 chain C region OS=Homo sapiens GN=IGHA1 PE=1 SV=2	150.58	0	2	0	0	0	0	0	0	0
P13639	Elongation factor 2 OS=Homo sapiens GN=EEF2 PE=1 SV=4	54.99	0	1	0	0	0	1	0	1	0
P49411	Elongation factor Tu, mitochondrial OS=Homo sapiens GN=TUFM PE=1 SV=2	77.94	0	0	0	2	0	1	1	2	0

P06702	Protein S100-A9 OS=Homo sapiens GN=S100A9 PE=1 SV=1	63.61	0	2	1	0	0	0	0	0	1
P14324	Farnesyl pyrophosphate synthase OS=Homo sapiens GN=FDPS PE=1 SV=4	29.79	0	0	0	0	0	0	0	1	0
P09651;Q32P51	Heterogeneous nuclear ribonucleoprotein A1 OS=Homo sapiens GN=HNRNPA1 PE=1 SV=5	166.46	0	2	0	1	2	0	0	2	0
P80723	Brain acid soluble protein 1 OS=Homo sapiens GN=BASP1 PE=1 SV=2	73.85	0	0	0	2	0	2	0	1	0
P61353	60S ribosomal protein L27 OS=Homo sapiens GN=RPL27 PE=1 SV=2	42.6	1	0	0	0	0	0	0	1	0
P08195	4F2 cell-surface antigen heavy chain OS=Homo sapiens GN=SLC3A2 PE=1 SV=3	60.35	0	0	0	0	0	0	0	1	0
P67936	Tropomyosin alpha-4 chain OS=Homo sapiens GN=TPM4 PE=1 SV=3	58.68	0	0	0	1	0	0	0	0	0

P60174	Triosephosphate isomerase OS=Homo sapiens GN=TPI1 PE=1 SV=3	67.55	0	2	0	1	0	0	0	1	0
P05090	Apolipoprotein D OS=Homo sapiens GN=APOD PE=1 SV=1	84.21	0	0	0	0	2	0	0	0	0
P31944	Caspase-14 OS=Homo sapiens GN=CASP14 PE=1 SV=2	107.46	0	0	0	0	0	2	0	0	0
P62263	40S ribosomal protein S14 OS=Homo sapiens GN=RPS14 PE=1 SV=3	38.82	0	0	0	0	1	0	1	0	0
Q8NHW5	60S acidic ribosomal protein P0-like OS=Homo sapiens GN=RPLP0P6 PE=5 SV=1	42.38	0	0	0	0	1	0	1	0	0
Q07021	Complement component 1 Q subcomponent-binding protein, mitochondrial OS=Homo sapiens GN=C1QBP PE=1 SV=1	131.41	0	2	0	2	0	2	0	3	0
P61604	10 kDa heat shock protein, mitochondrial OS=Homo sapiens GN=HSPE1 PE=1 SV=2	91.1	0	0	0	1	1	2	0	1	0

P26373	60S ribosomal protein L13 OS=Homo sapiens GN=RPL13 PE=1 SV=4	71.1	0	0	0	0	2	0	1	2	0
P49207	60S ribosomal protein L34 OS=Homo sapiens GN=RPL34 PE=1 SV=3	45.29	0	0	0	0	1	0	1	1	0
P07737	Profilin-1 OS=Homo sapiens GN=PFN1 PE=1 SV=2	234.11	0	3	0	2	1	0	4	3	0
Q00325	Phosphate carrier protein, mitochondrial OS=Homo sapiens GN=SLC25A3 PE=1 SV=2	42.43	0	1	0	1	0	1	0	1	0
P60709;A5A3E0;P0CG38;P0CG39;P62736;P68032;Q6S8J3;Q9BYX7	Actin, cytoplasmic 1 OS=Homo sapiens GN=ACTB PE=1 SV=1	1302.01	8	14	9	12	9	10	9	8	9
P62701;P22090	40S ribosomal protein S4, X isoform OS=Homo sapiens GN=RPS4X PE=1 SV=2	52.87	0	1	0	0	1	0	1	1	0
P62857	40S ribosomal protein S28 OS=Homo sapiens GN=RPS28 PE=1 SV=1	82.27	0	1	0	0	0	1	0	2	0

P07910;O60812	Heterogeneous nuclear ribonucleoproteins C1/C2 OS=Homo sapiens GN=HNRNPC PE=1 SV=4	229.73	0	0	0	0	5	0	0	1	0
P36578	60S ribosomal protein L4 OS=Homo sapiens GN=RPL4 PE=1 SV=5	27.48	0	0	0	0	1	0	0	1	0
P43307	Translocon-associated protein subunit alpha OS=Homo sapiens GN=SSR1 PE=1 SV=3	50.78	0	0	0	1	0	0	0	0	0
P00338;P07864	L-lactate dehydrogenase A chain OS=Homo sapiens GN=LDHA PE=1 SV=2	328.54	0	5	0	1	3	0	5	5	0
P45880	Voltage-dependent anion-selective channel protein 2 OS=Homo sapiens GN=VDAC2 PE=1 SV=2	263.79	2	2	3	2	3	1	4	2	3
P30041	Peroxiredoxin-6 OS=Homo sapiens GN=PRDX6 PE=1 SV=3	30.93	0	0	0	1	0	0	0	0	0

Q71U36;A6NHL2;Q13748;Q6PEY2;Q9BQE3;Q9H853;Q9NY65	Tubulin alpha-1A chain OS=Homo sapiens GN=TUBA1A PE=1 SV=1	766.63	0	1	0	1	1	0	0	1	0
P06576	ATP synthase subunit beta, mitochondrial OS=Homo sapiens GN=ATP5B PE=1 SV=3	78.68	1	1	2	0	1	2	1	1	1
Q15366	Poly(rC)-binding protein 2 OS=Homo sapiens GN=PCBP2 PE=1 SV=1	40.28	0	1	0	1	0	0	1	1	0
P07339	Cathepsin D OS=Homo sapiens GN=CTSD PE=1 SV=1	42.11	0	0	0	0	0	1	0	0	0
P02795	Metallothionein-2 OS=Homo sapiens GN=MT2A PE=1 SV=1	38.88	0	0	0	1	0	0	0	0	0
Q9NQ39	Putative 40S ribosomal protein S10-like OS=Homo sapiens GN=RPS10P5 PE=5 SV=1	65.03	0	1	0	1	1	0	1	1	0
P01834	Ig kappa chain C region OS=Homo sapiens GN=IGKC PE=1 SV=1	366.96	0	5	0	0	1	0	0	0	0
P08779;O76013;P35900;Q7Z3Y9;Q8N1A0;Q99456	Keratin, type I cytoskeletal 16 OS=Homo sapiens GN=KRT16 PE=1 SV=4	2566.41	4	11	14	3	0	3	0	24	5

P07195	L-lactate dehydrogenase B chain OS=Homo sapiens GN=LDHB PE=1 SV=2	266.08	0	0	0	0	0	0	2	4	0
Q07020	60S ribosomal protein L18 OS=Homo sapiens GN=RPL18 PE=1 SV=2	111.5	1	0	0	0	1	0	1	2	0
P63244	Guanine nucleotide-binding protein subunit beta-2-like 1 OS=Homo sapiens GN=GNB2L1 PE=1 SV=3	74.99	0	1	0	0	0	1	1	2	0
P56134	ATP synthase subunit f, mitochondrial OS=Homo sapiens GN=ATP5J2 PE=1 SV=3	34.48	0	0	0	1	0	0	0	0	0
P50914	60S ribosomal protein L14 OS=Homo sapiens GN=RPL14 PE=1 SV=4	55.85	1	0	0	0	1	0	1	1	0
P58107	Epiplakin OS=Homo sapiens GN=EPPK1 PE=1 SV=2	186.01	0	0	0	0	2	0	0	0	0

P63313;P62328	Thymosin beta-10 OS=Homo sapiens GN=TMSB10 PE=1 SV=2	56.95	0	1	0	2	1	0	0	2	0
P06454	Prothymosin alpha OS=Homo sapiens GN=PTMA PE=1 SV=2	172.65	0	3	0	2	2	0	0	2	0
P14174	Macrophage migration inhibitory factor OS=Homo sapiens GN=MIF PE=1 SV=4	62.76	1	0	0	1	0	0	1	1	1
P25705	ATP synthase subunit alpha, mitochondrial OS=Homo sapiens GN=ATP5A1 PE=1 SV=1	353.95	0	2	0	3	3	2	3	4	0
P06733;P09104;P13929	Alpha-enolase OS=Homo sapiens GN=ENO1 PE=1 SV=2	410.48	1	5	0	5	1	3	0	5	0
P02787	Serotransferrin OS=Homo sapiens GN=TF PE=1 SV=3	579.73	0	13	0	0	0	0	0	0	0
P46781	40S ribosomal protein S9 OS=Homo sapiens GN=RPS9 PE=1 SV=3	43.65	0	0	0	0	1	0	1	0	0
P05387	60S acidic ribosomal protein P2 OS=Homo sapiens GN=RPLP2 PE=1 SV=1	110.97	1	0	0	1	3	0	1	1	1

P67809	Nuclease-sensitive element-binding protein 1 OS=Homo sapiens GN=YBX1 PE=1 SV=3	148.56	2	2	0	2	2	1	1	3	0
P01024	Complement C3 OS=Homo sapiens GN=C3 PE=1 SV=2	83.75	0	2	0	0	0	0	0	0	0
P05787;P41219;Q9NSB2	Keratin, type II cytoskeletal 8 OS=Homo sapiens GN=KRT8 PE=1 SV=7	1242.71	2	4	3	2	16	2	7	8	3
Q02543	60S ribosomal protein L18a OS=Homo sapiens GN=RPL18A PE=1 SV=2	38.05	0	1	0	0	1	0	0	1	0
P04075	Fructose-bisphosphate aldolase A OS=Homo sapiens GN=ALDOA PE=1 SV=2	44.62	0	1	0	0	0	0	0	0	0
P11940;Q13310	Polyadenylate-binding protein 1 OS=Homo sapiens GN=PABPC1 PE=1 SV=2	74.01	0	1	0	0	0	0	0	2	0
P01040	Cystatin-A OS=Homo sapiens GN=CSTA PE=1 SV=1	102.86	2	0	0	1	1	3	1	2	1
P62854	40S ribosomal protein S26 OS=Homo sapiens GN=RPS26 PE=1 SV=3	28.01	0	1	0	1	1	0	0	1	0

P52272	Heterogeneous nuclear ribonucleoprotein M OS=Homo sapiens GN=HNRNPM PE=1 SV=3	33.17	0	0	0	0	1	0	0	0	0
P05109	Protein S100-A8 OS=Homo sapiens GN=S100A8 PE=1 SV=1	73.83	0	1	1	0	0	0	0	0	1
P02538	Keratin, type II cytoskeletal 6A OS=Homo sapiens GN=KRT6A PE=1 SV=3	1928.01	1	3	1	1	0	0	0	1	1
P61204	ADP-ribosylation factor 3 OS=Homo sapiens GN=ARF3 PE=1 SV=2	38.44	0	0	0	0	0	0	0	1	0
P49327	Fatty acid synthase OS=Homo sapiens GN=FASN PE=1 SV=3	39	0	0	0	0	0	0	0	1	0
P39023	60S ribosomal protein L3 OS=Homo sapiens GN=RPL3 PE=1 SV=2	54.47	0	0	0	0	0	0	0	1	0
Q5VTE0;Q05639	Putative elongation factor 1-alpha-like 3 OS=Homo sapiens GN=EEF1A1P5 PE=5 SV=1	385.21	3	8	1	5	4	4	6	5	4

P10412;P16401	Histone H1.4 OS=Homo sapiens GN=HIST1H1E PE=1 SV=2	115.86	3	2	0	0	3	0	2	0	2
P63104;P31946	14-3-3 protein zeta/delta OS=Homo sapiens GN=YWHAZ PE=1 SV=1	218.97	0	3	0	1	0	0	0	0	0
P05783	Keratin, type I cytoskeletal 18 OS=Homo sapiens GN=KRT18 PE=1 SV=2	564.7	0	0	4	1	9	0	5	4	0
P0CG05;A0M8Q6;B9A064; P0CF74	Ig lambda-2 chain C regions OS=Homo sapiens GN=IGLC2 PE=1 SV=1	230.15	0	4	0	0	0	0	0	0	0
Q8TF72	Protein Shroom3 OS=Homo sapiens GN=SHROOM3 PE=1 SV=2	30.43	1	1	1	1	1	1	1	1	1
P15924	Desmoplakin OS=Homo sapiens GN=DSP PE=1 SV=3	304.75	1	6	1	2	1	5	0	3	2
P68371;P04350;Q3ZCM7	Tubulin beta-4B chain OS=Homo sapiens GN=TUBB4B PE=1 SV=1	784.15	0	0	0	1	0	0	0	1	0
Q14240	Eukaryotic initiation factor 4A-II OS=Homo sapiens GN=EIF4A2 PE=1 SV=2	74.44	0	0	0	1	0	0	2	1	0

P40926	Malate dehydrogenase, mitochondrial OS=Homo sapiens GN=MDH2 PE=1 SV=3	31.05	0	1	0	0	0	0	0	0	0
P13647;P12036;Q3SY84;Q7RTS7;Q8N1N4	Keratin, type II cytoskeletal 5 OS=Homo sapiens GN=KRT5 PE=1 SV=3	2089.03	14	23	15	9	3	12	7	19	12
Q01105	Protein SET OS=Homo sapiens GN=SET PE=1 SV=3	50.97	0	0	0	1	0	0	0	0	0
Q6UWP8	Suprabasin OS=Homo sapiens GN=SBSN PE=2 SV=2	41.22	0	0	0	0	0	1	0	0	0
P02545	Prelamin-A/C OS=Homo sapiens GN=LMNA PE=1 SV=1	171.79	0	3	0	0	1	0	1	1	0
P27797	Calreticulin OS=Homo sapiens GN=CALR PE=1 SV=1	30.31	0	1	0	0	1	1	1	0	0
P14618	Pyruvate kinase PKM OS=Homo sapiens GN=PKM PE=1 SV=4	166.69	0	3	0	1	1	1	1	2	0
P62241	40S ribosomal protein S8 OS=Homo sapiens GN=RPS8 PE=1 SV=2	94.36	1	0	0	0	2	0	0	1	0
Q9NZT1	Calmodulin-like protein 5 OS=Homo sapiens GN=CALML5 PE=1 SV=2	31.01	0	1	0	0	1	0	0	0	1

P07900;Q58FG0	Heat shock protein HSP 90-alpha OS=Homo sapiens GN=HSP90AA1 PE=1 SV=5	763.65	0	2	0	0	0	0	3	3	0
P08238;P14625;Q12931;Q14568;Q58FF6;Q58FF7;Q58FF8;Q58FG1	Heat shock protein HSP 90-beta OS=Homo sapiens GN=HSP90AB1 PE=1 SV=4	970.68	1	4	0	2	3	2	8	7	0
P08729	Keratin, type II cytoskeletal 7 OS=Homo sapiens GN=KRT7 PE=1 SV=5	1202.7	1	1	8	2	14	0	3	5	1
P01857	Ig gamma-1 chain C region OS=Homo sapiens GN=IGHG1 PE=1 SV=1	307.25	0	3	0	0	0	0	0	0	0
Q5D862	Filaggrin-2 OS=Homo sapiens GN=FLG2 PE=1 SV=1	165.55	1	0	1	2	0	2	1	2	2
Q09666	Neuroblast differentiation-associated protein AHNAK OS=Homo sapiens GN=AHNAK PE=1 SV=2	63.72	0	2	0	0	0	0	0	1	0

Q9H299	SH3 domain-binding glutamic acid-rich-like protein 3 OS=Homo sapiens GN=SH3BGRL3 PE=1 SV=1	28.5	0	1	0	0	0	0	0	0	0
P04264;P14136	Keratin, type II cytoskeletal 1 OS=Homo sapiens GN=KRT1 PE=1 SV=6	3176.55	38	25	33	36	27	25	29	35	31
P22528	Cornifin-B OS=Homo sapiens GN=SPRR1B PE=1 SV=2	27.66	0	1	0	0	0	0	0	1	0
P31947	14-3-3 protein sigma OS=Homo sapiens GN=SFN PE=1 SV=1	256.38	0	3	0	0	0	1	0	0	0
Q5QNW6;Q96A08	Histone H2B type 2-F OS=Homo sapiens GN=HIST2H2BF PE=1 SV=3	226.48	0	0	0	0	1	0	0	0	0
P61313	60S ribosomal protein L15 OS=Homo sapiens GN=RPL15 PE=1 SV=2	41	1	0	0	0	1	0	1	0	0
P84098	60S ribosomal protein L19 OS=Homo sapiens GN=RPL19 PE=1 SV=1	103.26	1	1	0	0	2	1	1	2	1
P05386	60S acidic ribosomal protein P1 OS=Homo sapiens GN=RPLP1 PE=1 SV=1	64.79	1	1	0	1	1	0	1	1	0

P62269	40S ribosomal protein S18 OS=Homo sapiens GN=RPS18 PE=1 SV=3	115.09	1	1	1	2	1	0	2	0	3
P61247	40S ribosomal protein S3a OS=Homo sapiens GN=RPS3A PE=1 SV=2	47.31	0	1	0	0	0	0	1	1	0
Q71DI3;Q6NXT2	Histone H3.2 OS=Homo sapiens GN=HIST2H3A PE=1 SV=3	91.14	0	0	0	0	3	0	0	0	1
P12273	Prolactin-inducible protein OS=Homo sapiens GN=PIP PE=1 SV=1	151.5	0	0	0	0	3	0	0	0	0
P02647	Apolipoprotein A-I OS=Homo sapiens GN=APOA1 PE=1 SV=1	47.44	1	0	0	0	1	1	0	0	0
P00558	Phosphoglycerate kinase 1 OS=Homo sapiens GN=PGK1 PE=1 SV=3	89.01	0	2	0	1	0	0	1	1	0
Q04695;Q9C075	Keratin, type I cytoskeletal 17 OS=Homo sapiens GN=KRT17 PE=1 SV=2	2147.65	0	23	9	1	14	0	2	13	2
P0C0S8;P0C0S5;P16104;Q8IUE6	Histone H2A type 1 OS=Homo sapiens GN=HIST1H2AG PE=1 SV=2	157.98	0	1	0	0	4	0	0	0	1

P08670;P17661	Vimentin OS=Homo sapiens GN=VIM PE=1 SV=4	622.22	0	0	0	0	11	0	0	0	0
Q86YZ3	Hornerin OS=Homo sapiens GN=HRNR PE=1 SV=2	832.02	3	4	3	16	1	1	2	9	9
P20930	Filaggrin OS=Homo sapiens GN=FLG PE=1 SV=3	28.91	0	0	0	1	0	1	0	1	1
P04406	Glyceraldehyde-3-phosphate dehydrogenase OS=Homo sapiens GN=GAPDH PE=1 SV=3	518.16	1	5	1	6	3	0	4	8	1
P04259	Keratin, type II cytoskeletal 6B OS=Homo sapiens GN=KRT6B PE=1 SV=5	1965.26	0	2	1	0	0	0	0	2	0
P32969	60S ribosomal protein L9 OS=Homo sapiens GN=RPL9 PE=1 SV=1	26.05	0	0	0	0	0	0	0	1	0
P62805	Histone H4 OS=Homo sapiens GN=HIST1H4A PE=1 SV=2	387.46	0	1	0	0	7	0	0	0	3
P02533	Keratin, type I cytoskeletal 14 OS=Homo sapiens GN=KRT14 PE=1 SV=4	2344.3	5	14	9	4	1	4	1	13	6
Q01469;A8MUU1	Fatty acid-binding protein, epidermal OS=Homo sapiens GN=FABP5 PE=1 SV=3	228.68	1	4	1	0	0	5	0	1	0

P62917	60S ribosomal protein L8 OS=Homo sapiens GN=RPL8 PE=1 SV=2	38.43	0	0	0	0	1	0	1	0	0
P35908;Q7Z794;Q9NY12	Keratin, type II cytoskeletal 2 epidermal OS=Homo sapiens GN=KRT2 PE=1 SV=2	2525.26	25	14	23	14	9	18	15	19	24
P68363;P68366	Tubulin alpha-1B chain OS=Homo sapiens GN=TUBA1B PE=1 SV=1	780.23	1	1	0	1	1	0	1	1	0
P62753	40S ribosomal protein S6 OS=Homo sapiens GN=RPS6 PE=1 SV=1	31.64	0	0	0	0	1	0	0	0	0
P13645;Q2M2I5;Q7Z3Y7;Q7Z3Y8;Q7Z3Z0	Keratin, type I cytoskeletal 10 OS=Homo sapiens GN=KRT10 PE=1 SV=6	2847.53	31	20	26	25	17	29	25	28	30
P02768	Serum albumin OS=Homo sapiens GN=ALB PE=1 SV=2	629.14	1	12	0	2	3	1	3	3	0
P62258	14-3-3 protein epsilon OS=Homo sapiens GN=YWHAE PE=1 SV=1	105.7	0	1	0	1	0	0	0	0	0
P46777	60S ribosomal protein L5 OS=Homo sapiens GN=RPL5 PE=1 SV=3	37.52	0	0	0	0	1	0	0	0	0

P35579	Myosin-9 OS=Homo sapiens GN=MYH9 PE=1 SV=4	200.19	1	4	0	0	0	0	0	1	0
P43243	Matrin-3 OS=Homo sapiens GN=MATR3 PE=1 SV=2	31.45	0	0	0	0	1	0	0	0	0
P06744	Glucose-6-phosphate isomerase OS=Homo sapiens GN=GPI PE=1 SV=4	35.13	0	1	0	0	0	0	0	1	0
P14923	Junction plakoglobin OS=Homo sapiens GN=JUP PE=1 SV=3	71.32	0	1	0	1	0	2	0	1	0
P22531;P22532;P35326;Q96RM1	Small proline-rich protein 2E OS=Homo sapiens GN=SPRR2E PE=2 SV=2	97.24	1	2	0	2	0	2	0	2	2
Q5T749	Keratinocyte proline-rich protein OS=Homo sapiens GN=KPRP PE=1 SV=1	93.97	2	0	1	1	0	2	0	0	2
Q02878	60S ribosomal protein L6 OS=Homo sapiens GN=RPL6 PE=1 SV=3	61.84	1	1	0	0	2	0	2	1	1
P61626	Lysozyme C OS=Homo sapiens GN=LYZ PE=1 SV=1	80.42	0	0	1	1	0	2	0	1	1
Q02413	Desmoglein-1 OS=Homo sapiens GN=DSG1 PE=1 SV=2	104.91	1	0	0	1	0	2	0	2	0

P07355;A6NMY6	Annexin A2 OS=Homo sapiens GN=ANXA2 PE=1 SV=2	283.63	0	4	1	1	0	2	0	1	2
P47929	Galectin-7 OS=Homo sapiens GN=LGALS7 PE=1 SV=2	412.47	0	5	0	0	0	2	0	0	0
P81605	Dermcidin OS=Homo sapiens GN=DCD PE=1 SV=2	222.59	2	2	4	3	4	2	3	1	4
P01859	Ig gamma-2 chain C region OS=Homo sapiens GN=IGHG2 PE=1 SV=2	245.3	0	2	0	0	0	0	0	0	0
P31949	Protein S100-A11 OS=Homo sapiens GN=S100A11 PE=1 SV=2	55.84	0	1	0	1	1	1	0	1	1
P35527	Keratin, type I cytoskeletal 9 OS=Homo sapiens GN=KRT9 PE=1 SV=3	3074.34	37	30	34	41	28	11	20	32	38

Appendix 2:

Methods Supplement - Recipes

DNA Analysis:

Stock 5x TBE:

Tris	54 g
Orthoboric acid	27.5 g
0.5M EDTA, pH 8.0	20 mL
dH_2O	800 mL

pH to 8.3 with orthoboric acid

Make to 1 litre with dH_2O

DNA Glycerol loading buffer

dH_2O	5 mL
Glycerol	1.5 mL
Bromophenol blue	0.25% (w/v)
0.5M EDTA	5 µL

NZY+ Broth (per litre)

NZ amine (casein hydrolysate)	10 g
Yeast extract	5 g
NaCl	5 g
NaOH	pH to 7.5

Add prior to use:

1 M $MgCl_2$	12.5 mL
1 M $MgSO_4$	12.5 mL
20% (w/v) glucose	20 mL

Protein Analysis:

Lysis buffer:

β-mercaptoethanol	0.128 M
Tris	40 mM
glycerol	10 % v/v
SDS	1 % w/v
bromophenol blue	~0.01 % w/v

Use volume appropriately to sample size or tissue culture vessel area. Approximately 200 to 500 µL per well of a 6 well plate.

10x Loading buffer (Lemmli buffer)

β-mercaptoethanol	0.625 M
Tris pH 6.8	62.5 mM
glycerol	10 % v/v
SDS	2 % w/v
bromophenol blue	0.00125% w/v

Used at 2x concentration; with ¼ volume added to sample before heating to denature proteins.

Resolving gel buffer:

Tris	3 M
HCl	pH 8.85

Stacking gel buffer:

Tris	0.25 M
HCl	pH 6.8

Stock 5x Running Buffer:

(Use at 1x.)

Tris	0.125 M
Glycine	1.25 M
SDS	0.5 % w/v

Transfer buffer:

Produced from 5x Running buffer as follows: 100 mL 5x Running Buffer, 233 mL Ethanol, up to 1 L with dH_2O.

Tris	0.0125 M
Glycine	0.125 M
SDS	0.05 % w/v
Ethanol	23.3 % v/v

Wash buffer:

Tris	0.02 M
NaCl	0.137 M
Tween-20	0.1 % v/v

Blocking Buffer:

Tris	0.02 M
NaCl	0.137 M
Tween-20	0.1 % v/v
Milk powder	5 % w/v

Stripping solution:

Tris	0.0624 M
SDS	2 % w/v
HCl	pH 6.7
β-mercaptoethanol	0.7 % v/v

Add β-mercaptoethanol just prior to usage.

RIPA buffer (pH to 8.0):

NaCl	150 mM
Tris	10 mM
IGEPAL CA630	1 %
Cholic Acid	0.5 %
EDTA	5 mM

Add protease inhibitors just prior to use (Promega Protease Inhibitor Cocktail, G6521).

SDS Gel recipes:

Resolving gel (12%):

- 3.5 mL dH_2O
- 2.5 mL resolving gel buffer
- 4 mL acrylamide (30%,)
- 100 µL 10 % SDS
- 100 µL 10 % APS
- 10 µL TEMED

Stacking gel (4%):

- 1.85 mL dH_2O
- 2.5 mL stacking gel buffer
- 650 µL acrylamide (30%,)
- 50 µL 10 % SDS
- 50 µL 10 % APS
- 10 µL TEMED